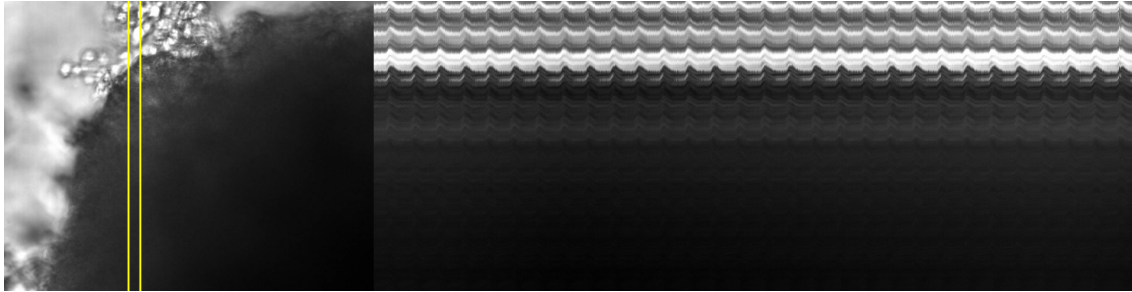


Effects of ultrasound on cardiomyocyte contractions

Dafne Groener (s1534092)

July 1, 2020



Biomedical Engineering - Imaging & in vitro diagnostics

Physics of Fluids

Master committee:

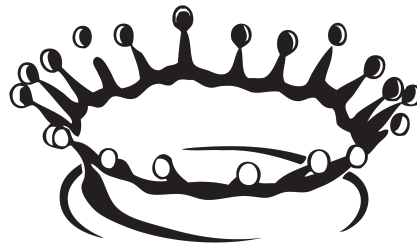
Prof.Dr M. Versluis (chairman)

Dr. G.P.R. Lajoinie

Pof.Dr. P.C.J.J. Passier

Dr. V. Schwach

Dr. K. Broersen (external member)



Physics of Fluids

**UNIVERSITY
OF TWENTE.**

Contents

1	Introduction	6
1.1	Cardiomyocyte contraction	6
1.2	Ultrasound	10
1.3	Study	12
2	Materials and methods	15
2.1	Sample	15
2.2	Setup	16
2.3	Experimental methods	16
2.4	Processing	18
2.5	Analysis	19
3	Results	21
3.1	Single measurement analysis	22
3.2	Effect of pulse duration	24
3.3	Effect of pulse pressure and center frequency	25
4	Discussion	29
5	Conclusion	32
6	Recommendations	33
	Bibliography	35
	Appendices	40
A	Extra figures	40
A.1	Contractions: histograms and shape	40
A.2	Histogram view	42
B	Recommendation calcium imaging	45
B.1	Theory	45
B.2	Method	45
B.3	Experiments	45
B.4	Data analysis	46
C	Matlab scripts	47
C.1	Script to process .tif files to one .AVI file	47
C.2	Script to do PIV analysis at .AVI movies	48
C.3	Script to define the movement of the tissue based on the PIV analysis results	55
C.4	Script to extract contractions and determine contraction parameters	63

Samenvatting

Contractie van cardiomyocyten is het gevolg van een cascade van gebeurtenissen, waarbij allereerst een calciumflux wordt veroorzaakt door een actiepotentiaal. Deze calciumstroom is benodigd voor het samentrekken van actine- en myosinefilamenten. Deze cascade kan extern in gang worden gezet op verschillende wijzen: namelijk activatie van calciumkanalen, resulterend in een verhoogde calciumflux, directe activering van myosinefilamenten, met als gevolg samentrekkingen, en cAMP toename wat leidt tot calciumkanaal activatie. Electricische en optische stimulatie zijn methoden die momenteel veelal gebruikt worden.

Het project '*Acoustical pacing of advanced human cardiac microtissues as platform to model heart rhythm disorder*' heeft als doel om om hartcellen te laten samentrekken door ultrasound stimulatie. Dit is nuttig bij *in vitro* ziektemodellering, screening van geneesmiddelen en studie van de farmacologie van geneesmiddelen. Het primaire doel van deze masterthesis is om de effecten van ultrasound puls duratie en frequentie op de contractiedynamiek van cardiomyocyten te bepalen. Dit kan gebruikt worden om werkingsmechanismen te achterhalen, zowel op fysisch als biologisch vlak.

Experimenten werden uitgevoerd met microtissues van ventriculaire cardiomyocyten geplaatst op Mylar-dekglaasjes. De samples werden geplaatst in een temperatuurgecontroleerd bad, waarna video's werden vastgelegd met 50 fps door middel van een microscoop. Ultrasound werd toegediend middels een transducer op de bodem van het bad. Een gemodificeerde PIV-analyse in MATLAB is gebruikt om bewegingen te kwantificeren. Vervolgens werden contracties geanalyseerd in termen van frequentie, maximale verplaatsing, piekoppervlak, maximale snelheden gedurende contractie en relaxatie, totale contractieduur en vertraging na ultrasone puls.

Tijdens de uitvoer van experimenten traden zeer wisselende weefsel reponses op, variërend van geen effect tot tachycardie. Pulsduraties onder 0.5 ms resulteerden niet in zichtbare veranderingen in contractiedynamiek, maar pulsen van 0.5 ms en 0.7 ms resulteerden vaak in een hogere contractiefrequentie, hogere contractie- en relaxatiesnelheden en kortere contractie duraties. Ook werd vastgesteld dat de contractieparameters voor en na ultrasound gelijk waren, wat een omkeerbaar effect suggereert.

De specifieke veranderingen in de contractiedynamiek suggereren dat ultrasound niet tot directe activering van actine-myosinefilamenten en niet tot triggering van calciumkanalen leidt. Het is zeer waarschijnlijk dat verhoging van cAMP het mechanisme is dat celcontractie door middel van ultrageluid triggert. Echter was de onderzochte ultrasound parameterset niet toereikend om de belangrijkste ultrasone mechanismes vast te stellen.

Aanbevelingen voor verder onderzoek kunnen worden gedaan voor methoden, data-analyse en experiment-plan. Er zijn meerdere richtingen mogelijk voor verder onderzoek: focus op de betrokken ultrasone mechanismen, uitbreiding van de ultrasone parameter ruimte of het versterken van de conclusie over het biologische mechanisme, door het mechanisme tijdelijk uit te schakelen.

Summary

Typically cardiomyocyte contraction results from a cascade of events, whereby a calcium flux is induced by an action potential. This calcium flux is at the origin of actin and myosin filaments motion. This cascade can be externally triggered at various key nodes, namely by activation of calcium channels, by direct activation of myosin filaments, or by cAMP enhancement. Activation of calcium channels leads to an increased calcium flux, cAMP enhancement causes calcium channel activation and direct activation of myosin filaments leads to actin-myosin motion. Pacing is generally achieved either electrically or optically.

The aim of this project is to investigate the use of '*Acoustical pacing of advanced human cardiac microtissues as platform to model heart rhythm disorders*'. Ultrasonic pacing is useful in *in vitro* disease modeling, drug screening and study of drug pharmacology. More specifically, the primary purpose of this thesis is to determine the effects of ultrasound pulse duration and center frequency on cardiomyocyte contraction dynamics so as to unravel the mechanisms behind ultrasound-induced contractions.

Experiments were conducted on ventricular cardiomyocyte microtissues placed on Mylar coverslips immersed in a temperature-controlled bath. A video was captured with 50 fps through a microscope, and ultrasound was applied via a transducer located at the bottom of the bath. A modified PIV approach performed in MATLAB was used to quantify movement. Contractions were subsequently analyzed in terms of frequency, maximum displacement, peak area, maximum speed during contraction, maximum speed during relaxation, total contraction duration, and delay after ultrasound pulse.

The responses were highly variable within the parameter space, varying from no effect at all to tachycardia. Pulse durations below 0.5 ms did not result in any visible alterations of the contractions, whereas pulses of 0.5 ms and 0.7 ms often resulted in a higher contraction frequency, higher contraction and relaxation speeds and shorter contraction times. After ultrasound driving, contraction parameters returned to their nominal values, suggesting a reversible effect of ultrasound.

The specific alterations to contraction dynamics suggest that ultrasound does not drive cell contraction via direct activation of actin-myosin filaments and calcium channels, but most likely enhanced cAMP in the cell contraction cascade. However, during these experiments, the investigated range of ultrasound parameter set was not extensive enough to ascertain the main mechanism behind ultrasound pacing.

Recommendations for further research can be done for methods, data analysis and experimental protocol. Optional research directions can be split in three categories: either focus on the ultrasound mechanisms that are involved, or extension of the ultrasound parameter space, or try to strengthen the conclusion regarding the biological mechanism by temporally disabling this mechanism and analyzing the results.

List of symbols and abbreviations

Abbreviation	Definition
AM	AcetoxyMethyl ester
AP	Action Potential
ARF	Acoustic Radiation Force
AST	Applied Stemcell Technology
CICR	Calcium Induced Calcium Release
CM	CardioMyocyte
EB	Embryonic Body
EC coupling	Excitation-Contraction coupling
FITC	Fluorescein IsoThioCyanate
hESC	Human Embryonic Stem Cell
HIFU	High Intensity Focussed Ultrasound
MDC	Membrane Deformation Currents
MEF	Mechano-Electric Feedback
MI	Mechanical Index
POF	Physics Of Fluids
PRF	Pulse Repetition Frequency
PRP	Peak Rarefraction Pressure
PVC	Premature Ventricular Contraction
RyR	Ryanodine Receptor
SA node	SinoAtrial node
SAC	Stretch Activated Channel
SFR	Slow Force Response
SLMC	Sarcomere Length Modulation Current
SR	Sarcoplasmic Reticulum
TI	Thermal Index
US	UltraSound

Chapter 1

Introduction

Today, cardiomyocyte pacing most commonly is achieved by electrical means [1]. However, two major disads of electrical pacing are 1) its potential to cause Faradaic reactions that permanently alter the chemical properties of the tissue and 2) that electrical stimulation cannot be spatially targeted [1, 2]. Another method, optogenetic pacing, requires genetic manipulation to append the expression of light-sensitive ion channels and pumps [2, 3]. In addition, the insertion of genetic materials also affects other cell functions. Acoustical pacing would allow for a spatially resolved actuation at the ultrasound focus, and can penetrate deep into biological tissues. It doesn't require genetic modification and cannot induce Faradaic effects [2, 4]. Artificial pacing is especially crucial in the design of advanced disease models, studies into drug pharmacology or drug screening and regenerative medicine [5].

The effect of ultrasound on the heart has been studied *in vivo* for many years [6, 7, 8, 9]. Recently cultured cardiomyocytes have been used for *in vitro* studies [10, 11]. The impact of ultrasound on cardiac muscle function, regulated by stretch and calcium, is also been investigated to determine the potential occurrence of premature ventricular contractions (PVCs) [12, 13, 14].

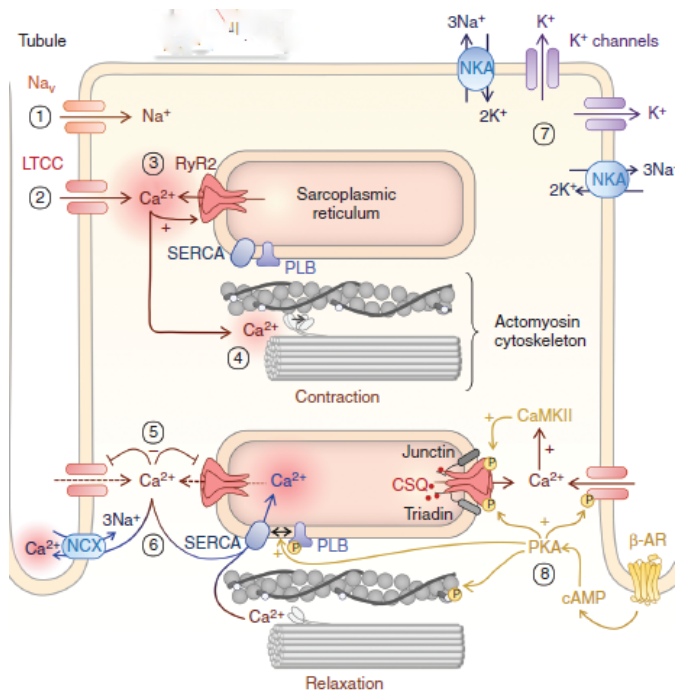
A wide variety of ultrasound exposure conditions, varying in pulse duration, peak to peak pressure, pulse repetition frequency, center frequency and pulse timing relative to contraction cycle, are being examined by various research groups [11, 15, 16]. However, no clear conclusions have yet been reached regarding the physical and biological processes involved in acoustical pacing of cardiomyocytes.

1.1 Cardiomyocyte contraction

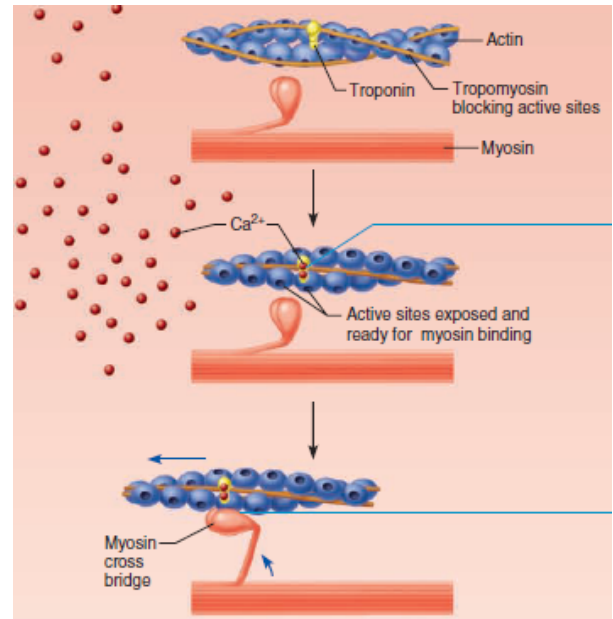
Excitation-contraction coupling is the process by which an electrical stimulus initiates a mechanism of muscle contraction by sarcomere shortening [17, 18, 19]. The electrical stimulus is the action potential (AP), fired off by the sinoatrial node (SA node) of the heart [20]. This leads to a cascade of events in terms of ion fluxes. This cascade leads to mechanical events in the cells, namely at the actin-myosin filaments.

1.1.1 Ion cascade

The cardiac cycle is the collection of electrical and mechanical events that repeat with every heartbeat [20]. Cardiomyocyte dynamics are the foundation of these events. The heart contraction cycle is controlled by the sinoatrial node (SA node) of the heart [20]. It fires off action potentials (APs) which propagate via gap junctions and the intrinsic cardiac conduction system and eventually reach cardiomyocytes [20]. Cardiac myocytes are well known for their ability to initiate their own depolarization, which is called *automaticity*. Cardiomyocytes are also capable of depolarizing surrounding cells. Figure 1.1a depicts the mechanisms that take place after an action potential has reached a cardiomyocyte. APs lead to depolarization, which opens fast voltage-gated Na^+ channels in the sarcolemma (step 1) [21]. As a result Na^+ will enter the cell and increase the membrane voltage. This activates the slow voltage-gated L-type channels and the influx of Ca^{2+} into the cytoplasm (step 2) [17]. This internalized calcium stimulates the ryanodine receptor calcium channels (RyR) on the sarcoplasmic reticulum which release its stored calcium. This step is called calcium induced calcium release (CICR) and is shown in step 3 of figure 1.1a. Finally, the sharp increase in calcium concentration enables the binding of calcium to troponin C, which causes motion of tropomyosin and exposes the active sites on actin which is necessary for muscle contraction (step 4).



(a) Schematic figure of the mechanisms in cardiomyocytes after an action potential arrives [17]. 1) Opening voltage gated Na^+ channels, 2) Ca^{2+}_i increase through voltage-gated L-type channels, 3) calcium induced calcium release via RyR2, 4) Calcium binding to troponin, enabling contraction. Step 5) inactivation of voltage gated L-type calcium channels, 6) calcium extrusion, 7) opening of K^+ channels bringing the membrane potential back to the resting potential.



(b) Actin and myosin filaments and their cross-bridging [21]. Calcium binding with troponin moves the tropomyosin, after which active sites at actin are exposed.

Figure 1.1: Overview of cardiomyocyte contraction, from ion cascade to muscle contraction.

1.1.2 Muscle contraction

Cardiomyocytes are striated and use the sliding filament mechanism to contract [21]. The actin and myosin complexes and their interactions are depicted in figure 1.1b. To enable contraction, intracellular calcium binds to troponin C thereby exposing myosin binding sites on actin, as seen in figure 1.1b [21]. The binding of myosin heads to active sites at actin results in cross bridges. The myosin heads tilt, which results in sliding of myofilaments (step 4). This repeatedly takes place, resulting in sliding of myofilaments which contracts the cardiomyocyte.

Thereafter a well-regulated process namely cardiac muscle relaxation takes place [22]. The relaxation rate is limited by intracellular calcium decline, actin de-activation and cross-bridge cycling speed [22]. After EC coupling, the voltage-gated L-type Ca^{2+} channels are inactivated and the RyR channels close (step 5) [17]. Thereafter an intracellular calcium decrease is realized for 28% by Ca^{2+} extrusion by sarcolemmal Na^+/Ca^{2+} exchanger (NCX1) and for 70% by Ca^{2+} uptake by the sarcoplasmic reticulum via Ca^{2+} pump SERCA2a (step 6). The calcium decline will cause repolarization. Two other methods to lower cytosolic calcium levels, which make up approximately 2% of the calcium decline, are via the calcium uniporter from the mitochondria and from the myocyte via the sarcolemmal (SL) Ca^{2+} ATPase [22].

This decreased cytosolic calcium results in disassociation of Ca^{2+} from troponin C, since the free cytosolic calcium concentration eventually drops below the binding threshold of calcium for troponin C [17, 20, 22]. After calcium disassociation of troponin C, the rebinding of troponin I to actin, structural changes in troponin troponin T and movement of tropomyosin must take place in order to cause actin de-activation, muscle relaxation in short [17, 20, 22]. The maximum speed of muscle relaxation exhibits a linear relationship with myosin's ATPase rate [22]. Furthermore, the contraction speed and relaxation speed show a strong correlation [22]. After muscle relaxation, K^+ membrane channels will open (step 7), they cause a K^+ flux to extracellular space. This brings the membrane potential back to the resting potential. Concluding, action potentials affect intracellular calcium concentration and intracellular calcium enables cell contraction.

1.1.3 Time course of action potential, calcium and contraction

The time-course and features of action potential, intracellular calcium and EC coupling are strongly interrelated [23, 24]. Figure 1.2 shows an example of the relation between action potential, intracellular calcium concentration and relative cell length decrease in cardiomyocytes obtained from human induced pluripotent stem cells [24]. Van Meer et al. have developed a method to study action potential, calcium flux and contraction simultaneously. They studied the effect of various drugs on cardiomyocyte monolayers: aspirin has no effect on the cardiomyocytes and is therefore used as reference, shown in figure 1.2. They found that cardiomyocytes from human induced pluripotent stem cells (hiPSC-CMs) have APs (blue) of 90 ms, a calcium increase (yellow) duration of 170 ms and contractions (red) of 110 ms [24]. The contraction rise starts 20 ms after the AP rise and the contraction peak has a delay of 75 ms.

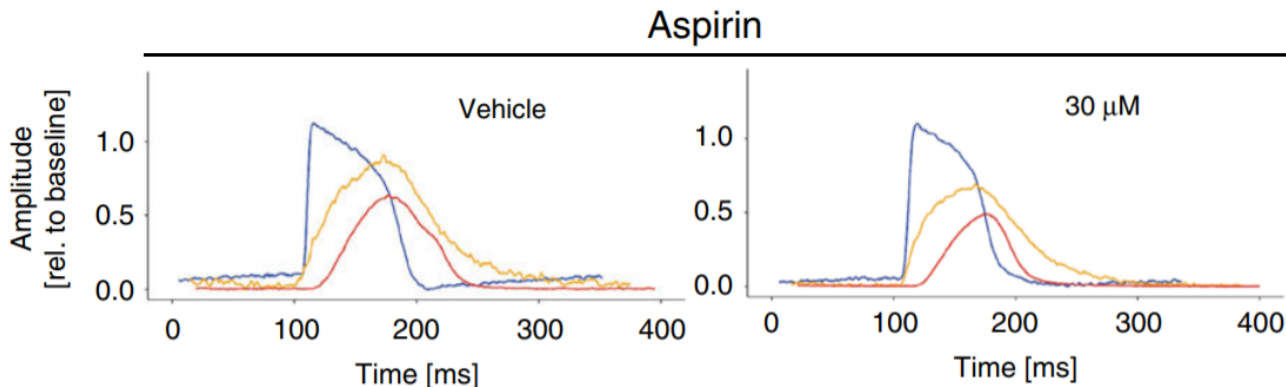


Figure 1.2: Timecourse of **action potential** (blue), **cytosolic calcium** (orange) and **contraction length** (red) of monolayer hiPSC-CMs [24]. On the left is a reference without drugs, the right depicts the effect of non-cardioactive drug aspirin ($30 \mu\text{M}$).

Another connection is found between electrophysiology of cardiomyocytes and the contraction force & duration [20]. Contraction force is described as the relative magnitude of cardiac contraction, which equals the contraction displacement [25]. A rise in intracellular calcium results in increased binding of calcium to troponin C on actin, which allows for myosin to pull on the thin filaments which results in increased sarcomere shortening, thus increased force [23, 26, 27]. Furthermore, the total contraction strength is altered by the calcium transient duration, calcium transient amplitude and by troponin C calcium sensitivity [28]. In a myocyte with a resting level of $150 \mu\text{M}$ free $[Ca_i^{2+}]$, it is found that the first $30 \mu\text{M}$ added calcium develops very little force, whereas a steep force increases after 40 to $80 \mu\text{M}$ of added calcium [27].

Furthermore, the force of contraction increases with frequency, which enhances calcium cycling and causes a net influx of calcium to the sarcoplasmic reticulum [22]. Contraction speed increases with increased contraction frequency [22]. However, contractile kinetics acceleration is not yet clearly understood; calcium transient changes are involved just as myofilament responsiveness and cross-bridge kinetics [22]. Besides, the speed of calcium influx affects the contractile rate of the cell. Biesiadecki et al. show an overview of the processes involved in cardiac muscle relaxation, reproduced in figure 1.3 [22]. The orange ovals represent the main physiological processes and two-headed blue arrows indicate major direct interactions. Dashed gray arrows indicate unresolved or minor interactions. One sided green and red arrows indicate acceleration and slowing respectively. This figure shows that the processes are very complex and interconnected.

Van Meer et al. have stated what mechanisms do enhance cardiomyocyte contraction targetted by drugs [24]. The first is increased free cytosolic calcium concentration, the second direct thick- or thin myosin filament activation and lastly enhancement of the complete contractile cascade by beta-adrenergic stimulation. Causes of reduced contraction are either reduction of intracellular calcium or cardiotoxicity due to mitochondrial dysfunction. They work out expected effect of these mechanisms on the contraction kinetics in terms of amplitude, contraction duration and relaxation duration. The effects are included in table 1.1.

1.1.4 Mechano-electric feedback

In addition to excitation-contraction coupling, intracellular mechano-electric feedback (MEF) is a mechanism that couples mechanical activity to electrical function in cardiac cells and tissues [8, 28, 29, 30, 31, 32]. MEF modifies

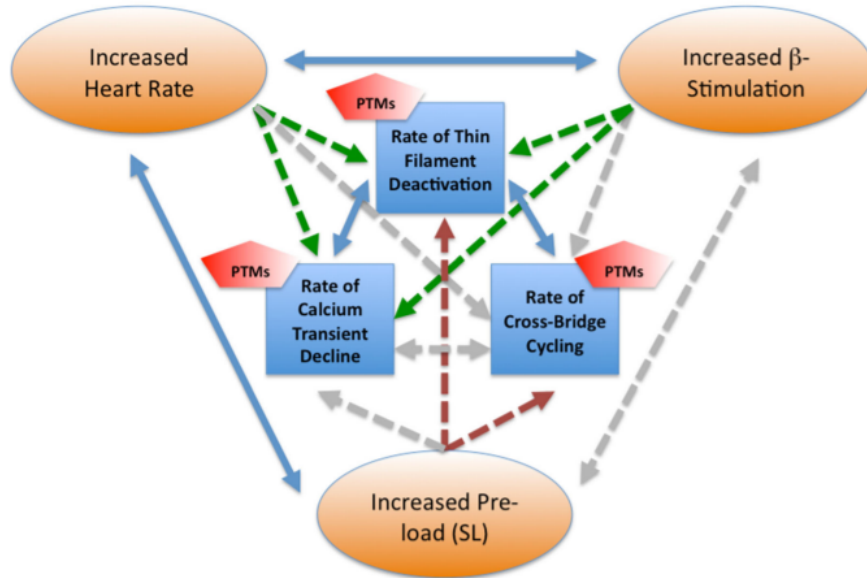


Figure 1.3: Overview of the processes involved in cardiac muscle relaxation [22]. The orange ovals represent the main physiological processes and two-headed blue arrows indicate major direct interactions. Dashed gray arrows indicate unresolved or minor interactions. One sided green and red arrows indicate acceleration and slowing respectively. This figure shows that the processes are very complex and interconnected.

contractile function by mechanical loading and interactions via electrophysiology and calcium handling [8, 29]. It alters cardiac electrophysiology (EP) and calcium handling due to mechanical perturbations [30, 33]. In particular voltage-gated channels respond to stretch and physical membrane deformations, so they are able to transduce mechanical force [8, 34, 35, 36, 37, 38].

Mechanical stress is caused by physical impact, e.g. by applying an ultrasound (US) pulse [39, 40, 41]. Cohen and Safran identified some options for coupling of external mechanical impact to cell contraction [42]. The first option is via adhesion points that connect substrate with acto-myosin contractile units. Mechanical force pulls on the adhesion points, after which motion occurs within the actin-myosin contractile unit. Another scenario is that mechanical force leads to tension in the sarcolemma, which stretches the membrane which becomes thinner. This activates stretch sensitive proteins, which are able to adapt the calcium concentration and therefore modulate contractility. The last option is that a mechanical impact releases calcium from troponin C, after which the cytosolic calcium is increased which ends the contraction cycle.

For cardiomyocytes in particular, application of membrane tension increases the opening probability of stretch activated channels (SACs) such as TRPC6 channels [13, 26, 43]. Opening of SACs leads to transmembrane currents which are able to increase the membrane potential directly and indirectly, which may result in triggering of an action potential [14, 43]. Furthermore, it is found that mechanosensitivity of cardiomyocytes is highest when the cardiomyocytes are relaxed [18, 30]. During diastole local mechanical stress sometimes leads to cardiac depolarization, whereas local mechanical stress during systole affects the action potential re-polarisation timecourse and shape [44]. Along with relative timing, features of the affected membrane region play a part. Kubanek et al. state that the effect of mechanical impact depends on the specific mechanosensitive ion channels that are dominant at the cell membrane: excitation takes place when Na^+ ($Na_v1.5$) or Ca^{2+} channels are most abundant, whereas inhibition takes place if K^+ channels are abundant [4].

Supplementary to a mechanical impact, change in cells can be due to myofilament stretching. It boosts the calcium sensitivity of troponin C and it enables the heart to adjust to altered diastolic filling. This results in an increased aortic pressure on the short (the next contractions) and the long term (several minutes) [28, 45]. This mechanism is called the Frank-Starling mechanism [14, 28, 46]. In short the degree of stretch experienced by myocytes before activation, regulates their contractile force [45]. Various cellular mechanism are involved in this mechanism: a larger affinity of troponin C for Ca^{2+} , an increased overlap between contractile protein myofilaments, and increased Ca^{2+} transient minutes after a stretch [45]. This delayed calcium transient response to stretch is named the slow force response (SFR). The cellular mechanism underlying the SFR is not yet fully understood [45]. However, potential mechanism are identified. One mechanism is stretch-activation of ion channels at the

sarcolemma, which results in a steady increase in calcium within the sarcoplasmic reticulum. The other is stretch-activation of autocrine and paracrine signaling pathways. The result of those pathways is an increased calcium flux in the cell and nearby cells at a longer timescale. another effect is 'the Anrep effect'. It states that increased afterload causes increased contractility. The Anrep effect is due to an increase in intracellular Na^+ concentration and an increase in calcium transient amplitude, after which contractility (contraction force and speed) increases and SFR is triggered.

1.1.5 State of the art in ultrasound pacing

Various experiments are done in pigs [47, 48], rats [9], frogs [6, 39, 49, 50, 51, 52] and human cardiomyocytes [3]. *Ex vivo* pig and swine heart studies resulted in a 90% success rate in inducing PVCs, whereby at least 4MPa and 10 ms were necessary at 1 MHz [47, 48]. Buiocci et al. have found that a variable (decreasing) PRF was more successful in decreasing the heart rate of rats than using a standard low PRF [9]. Furthermore, until 45 minutes after the experiment the negative chronotropic effect was still noticeable [9]. The acoustic parameters were 1 MHz, peak rarefactional pressure 3 MPa, 1% duty cycle (2.0-2.5 ms pulses) and PRF from 2 Hz less than the heart rate to slightly above [9].

In the frog heart a single high intensity ultrasound pulse has reduced the aortic pressure or caused a premature ventricular contraction [49]. Furthermore, it was found that 5 ms, 1.2 MHz ultrasound with a pressure higher than 2 MPa is able to induce PVCs [49]. The pressure threshold increases with increasing frequency and increases with decreasing pulse duration [6]. Besides, the occurrence of reduced aortic pressure was directly correlated with the radiation force [52]. However, after application of an acoustic reflector the heating and cavitation were eliminated, as well as the premature ventricular contractions [52]. Yet the reduced aortic pressure effect could still be identified [52]. For the frog heart, heat is ruled out as primary physical mechanism causing PCVs [51]. High intensity pulsed ultrasound at 1.2 MHz, 10 MPa has an increased effectiveness in inducing PVCs with an increasing pulse duration from 1 to 5 ms [6].

At the moment, the research group of Chen et al. is establishing a systematic view of the parameter space in terms of the electromechanical function of cardiomyocytes [3]. They try to find optimal ultrasound parameters to safely and effectively control cardiac electromechanical activity of human cardiomyocytes [3]. In order to do so they track the intracellular calcium and membrane voltage and try to time the US application [3]. Kudo et al. use the phase-contrast light intensity for real-time detection of beating of cultured cardiomyocytes [11]. With this real-time detection, the timing of application of ultrasound is determined relative to the contraction cycle.

1.2 Ultrasound

1.2.1 Definitions and quantities

Ultrasound consists of sound waves with a frequency range above 20 kHz and can be generated using piezoelectric transducers, that are able to convert an electrical signal into a pressure wave [4, 15]. Ultrasound parameters are center frequency, negative and positive pressure amplitude [4]. Ultrasound transducers have focused and non-focused variants [47]. Quantities used in ultrasound are divided into two groups: amplitude quantities, and energy-based quantities [15]. The amplitude quantities are directly proportional to each other, just as all energy-based quantities [15]. Next the product of any two amplitude quantities is proportional to any energy-based quantity [15]. Amplitude-based quantities are: ultrasonic pressure, driving voltage, particle displacement, particle velocity and particle acceleration [15]. Energy-based quantities are energy, energy density, intensity and power [15]. Stimulus intensity (average power per unit area in W/cm^2) is the effective pressure squared divided by the acoustic impedance of the material [4].

1.2.2 Effects of ultrasound

In order to provide information about risk and safety the mechanical index is defined (MI , see equation 1.1) [15, 53]. It indicates the possibility of mechanical damage to the tissue due to bubbles or gas bodies [53]. It depends on the peak negative pressure (PNP) and the center frequency (f_c). Thus higher peak negative pressure and lower center frequency leads to more mechanical damage; cavitation $\propto PNP/\sqrt{f_c}$

$$MI = PNP/\sqrt{f_c} \quad (1.1)$$

The bio-effects of ultrasound are studied extensively with various exposure conditions [7, 8, 39, 54, 55, 56]. This resulted in a distinction between thermal and non-thermal (or mechanical) effects of ultrasound [57]. Thermal energy is the result of tissue absorption of ultrasound energy [47, 57]. When heating of 1 degree Celsius or more occurs, an effect is defined as thermal by Abramowicz [58]. Smaller temperature changes, classified as non-thermal effects, can still lead to activation of temperature sensitive channels and rate of temperature change can also contribute to stimulatory effects [59, 60]. The thermal dose is directly related to exposure time and intensity [47]. Generally low intensities (10^2 W/cm²) with continuous sonification cause thermal effects [47].

The maximum temperature increase in Kelvin depends on the rate of heat generation per unit volume, the size of the ultrasound focus and the time duration of exposure [15]. Equation 1.3 states the maximum temperature increase under the assumption that no heat is lost by conduction and convection. In equation 1.3 C_v is the heat capacity per unit volume of the medium. Equation 1.2 shows the rate of heat generation per unit volume in J/cm³s, \dot{Q} , which depends on ultrasonic pressure amplitude squared, ultrasonic amplitude absorption coefficient in cm⁻¹, density and speed of sound in the material. Since the heat capacity per unit volume, the amplitude absorption coefficient, density and speed of sound are constant, the total temperature increases scales with pulse duration and squared peak positive pressure. Thus $Q \propto P_0^2 \tau$

$$\dot{Q} = \alpha p_0^2 / \rho c \quad (1.2)$$

$$\Delta T = \dot{Q} \Delta t / C_v \quad (1.3)$$

Non-thermal effects, also called mechanical effects, are effects that are the result of heating less than 1° Celsius. Consequently, processes that are not literally mechanical but indirectly affected by mechanical processes are also called mechanical effects [61]. In general, short exposures (<0.05 ms) with high pressure (>20 MPa) or low pressure (55 kPa) with longer exposure do not induce significant heating; therefore non-thermal effects occur [47]. Cavitation is a non-thermal effect that occurs in acoustic fields at high negative pressures and low US frequencies [57]. It is the formation then optionally collapse of gaseous bodies in liquid media or soft tissues [4, 47].

Acoustic cavitation is divided into two subclasses: stable and inertial cavitation [62]. In inertial (also known as transient or unstable) cavitation gas bodies collapse due to inertial forces. In stable cavitation the bubbles do not collapse. Other non-thermal effects are radiation torque, acoustic streaming, membrane oscillation and shock waves [16]. Acoustic radiation force (ARF) results in radiation torque and acoustic streaming effects and it is defined as a period-averaged force exerted on the medium by a sound wave [16]. Acoustic streaming is caused by a rise in fluid flow, which may occur when acoustic field propagates in a fluid [16]. ARF is proportional to total acoustic power, which depends on intensity and area. Since the focus area decreases quadratically with the center frequency, $ARF \propto P_0^2 / f_c^2$.

1.2.3 Ultrasound and cardiomyocytes

Ultrasound is defined by several parameters. Application of ultrasound to contracting cardiomyocytes introduces new parameters. Ultrasound application to cardiomyocytes varies in terms of relative timing with respect to cardiomyocyte cycle and pulse repetition frequency.

Ultrasound is known for its ability to induce effects in a medium or solid [4]. Acoustic radiation force for example can cause movement of medium or tissue [47]. In solids, time constant radiation force causes internal stress, whereas time-varying radiation force creates motion [63]. It is also shown that ARF and stable cavitation create mechanical forces which activate the mechano-electric feedback system in cardiomyocytes [8]. Furthermore, it has been shown that cardiomyocytes may synchronize to a cyclic mechanical perturbation with a new frequency, at maximum 25% of their natural frequency [18].

Cohen and Safran have also identified that it takes approximately 15 minutes for a cell that is spontaneously beating to adapt to entrained beating by an oscillating mechanical probe. The cell will synchronize with the new frequency for about 1 hour [42].

Livneh et al. suggest two cellular level mechanisms in high intensity focused ultrasound (HIFU) pacing: membrane deformation currents (MDC) and sarcomere length modulation current (SLMC) [8]. Membrane deformation currents (MDCs) are triggered by mechanical stimulation, which results in pressure changes, shear force and mechanical deformations at cellular level [8]. Membranes affected are the sarcolemma and the sarcoplasmic reticulum membrane [8]. These effects cause deformations in the membrane, membrane proteins and cellular organelles [8]. Changes to membrane proteins result in ion channel conformation state change [59]. Another source of membrane potential variation and ionic flows is mechanical stretch on the membrane nearby channels or strain on mechanosensitive channels [8]. Another theory is that cavitation causes permeabilization, after which ions such as calcium can move freely [8]. SLMC takes place after cardiomyocyte size decrease as a result of ultrasound. When the length of

sarcomeres in cardiomyocytes is rapidly reduced, the intracellular Ca^{2+} concentration is rapidly increased [64, 65]. The increased intracellular Ca^{2+} concentration activates the Ca^{2+} induced Ca^{2+} release (CIRC), which can lead to contractions [66]. The probability of MDC is uniform, whereas the probability of SLMC varies during the cell cycle [65]. Based on this assumption, MDCs are at cellular level most prominent for inducing pacing [8].

Livneh et al. have described the cascade of processes that must take place to achieve ventricular contraction due to ultrasound [8]. When ultrasound reaches the tissue, a mechanical force is exerted at the tissue. This force plays a role in the mechano-sensitive pathway and results in activation of the mechano-electric feedback circuit. Activation of this circuit leads to cellular depolarization, which on its turn leads to an action potential. The action potential is necessary for cardiomyocyte contraction, as described in subsection 1.1.2. In the frog heart, heat is ruled out as the primary mechanism causing effect on the heart as a tenfold increase in temperature rise does not result in a significant bioeffect increase [51]. Concluding, ultrasound is able to induce premature ventricular contractions (PVCs) and this is identified as a non-thermal process [10, 49, 51, 52].

Control of producing PVCs was obtained by varying pulse duration, pulse intensity and pulse timing relative to the cardiac cycle [11, 40]. In full heart studies is shown that the heart is most susceptible for inducing PVCs after application of an ultrasound pulse during diastole [39, 40, 49, 50]. Others have found that after the ECG T-wave the HIFU pacing is most successful [8]. Recently it was found that ultrasound (peak to peak) pressure contributes more in inducing PVCs than pulse duration or total energy of the US pulse [10]. However, the cellular mechanism that is responsible for PVC induction is not yet known [57]. Suggestions are: cavitation, ARF, shear-stress activating mechano-sensitive cells of the cardiac tissue and direct vibration at cellular level [57]. ARF is eliminated as responsible ultrasound effect for inducing PVCs by Dalecki, since the use of an acoustic reflector which maximizes ARF and eliminates cavitation and heating did not result in PVCs [52]. Besides, it is known that an increased US pulse duration causes more bioeffect [6, 49].

A drawback of premature contractions in cardiomyocytes after ultrasound exposure is the link with cardiomyocyte death [56]. In addition the long-term effectiveness and safety is not known, just as the efficiency of energy transfer from US pulses to cardiomyocytes [56, 57, 67]. Livneh et al. could obtain a success rate greater than 90% up for maximum 30 seconds [8]. It is known that cell viability is decreased with increasing acoustic energy dose in the low frequency regime (20-100 kHz) [68]. Furthermore, the cell viability is increased with increasing acoustic frequency for energy densities between 0 and 150 J/cm² [68].

Contrast agents

Microbubbles are often used in ultrasound diagnostics and therapies [69, 70]. Tran et al. have shown that as well the cell membrane permeability as the uptake of substances is enhanced by microbubbles under ultrasound stimulation [13]. The impacted cells were all in direct contact with the microbubbles [13]. Furthermore, microbubbles amplify the mechanical deformations induced by ultrasound [71]. A few years later they have shown that microbubbles induce PVCs *in vivo* [7]. Next it is shown that microbubbles at target position decrease the PVC threshold after high-intensity focused ultrasound [40]. Concluding, microbubbles decrease the thresholds of US parameters in order to cause bioeffects [50].

1.3 Study

1.3.1 Research questions

In this master thesis the effect of ultrasound on human embryonic stem cell-derived cardiomyocytes is examined in terms of response. The main research question is:

Can ultrasound control cardiomyocyte pacing?

Subquestions are:

What is the behaviour of the cells within the ultrasound parameter space?

What is the mechanism driving cell contraction?

How to best control the contractile rate?

1.3.2 Hypothesis

In these theory sections various effects are named that can lead to tissue response to ultrasound pulses. In this subsection the proposed mechanisms are summed up with the resulting effects on contractions.

Van Meer et al. have identified three mechanisms of action leading to a higher contraction frequency in cardiomyocytes and hypothesise the effect on kinetic parameters of the action potential, calcium transient and contraction [24]. Table 1.1 is adapted from their article. The mechanisms are: increased cytosolic calcium ($[Ca^{2+}]_i$) via calcium- and sodium channels (Co_{Ca}^+), direct activation of myosin (Co_{Myosin}^+) or enhancement of contraction cascade via cyclic adenosine monophosphate by beta-adrenergic stimulation or PDE3 inhibition (Co_{cAMP}^+) [24].

In the table the following indicators are used: \uparrow indicates increase, \downarrow indicates decrease, $=$ indicates equality and NOT indicate the other options except the option stated. The subscripts at t are as follows: rise is the AP rise duration, APD is the total action potential duration, to peak means time of rising phase to peak, decay means from peak to resting phase, contraction is time from rise to peak and relaxation is time from peak to resting state. Triangulation is defined as the interval between APD at 30% of repolarization and at 90% of repolarization. Calcium transient and contraction parameters can be used to determine which MOA is dominant in increased pacing of cardiomyocytes, since the MOAs have distinctive effects. Based on the contraction amplitude, contraction speed and relaxation speed at least one MOA can be disregarded, so therefore the contraction amplitude and speeds are determined in this thesis.

Table 1.1: Overview of various modes of action on kinetic parameters of action potential, calcium transient and contraction by Van Meer et al. [24].

Kinetic parameters	Co_{Ca}^+	Co_{Myosin}^+	Co_{cAMP}^+
Action potential (AP)			
Amplitude	=	=	=
t_{rise}	\downarrow	=	\downarrow
t_{APD}	NOT=	=	\downarrow
Triangulation	\downarrow	=	\downarrow
Calcium transient (Ca)			
Amplitude	\uparrow	=	\uparrow
t_{topeak}	NOT \downarrow	NOT \uparrow	\downarrow
t_{decay}	NOT \downarrow	NOT \uparrow	\downarrow
Contraction (Co)			
Amplitude	\uparrow	\uparrow	\uparrow
$t_{contraction}$	NOT \downarrow	\uparrow	\downarrow
$t_{relaxation}$	NOT \downarrow	NOT \downarrow	\downarrow

Figure 1.4 depicts the effect of medicine with various MOAs at the action potential, calcium concentration and contraction. Subfigure A is blanco; no effect at all. Sub B) indicates the cAMP pathway, which results in higher contraction peak and shorter contraction duration. Sub C) indicates the direct myosin pathway, which results in higher contraction peak, slower contraction and equal relaxation. Sub D) indicates the calcium channel pathway, which results in higher contraction amplitude and equal contraction timing.

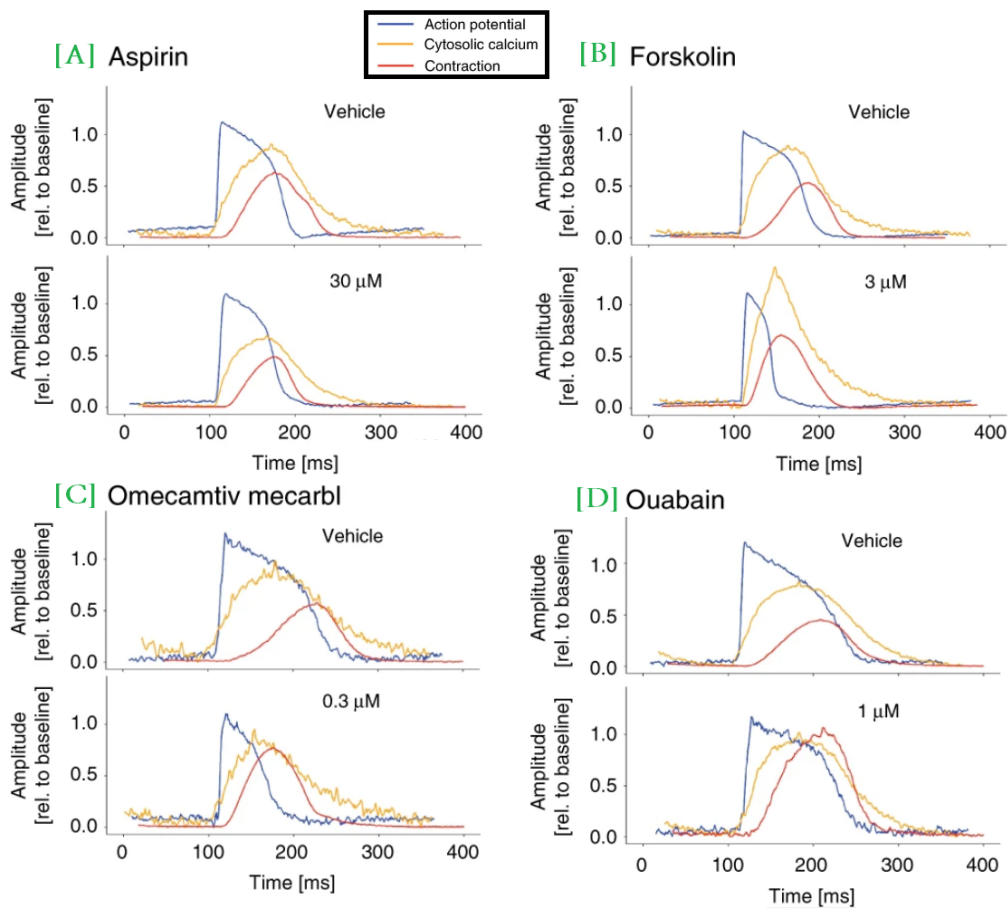


Figure 1.4: Overview of hypothetical effects: **action potential** (blue), **cytosolic calcium** (orange) and **contraction length** (red) of monolayer hiPSC-CMs [24]. All top figures (vehicle) are blanco's, all bottom graphs show effect of the drug in the indicated concentration. A) Aspirin, no effect. B) Forskolin, cAMP mechanism with shorter contraction & relaxation time and higher contraction peak. C) Omecamtiv mecarbil, myosin mechanism, with higher contraction peak and shorter contraction time. D) Ouabain, calcium channel mechanism with increased displacement peak and equal timecourse. [24]

Furthermore, ultrasound has various triggering mechanisms, namely cavitation, acoustic radiation force and heat generation. Ultrasound parameters such as pulse duration, pulse frequency and pressure are related with triggering mechanisms. Heat generation is proportional to pressure amplitude squared times pulse duration. Thus: $Q \propto P_0^2 \tau$. Mechanical index (MI) is an indicator for the likeliness of cavitation to occur. Thus cavitation $\propto P/\sqrt{f_c}$. Acoustic radiation force is proportional to total acoustic power which depends on intensity and area. Since the focus area decreases quadratically with center frequency, $ARF \propto P_0^2/f_c^2$.

1.3.3 Overview

Chapter 2 describes the materials and methods. It is divided into five parts: sample preparations, setup, experimental methods, data processing and data analysis methods. The chapter is concluded with an overview of data analysis parameters and cardiomyocyte contraction variables. In the following chapter, chapter 3, the results are displayed. Next off the results are discussed in chapter 4. Subsequently conclusions are drawn in chapter 5. Ultimately recommendations are done towards future research in chapter 6.

Chapter 2

Materials and methods

In this section is described what materials and methods are used to ultimately obtain the results. First the sample is described in detail, thereafter the setup is shown and described. Next the experimental protocol and measurement plan is explained. Lastly the data processing and data analysis is described.

2.1 Sample

The sample contains embryonic bodies (EBs) of ventricular and atrial myocytes placed at coverslips. The EBs were derived from a human embryonic stem cell line (hESC) and were generated as described by Schwach and Passier (2016); "generation of stem cell-derived CMs with the Spin-EB protocol" [72]. After fourteen days of EB culturing, the EBs are placed at the coverslips. The coverslips consist of polymer rings (inner diameter 10mm, outer diameter 14mm) glued with UV-curable glue (Norland optical adhesive 81) on a mylar membrane. The coverslips are disinfected by storage in ethanol solution for at least a day. In a 12 well suspension plate 10 μ L matrigel (10 mg/mL) solution is put on the coverslips, after which 10 to 15 EBs without medium are put at the coverslips covered with matrigel. Figure 2.1 depicts the EB at coverslip loading process. The construct is put in the 37 °C incubator for an hour: the matrigel will crosslink. Hereafter 3 mL cell medium can be added. After 5 to 7 days the EBs at the membrane are ready for measurements; meanwhile non-cardiomyocyte cells in the tissue have produced extracellular matrix components that enable binding to the gel. Every 3 to 4 days the cell medium is refreshed.

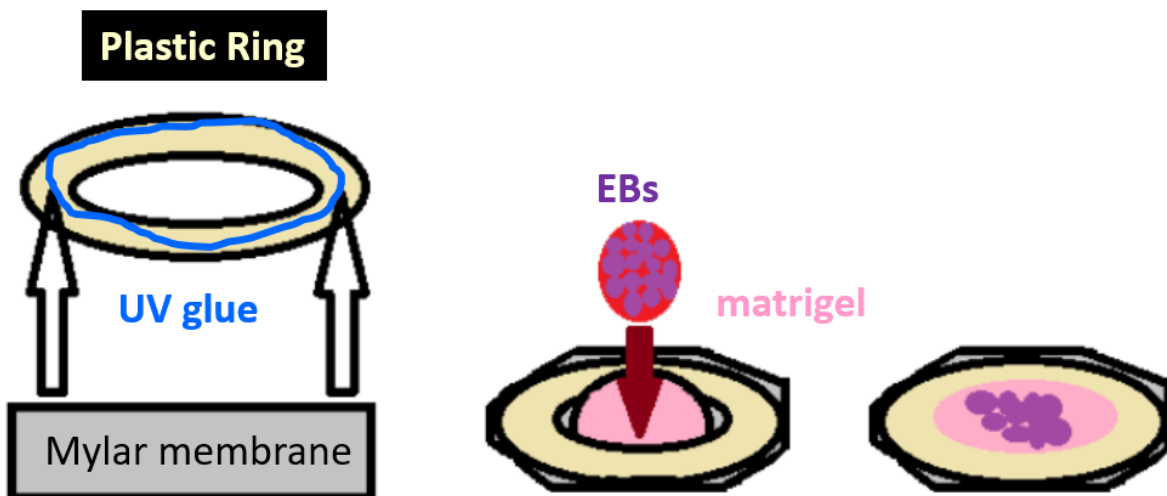


Figure 2.1: Sample construct of plastic ring, UV glue, mylar membrane, EBs and matrigel at coverslips, based on figure from Jeroen Bugter [73].

2.2 Setup

The setup is divided into parts with various functions. The first function is sample placement, which is provided by the **sample stage** which can be moved in x, y, and z direction. It can contain the EBs loaded at coverslips. Vacuum grease is used to stick the coverslips in the sample holder. The setup **reservoir** is used for liquid containment and temperature control by a **heating pad**, **temperature sensor** and **magnetic stirrer**. The third function is application of ultrasound pulses: an electrical signal is provided by a **signal generator** (Agilent 3310A) and a **power amplifier** (Electronics & Innovation), after which an **ultrasound transducer** (Olympus C302-SU-F1.63IN-PtF) converts the electrical signal into ultrasound pulses. The signal generator is dependent on two **pulse delay generators** (BNC 565-4C and BNC 575), which also control the camera timing. Another function is the image recording, which is enabled by a **microscope** (Olympus) with **20x objective**, a **lightsource**, and a **Ximea camera** (XiQ series, MQ013MG-ON). In figure 2.2 an schematic overview of the setup is given.

Ultrasound focus and imaging focus

A hydrophone(0.2mm Needle Hydrophone, Precision Acoustics) was used in order to locate the microscope focus at the same location as the ultrasound focus (focus distance 1.63 inch, 4.14 cm). First the microscope is used to focus the hydrophone tip. Thereafter the transducer and setup reservoir are moved until the hydrophone signal is maximized and is received with a time delay of $27.7 \mu\text{s}$.

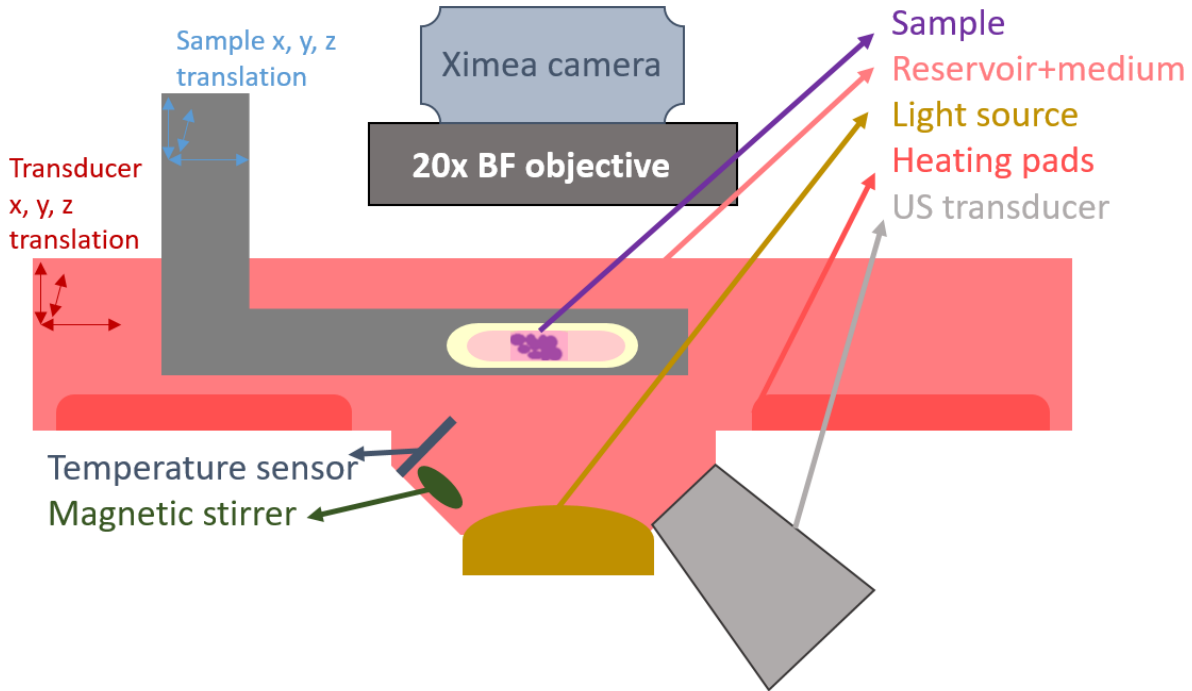


Figure 2.2: Schematic overview of the setup including sample stage, camera and ultrasound transducer.

2.3 Experimental methods

The experimental methods are divided into three parts: a description of the parameters that are varied, the protocol of an experiment and a measurement plan.

Parameters

The parameters that are varied determine the ultrasound pulses that are sent and the repetition frequency of those pulses. The pulse duration is varied: 0.001, 0.002, 0.005, 0.01, 0.02, 0.05, 0.1, 0.2, 0.3, 0.4, 0.5, 0.7, 1.0, 1.2, 1.4 ms. The center frequency and peak to peak pressure are varied from 0.5 MHz (1.6 MPa), 0.7 MHz (2.8 MPa), 1.0 MHz (3.7 MPa), to 1.5 MHz (5.0 MPa). The pulse repetition frequency is varied from 0.7 Hz to 1.5 Hz, whereas during experiments the PRF is always set higher than the automaticity frequency. In figure 2.3 and table 2.1 schematic overviews of the ultrasound parameters are given.

Table 2.1: Overview of experimental settings - the number indicate the number of completed measurements, the number in brackets the number of measurements tried.

Frequency (MHz)	Pressure (MPa)	Duration (ms)												
		0.001	0.002	0.004	0.005	0.008	0.01	0.02	0.04	0.05	0.1	0.2	0.3	0.4
1.0	3.7	4(5)	5(5)	0(0)	2(5)	0(0)	3(5)	3(5)	0(0)	3(5)	3(5)	2(5)	2(5)	2(5)
1.5	5.0	0(0)	4(6)	4(6)	0(0)	4(6)	0(0)	3(6)	4(6)	0(0)	7(7)	4(7)	0(0)	0(4)

Frequency (MHz)	Pressure (MPa)	Duration (ms)				
		0.5	0.7	1.0	1.2	1.4
0.5	1.6	0(5)	2(5)	0(3)	0(3)	0(3)
0.7	2.8	3(3)	2(3)	2(6)	0(3)	0(3)
1.0	3.7	6(12)	5(12)	7(25)	0(5)	0(5)
1.5	5.0	8(12)	8(12)	6(14)	2(7)	3(5)

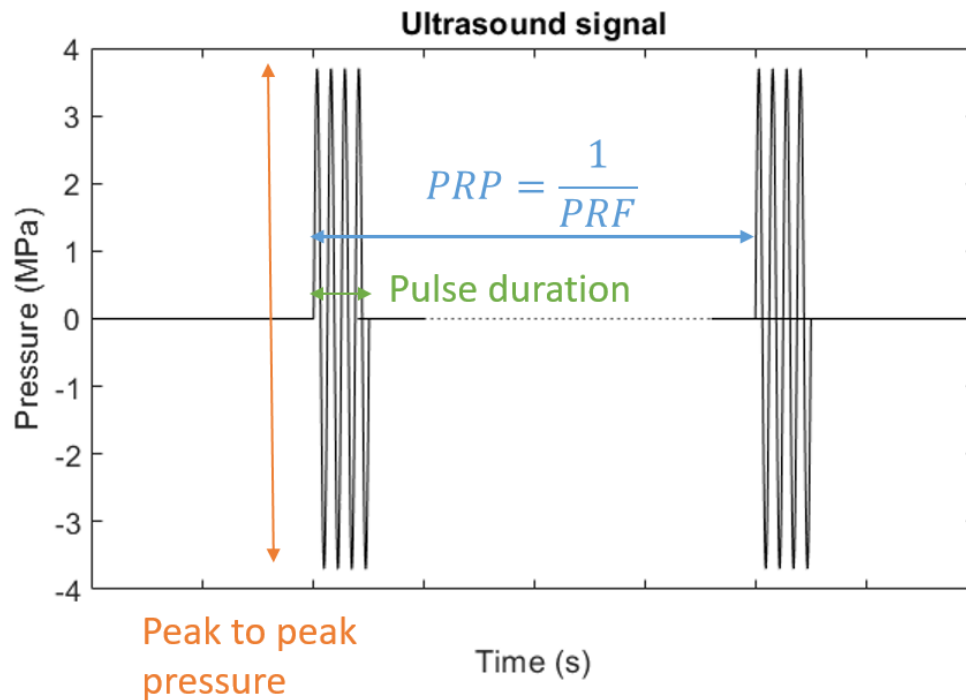


Figure 2.3: Schematic overview of the ultrasound parameters that are varied. Pulse duration in unit ms, PRF in unit Hz and peak to peak pressure in MPa.

Protocol

An experiment consists of four phases:

1. Onset time, 10 seconds
2. Pre-ultrasound, 20 seconds
3. Ultrasound, 40 seconds
4. Post-ultrasound, 20 seconds

After starting an experiment, there is delay before the acquisition camera starts. The pre-ultrasound phase starts as soon as the camera starts capturing frames with 50 frames per second. After a predefined waiting time, the ultrasound pulses appear with a chosen PRF at predefined parameters. When the ultrasound time is over, the camera still runs for the post-ultrasound measurement. In figure 2.4 the experimental protocol is schematically displayed.

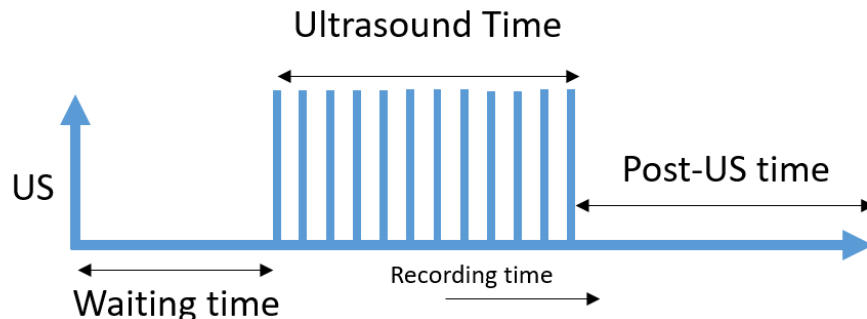


Figure 2.4: Schematic overview of the experimental protocol, typically with a waiting time of 20 seconds, 40 seconds of ultrasound and a post ultrasound time of 20 seconds.

Measurement plan

Since the ultrasound parameters from literature widely varied, the experiments started with a basic measurement of 1.0 MHz, 3.7 MPa, 1.0 Hz ultrasound. However, initially this resulted in tissue detachment. Therefore the ultrasound pressure and frequency were lowered and gradually increased. Every measurement is performed twice at the same tissue, which is a technical duplo. Furthermore, biological duplos are obtained by performing technical duplos at two or more samples.

2.4 Processing

In order to display the results, the raw data is processed into clearly defined measures. The raw data obtained during a measurement consists of 4000 (Q) frames of 1264x1016 (N x M) pixels, stored in .tif files. Furthermore, each measurement comes with a .xiseq file, which contains timestamps of every frame. With use of MATLAB .avi files are converted out of the .tif files without using .xiseq files, but with a constant framerate of 50. However, time domain representation of defined measures are based on the timestamps of the .xiseq files. In appendix C.1 .tif files are developed into .avi movies.

The .avi files are used for further processing. Processing is done frame by frame. The middle frame (arbitrary chosen) is set as reference frame; parts of all frames are compared to this frame. The first step of the analysis is dividing the reference frame into N kernels of 64x64 pixels with 50% overlap in both directions. For each kernel the 2-dimensional cross correlation within a range surrounding the kernel (156x156 pixels) at the frame of interest is determined. In figure 2.5 the kernel, range, overlap and frame are depicted. Assumed is that the pixel with highest cross correlation equals the movement of the kernel within the range. The highest cross correlation value is normalized by dividing it by the standard deviation of the cross correlation values within a kernel of a frame, and saved as Xcorr-contrast. The location of the highest cross-correlation is saved as (disp1, disp2) for every kernel and every frame. The MATLAB script used is displayed in appendix C.2.

Defining the mean displacement per unit time is the ultimate goal. In appendix C.3 the mean displacement per unit time is determined based on the PIV output data. The mean displacement is determined by first subtracting the "displacement" during 0.1 second (5 frames) without movement from all displacement values per frame. Thereafter the resulting x-direction displacement and y-direction displacement are both squared per frame. Next the square root is taken of these two values added. This value is the mean displacement in unit pixel per unit time for the full frame. The unit pixel is converted into a length scale in micrometers by using the pixel size (0.48 μm) and microscope resolution (20x).

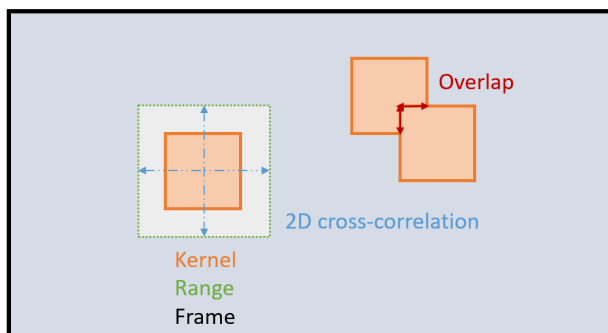


Figure 2.5: Schematic overview of data processing.

2.5 Analysis

During analysis the the mean displacement per unit time and the input ultrasound pulses are used. The script can be found in appendix C.4. The unfiltered frame averaged displacement, the contraction to contraction time (contractile period) and the contraction response time after an ultrasound pulse are shown. Contractions are identified as follows:

First the mean displacement is Fourier filtered; the data is Fourier transformed from time to frequency domain. In frequency domain, only data between 0.3 Hz and 3.0 Hz is kept. Next the frequency domain data is inverse Fourier transformed into the time domain. Thereafter a peakfinder is applied at the filtered data to identify local displacement maximums. The displacement maximums correspond with contraction peaks. From the raw data, 15 samples before and 14 samples after a displacement maximum are saved: this dataset represents the raw contraction shape. The contractile period of a contraction is defined as the time between two contraction maxima; in figure 2.6 this is indicated with the green arrows. For the displacement maximums during the ultrasound phase (see 2.3) the response delay is determined additionally. The response delay is defined as the time between the previous ultrasound pulse and the contraction maximum itself. In figure 2.6 this is indicated with the yellow arrows. For displacement maximums during the waiting time and post-ultrasound time, the response delay is set at NaN (not a known number), since there is not an ultrasound pulse to refer to.

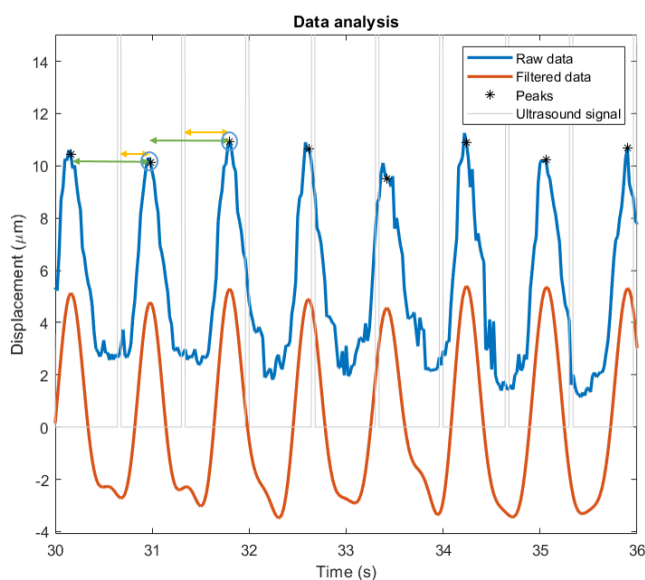


Figure 2.6: Schematic overview of data analysis; in yellow the response delay, defined as time between ultrasound signal and peak. In green the contractile period, defined as time interval between two peaks.

The contraction shape datasets are used for further quantification of the contractions. The defined parameters

are elaborated in figure 2.7. First the contraction shape is smoothed. The maximum displacement of the smooth contraction is determined. Furthermore, the integral of the contraction shape is determined using MATLAB's trapz. Thereafter the derivative is taken of the smooth contraction in order to quantify speed during contractions. The maximum speed equals the contraction speed, whereas the minimum speed quantifies the relaxation speed. The time between the minimum and maximum speed is quantified as contraction duration. The zero crossing timing between the maximum and minimum speed is also defined. It is stated as a percentage of the total contraction duration. In order to connect the theory with analysis parameters, table 2.2 connects the data analysis parameters with contraction variables.

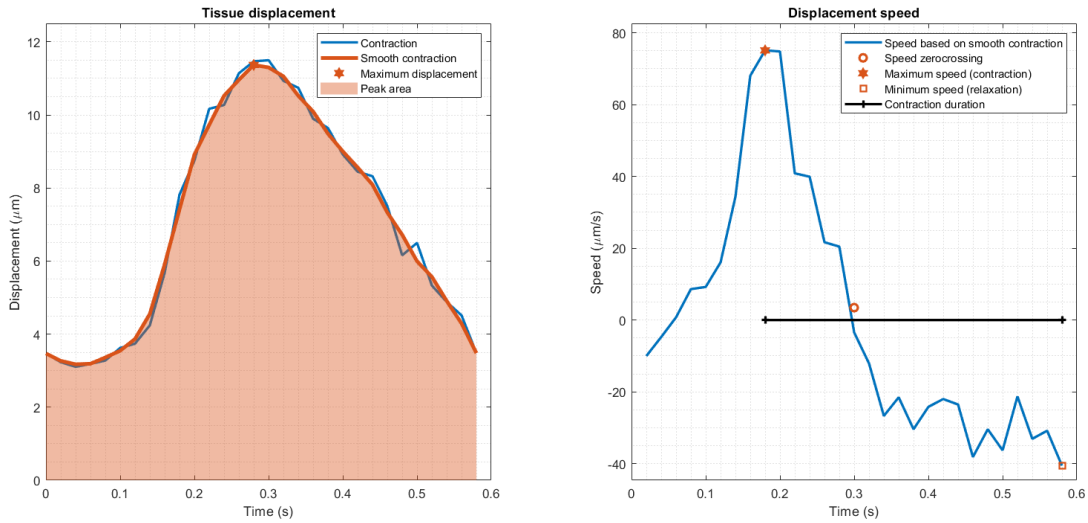


Figure 2.7: Schematic overview of peak analysis.

Table 2.2: Overview of data parameters and biological parameters.

Data analysis parameter (unit)	Contraction variables
Maximum displacement (μm)	Contraction force
Peak area (μms)	Contraction strength
Maximum speed ($\mu\text{m/s}$)	Contraction speed
Minimum speed ($\mu\text{m/s}$)	Relaxation speed
Speed zero-crossing timing (-)	Contraction shape
Peak duration (s)	Contraction duration

Chapter 3

Results

In this chapter the results obtained during the research will be shown and supplemented with explaining text. The structure of the result chapter is as follows: In section 3.1 single measurements with various responses to ultrasound are shown. In section 3.2 a measurement series consisting of 4 measurements per experimental parameter is used. The 4 measurements consists of two measurements (technical repeats) on two different samples (biological repeats). The series uses ultrasound at 1.5 MHz, 5 MPa with a PRF of 1.5 Hz. The pulse durations vary from 0.002 ms to 0.7 ms. In section 3.3, 1.0 MHz (3.7 MPa) versus 1.5 MHz (5.0 MPa), at pulse durations of 0.5 ms, 0.7 ms and 1.0 ms are analysed. In table 3.1 an overview is given of the used measurements, the number indicates in which result section the measurements are used. In figure 3.1 the starting frame of 0.2 ms, 1.5 MHz measurement can be seen on the left. The yellow bar indicates the line from the figure that is tracked for all frames, which resulted the right part of figure 3.1. It shows a repetitive pattern in top, which indicates repetitive movement of that line.

Table 3.1: Overview of measurements used for analysis, the number equals in which section the measurement is used.

Frequency (MHz)	Pressure (MPa)	Duration (ms)												
		0.001	0.002	0.004	0.005	0.008	0.01	0.02	0.04	0.05	0.1	0.2	0.3	0.4
1.0	3.7													
1.5	5.0		2	2		1,2		2	2		2	2		

Frequency (MHz)	Pressure (MPa)	Duration (ms)				
		0.5	0.7	1.0	1.2	1.4
0.5	1.6					
0.7	2.8					
1.0	3.7	1,3	1,3	3		
1.5	5.0	2,3	1,2,3	3		

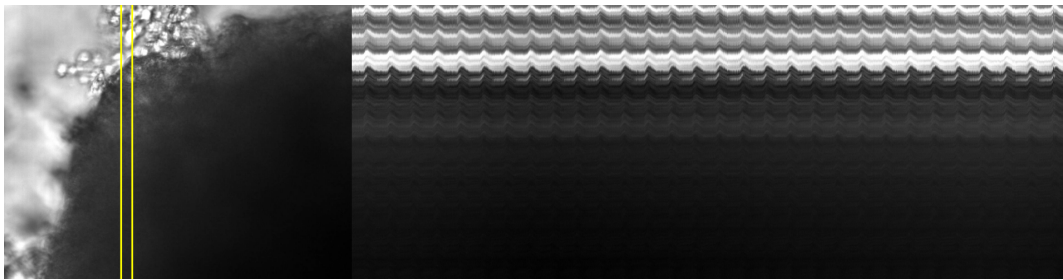


Figure 3.1: The start frame of a video; the yellow line indicate the line that is on the right displayed from frame 1 to 1600 (0 to 32 seconds). A repetitive pattern is visible at the top of the line.

3.1 Single measurement analysis

For all movies the data analysis is done as described in chapter 2. In this section the displacement data and US pulse will be shown, just as two examples of contraction shape and contraction speed. In appendix A the identified peaks, histograms of contraction periods during and without ultrasound, and all contraction (speed) shapes can be found.

In figure 3.2, upper row, ultrasound is present between 10 and 50 seconds, with a PRF of 1.0 Hz, a pressure of 3.7 MPa and a center frequency of 1.0 MHz. The pulse duration is 0.7 ms. The displacement shows peaks around 13 μm . Initially the contraction period is around 3 seconds. When the first ultrasound pulse is applied, the contraction period equals the pulse repetition period for two contractions. Thereafter the period of 3 seconds is resumed. At 23 seconds the contraction period becomes 0.7, where-after the contraction period gradually increases to 1.2 s at the end of the ultrasound at 60 s. The contraction peaks do not have a regular shape, as expected from literature. In short this is an example of an experiment with irregular response and unexpected contraction shape.

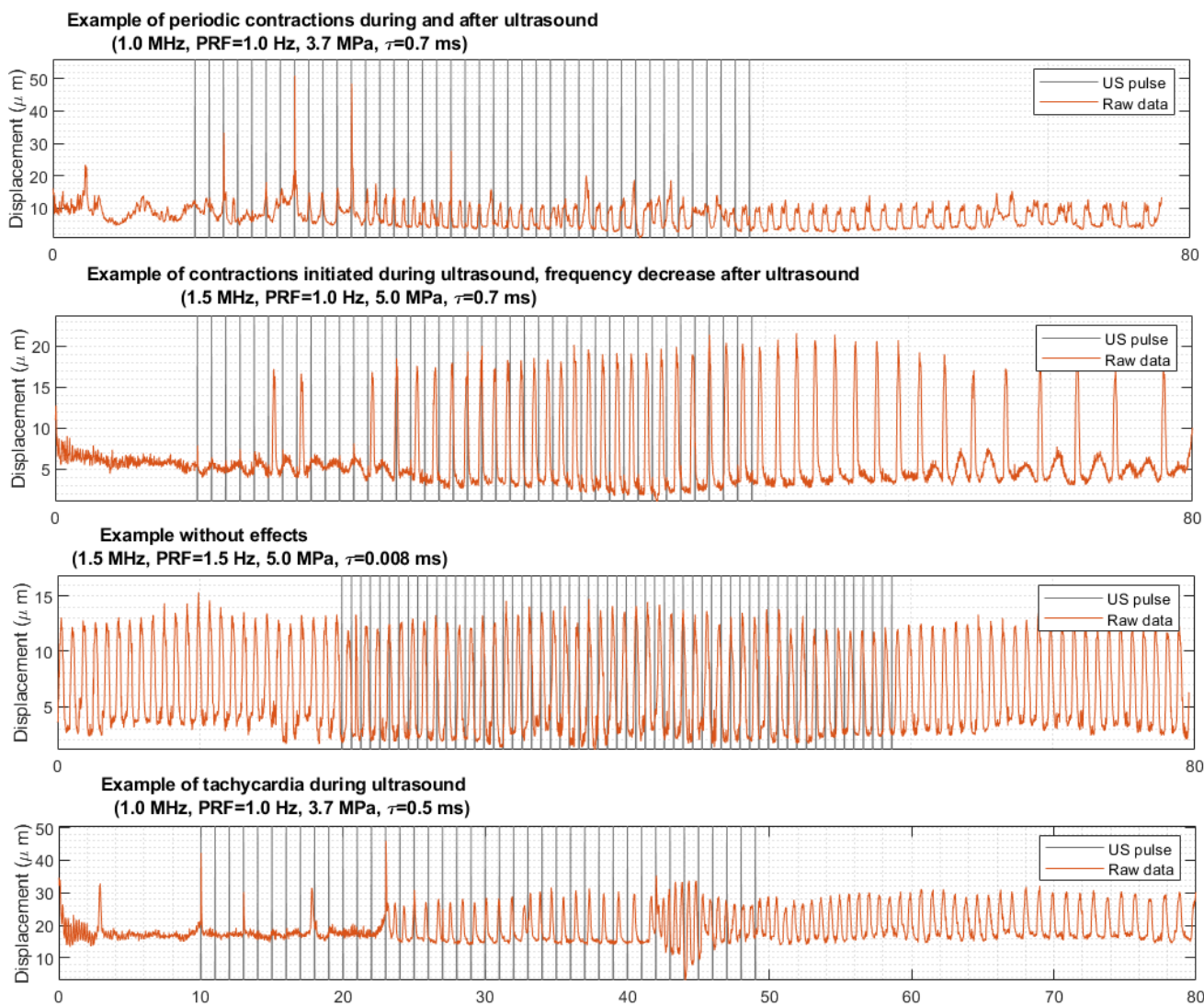


Figure 3.2: Four examples of ultrasound application to cardiomyocytes with various outcomes.

In figure 3.2, second row, ultrasound is present between 10 and 50 seconds, with a PRF of 1.0 Hz, a pressure of 5.0 MPa and a center frequency of 1.5 MHz. The pulse duration is 0.7 ms. The displacement shows peaks around $20 \mu\text{m}$. Initially the sample does not contract. At 15 s, 17 s and from 22 s to the end contractions do occur. At 22 s the period is 1.4 s, next the period decreases to 1.0 s and remains 1.0 s until the ultrasound pulses cease. Hereafter the contraction period gradually increases. In appendix, the contraction period probability histogram shows high probability of 1.0 contractions with ultrasound, which is desirable. Furthermore, the contraction peak shape and the contraction speed are equal to literature, with and without ultrasound. Concluding, this is an example of cardiomyocyte pacing as result of ultrasound pulses.

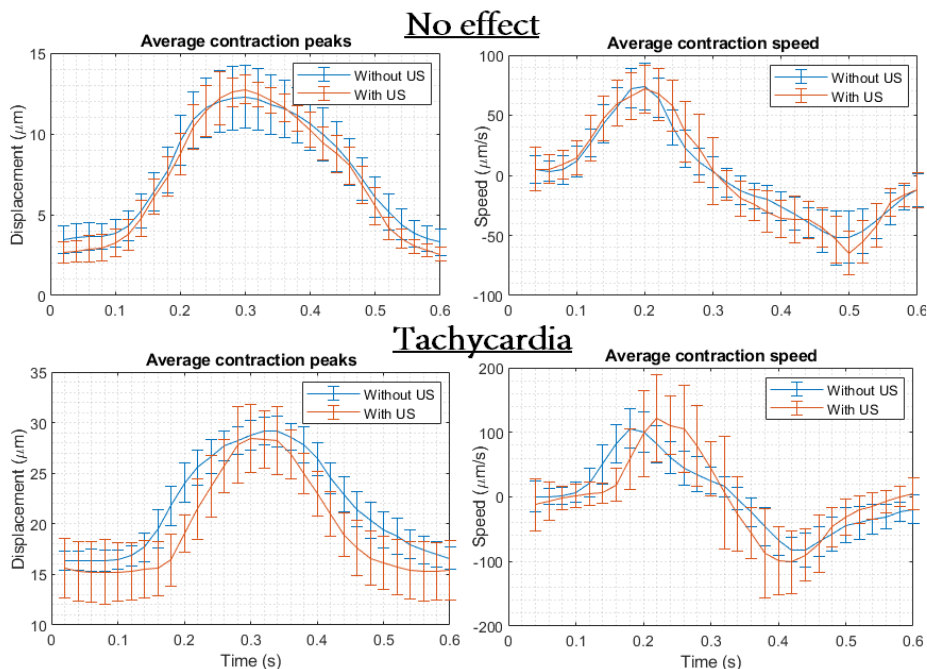


Figure 3.3: Two examples of contraction shape and contraction speed shape without and during ultrasound application to cardiomyocytes with various outcomes, on top without effect and on bottom with tachycardia. The tachycardia occurs during ultrasound; the contraction peak narrows and the contraction speed increases, just as the contraction speed standard deviation. This corresponds to the effect of Forskolin (cAMP mechanism) from figure 1.4.

In figure 3.2, third row, ultrasound is present between 20 and 60 seconds, with a PRF of 1.5 Hz, a pressure of 5.0 MPa and a center frequency of 1.5 MHz. The pulse duration is 0.008 ms. The displacement shows peaks around $12 \mu\text{m}$, with a constant contraction period of 0.8 s before, during and after ultrasound. The contraction period histogram shows the same pattern. The time delay varies, since the ultrasound PRF does not equal the contraction period. Furthermore, the average contraction peaks with and without ultrasound show similar shape, just as the average contraction speed. In figure 3.3, top subfigures, the average contraction peaks show high similarity without and with ultrasound. The average contraction speed show positive and negative peaks as expected from literature. In short this is an example of an experiment without response.

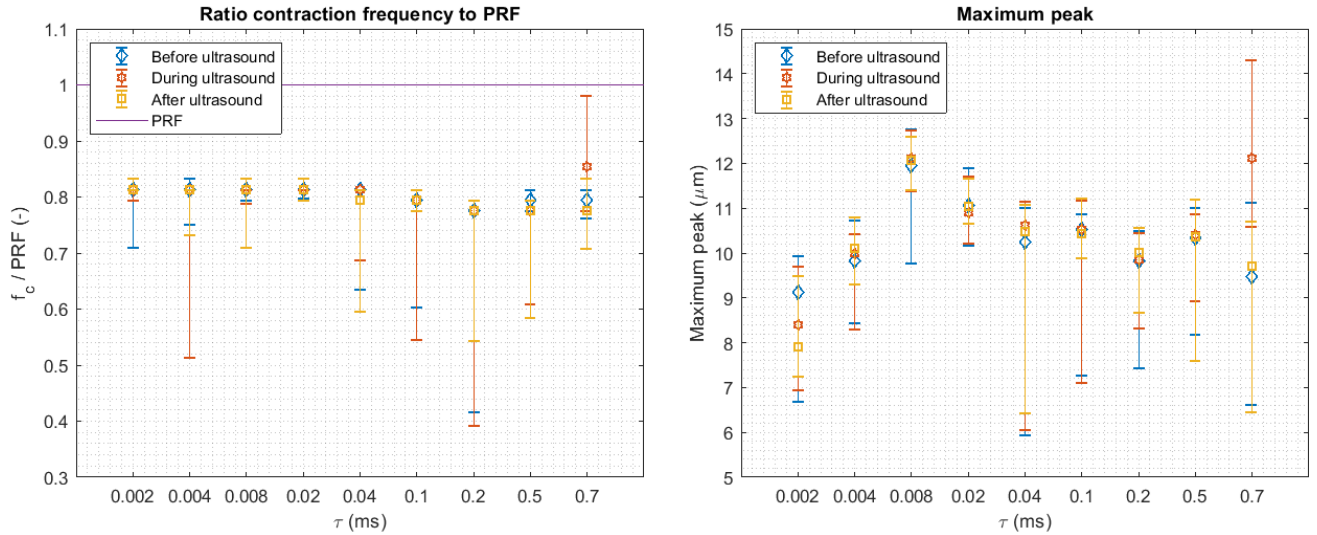
In figure 3.2, last row, ultrasound is present between 10 and 50 seconds, with a PRF of 1.0 Hz, a pressure of 3.7 MPa and a center frequency of 1.0 MHz. The pulse duration is 0.5 ms. It is seen that the displacement shows peaks around $30 \mu\text{m}$ with a baseline of $15 \mu\text{m}$. Initially the sample does not contract frequently. At 3 s, 13 s and 18 s contractions do occur. From 24 s to 78 s contractions occur. At 24 s the period is 0.8 s, next the period increases to 1.0 s and remains 1.0 s until 42 s. From 42 s on tachycardia occurs: the contraction period is 0.4 s. Hereafter the contraction period gradually increases to 1.0 s at 78 s. In figure 3.3, top subfigures, the average contraction peaks during ultrasound is narrowed and the contraction speeds are increased. This is an example of cardiomyocyte pacing and tachycardia due to ultrasound pulses, with altered contraction shapes.

Based on the results of this section is concluded that the application of ultrasound pulses (range 1.0 to 1.5 MHz, 0.001 to 1.0 ms, 3.7 to 5.0 MPa) on cardiomyocytes has various effects, ranging from no effect at all to adapted contraction peak shape and tachycardia. Also it is shown that after ultrasound application the effect prolongs, or declines and eventually disappears.

3.2 Effect of pulse duration

In this section multiple variables of the contractions are displayed. This series contains biological and technical duplos with ultrasound at 1.5 MHz and 5 MPa with a PRF of 1.5 Hz. The pulse durations vary from 0.002 ms to 0.7 ms. **Each figure in this section represents the median and the bars represent the 25th to 75th percentile.** The median contraction frequency (figure 3.4a) are before and after ultrasound pulses from 0.002 ms to 0.5 ms constant around 0.8. However the contraction frequency during 0.7 ms ultrasound pulses slightly increases, after which the initial frequency is restored after ultrasound. The peak maximum (figure 3.4b) varies without ultrasound (even for the samples) between 6 and 12 μm . During ultrasound the peak maxima are equal, except for 0.7 ms pulses. Then the peak maxima slightly increase from 9.5 to 11 μm .

Figure 3.5a shows a constant contraction speed between 45 and 70 $\mu\text{m}/\text{s}$ and a relaxation speed between 40 and 50 $\mu\text{m}/\text{s}$ without ultrasound and with ultrasound pulses until 0.5 ms. The interquartile range per pulse duration is very small. An ultrasound pulse of 0.7 ms result in a higher maximum speed, as well for relaxation as contraction speed maxima. It increases from approximately 40 $\mu\text{m}/\text{s}$ to 135 $\mu\text{m}/\text{s}$. After the ultrasound, the maximum speed as before ultrasound is resumed. The contraction durations are shown in figure 3.5b. Before ultrasound this is approximately 0.26 s, whereas the duration decreases to 0.15 s with ultrasound pulses of 0.7 ms. After 0.7 ms of ultrasound pulses the former peak duration is resumed. Other pulse durations do not alter the peak durations.

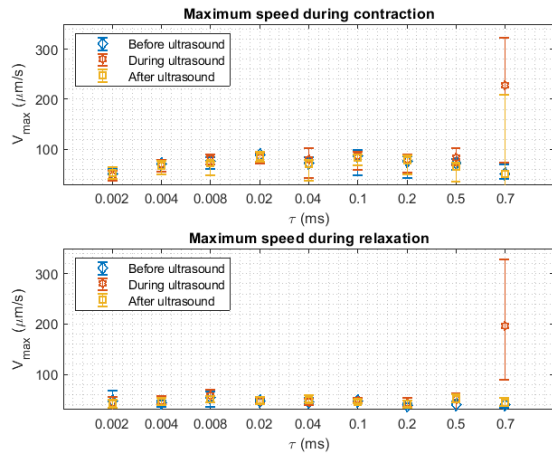


(a) Relative contraction frequencies per pulse duration.

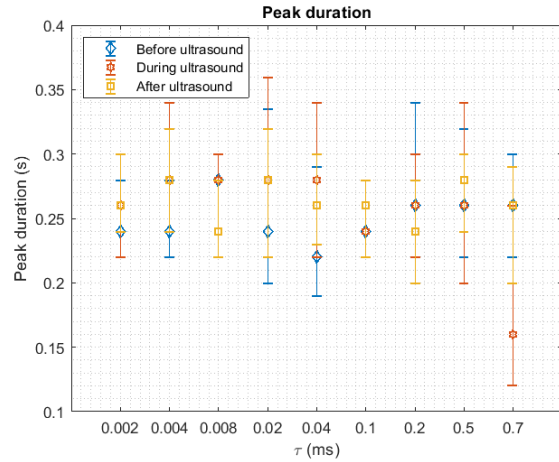
(b) Peak maxima per pulse duration.

Figure 3.4: Overview of contraction frequency and contraction maxima per pulse duration, 1.5 MHz, 5.0 MPa, 1.5 Hz.

Based on the increased relative contraction frequency, it is concluded that in this series only ultrasound pulses at 1.5 MHz of 0.7 ms result in a contraction frequency increase towards the pacing frequency. Next this ultrasound pulse does increase the maximum peak, which is a measure for contraction force. Also, the contraction speed and relaxation speed are significantly increased and show a higher variation, which indicates that the enhancement of the complete contractile cascade via higher levels of the second messenger 3,5-cyclic adenosine monophosphate (cAMP) is involved. It rejects the hypothesis of increased free cytosolic calcium concentration ($[Ca^{2+}]_i$) and direct thick- or thin myosin filament activation, since the contraction duration decreases, the amplitude increases and the maximum contraction & relaxation speeds increase.



(a) Speed maxima during contraction and relaxation.



(b) Peak durations, defined as time interval between maximum contraction speed and maximum relaxation speed.

Figure 3.5: Speed maxima and contraction durations per pulse duration, 1.5 MHz, 5.0 MPa, 1.5 Hz.

3.3 Effect of pulse pressure and center frequency

During the experiments over 20 measurement series have been performed with pulse duration from 0.001 ms to 1.0 ms. From all these series, the measurements with pulse durations of 0.5 ms and higher are involved in this results section. The following result series compares 1.0 MHz (3.7 MPa) and 1.5 MHz (5.0 MPa) experiments with ultrasound pulses of 0.5 ms, 0.7 ms and 1.0 ms. All the graphs show 1.0 MHz experiments on the left, 1.5 MHz experiments on the right. **Each figure in this section represents the median and the bars represent the 25th to 75th percentile.**

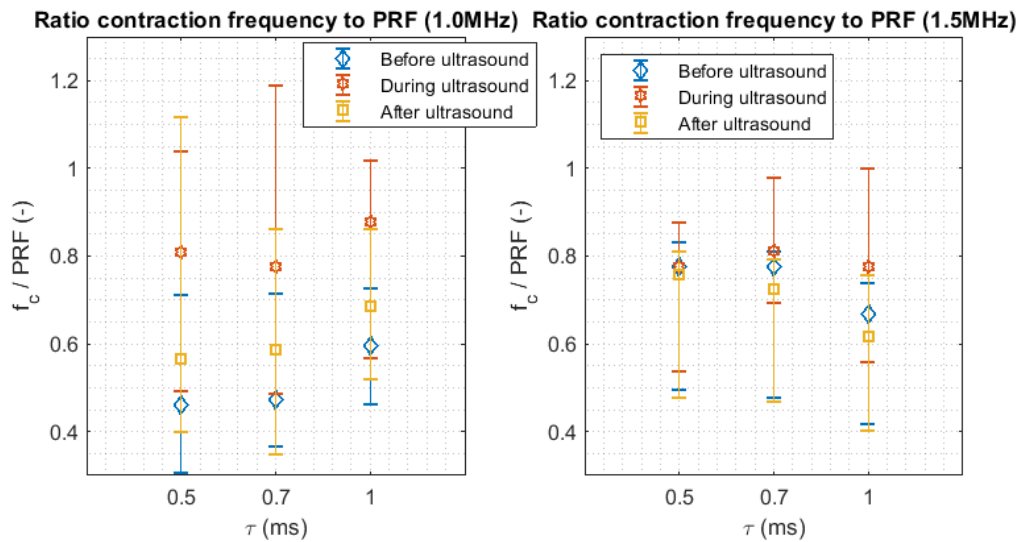


Figure 3.6: Relative contraction frequencies per pulse duration and center frequency combination.

Figure 3.6 depicts the contraction frequency relative to PRF; a value of 1 means that the contraction frequency equals the pulse repetition frequency, whereas a value of 0.5 means that the contraction frequency is half the PRF. During experiments the PRF was chosen such that pacing would increase the contraction frequency. The ratio would therefore increase to 1.0 in the ideal case. On the left is the contraction ratio before ultrasound 0.5, except for 1.0 ms signal where it's 0.6. Since the contraction frequencies without ultrasound are not uniform for the various pulse durations, it can not be used for comparison between variables. However, ultrasound pulses of 0.5 ms, 0.7 ms and 1.0 ms lead to an increase in contraction frequency. After ultrasound the contraction frequency is lower

than with ultrasound, but higher than before ultrasound. On the right are the contraction periods shown without and with 1.5 MHz ultrasound. The contraction frequencies before ultrasound are not constant, so the variables can not be compared. Pulses of 0.7 ms and 1.0 ms lead to a small increase in contraction frequency during ultrasound. After ultrasound the contraction frequency is even lower than before ultrasound.

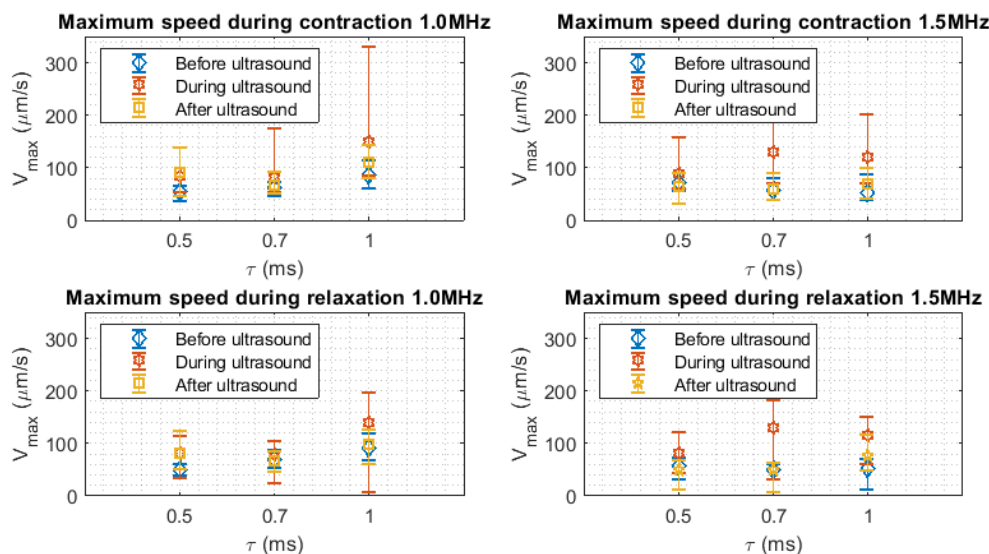


Figure 3.7: Speed maxima per pulse duration and center frequency combination.

The maximum contraction and relaxation speed for each center frequency are shown in figure 3.7. In general, the maximum contraction speed before ultrasound is around $60 \mu\text{m/s}$ and the maximum relaxation speed is around $50 \mu\text{m/s}$. The maximum contraction speed slightly increases during ultrasound, furthermore, the interquartile range is larger than before ultrasound. After ultrasound the contraction speed of before the ultrasound is restored. The relaxation speed is slightly increased during ultrasound (1.0 MHz 1.0 ms, 1.5 MHz all pulse durations); this is most prominent for 0.7 ms 1.5 MHz ultrasound. Besides, the interquartile spread is larger during ultrasound. After ultrasound the relaxation speed equals the relaxation speed of before ultrasound.

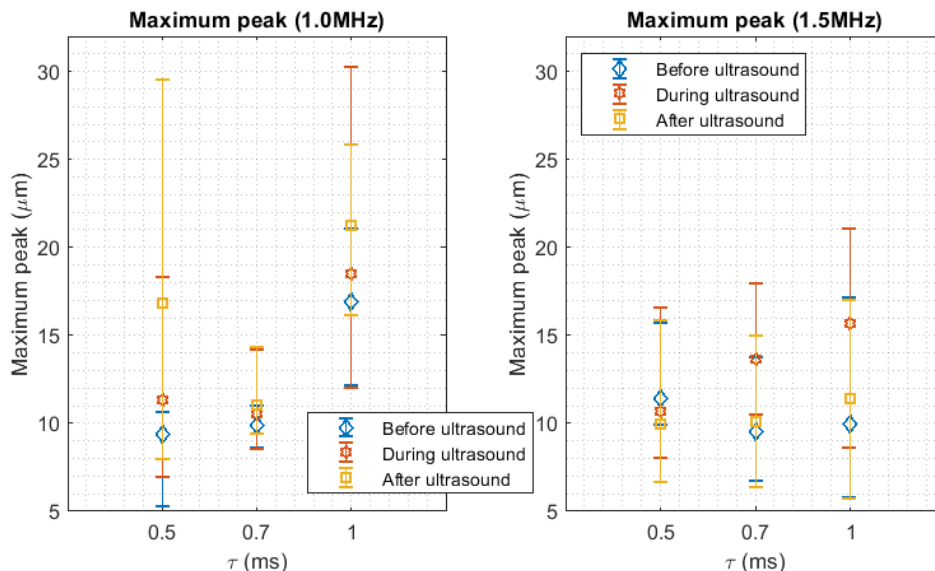


Figure 3.8: Peak maxima per pulse duration and center frequency combination.

In figure 3.8 the peak maxima per pulse duration and center frequency are shown. The maximum peak before 1.0 MHz and 1.5 MHz ultrasound is around $10 \mu\text{m}$, except for 1.0 MHz 1.0 ms blanco data. In that case before

ultrasound the maximum peak is around $16 \mu\text{m}$. The effect of 0.5 ms and 0.7 ms 1.0 MHz ultrasound is a slight increase in peak maxima. The effect of 1.5 MHz ultrasound is an increase in peak maxima; the maxima increases with increasing pulse duration. Furthermore, the variation in maxima is increased during ultrasound. After ultrasound the blanco peak maxima are restored for 1.5 MHz pulses, whereas the blanco peak maxima increases to $16 \mu\text{m}$ for 0.5 ms 1.0 MHz pulses.

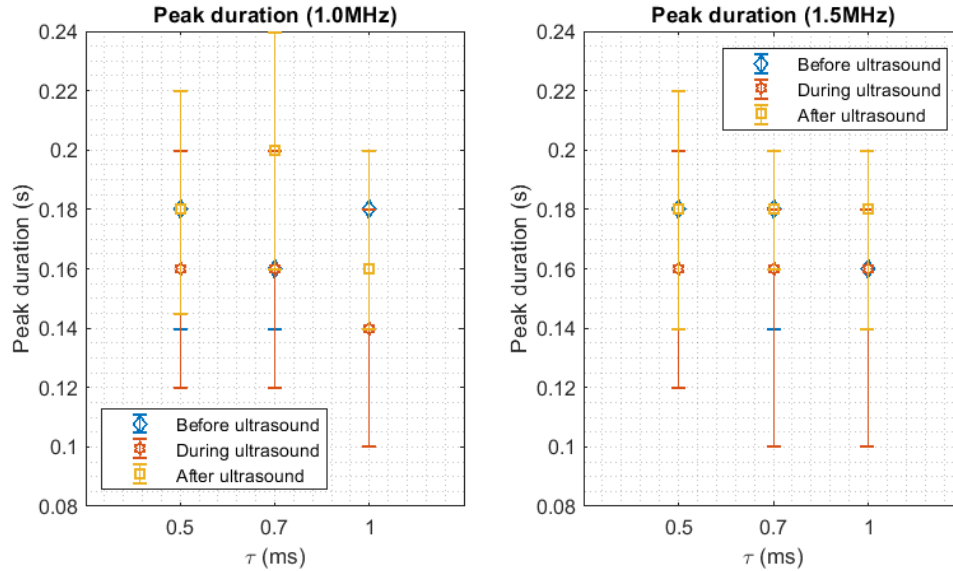


Figure 3.9: Peak duration per pulse duration and center frequency combination.

In figure 3.9 the peak durations per pulse duration and center frequency are shown. The peak duration median is within 0.14 s to 0.20 s, before, during and after ultrasound. The 25th and 75th percentiles lie within 0.10 s and 0.24 s. With the used fps, peak durations are determined in steps of 0.02 s. In all datasets, the median peak duration is lowest during ultrasound. However the variations are still very small.

3.3.1 Contraction delay

Another aspect of interest is the contraction timing with respect to ultrasound pulse timing. In figure 3.10 an overview is given of the delaytime of contractions after an ultrasound pulse. It is split up in contractions that synchronize with the PRF, and contractions that are not synchronized. Synchronization is determined as a frequency within 0.95 to 1.05 PRF value. The delay is highly variable for both groups. Unsynchronized contractions have time delays varying from 0 to 1.15 seconds. Most do have a delay between 0.60 & 0.66 (15%) and between 0.00 & 0.10 s (20%) for all pulse durations. For all three pulse durations, time delays are approximately equally represented. On the other hand, synchronized pulses occur mostly with a delay of 0.78 to 0.84 s (25% in total) and occur from 0.00 s to 0.20s for 40%. Between 0.20 and 0.40 the probability is almost zero, whereas the probability between 0.40 and 0.70 is varying from 0.00 to 0.05.

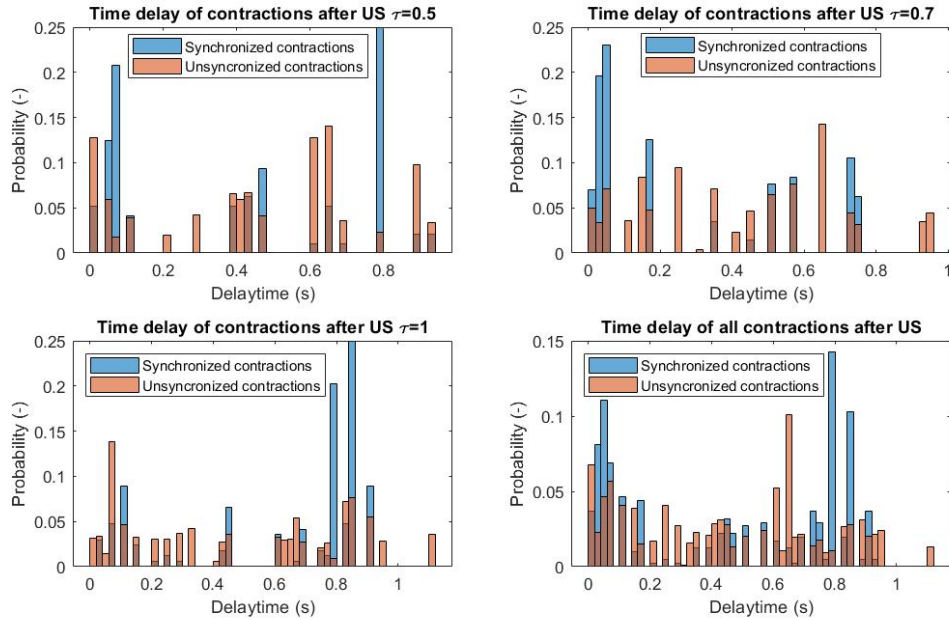


Figure 3.10: Delay timing per pulse duration, for synchronized and unsynchronized contractions.

3.3.2 Interim conclusion

Based on the figures in this section, the conclusions in the range 0.5 ms to 1.0 ms, 1.0 MHz to 1.5 MHz are as follows:

- Ultrasound increases the contraction frequency.
- This increase is constant for 1.0 MHz pulses of various durations.
- 1.5MHz pulses with increasing pulse durations, cause increasing contraction frequencies.
- Ultrasound also increases maximum speed during contraction and relaxation.
- Maximum speed increase is larger for 1.5 MHz 5.0 MPa pulses than for 1.0 MHz 3.7 MPa pulses.
- Maximum displacement peaks increase with increasing pulse duration.
- Contraction durations slightly decrease, but the decrease is not significant nor large.
- The delay of contractions after ultrasound is highly variable, but occurs mostly within 0.2 s after the ultrasound pulse or around 0.8 s after the pulse.

Based on the speed increase during contraction and relaxation, the direct link between ultrasound and increased free cytosolic calcium concentration can be rejected. The speed increase and the highly variable contraction delay also reject the direct myosin activation hypothesis. The hypothesis that ultrasound drives cell contraction by enhancement of the complete contractile cascade by beta-adrenergic stimulation or PDE3 inhibition can not be rejected, since the contraction amplitude and speed increase, just as the relaxation speed. Also, the time delay of contractions after ultrasound does not contradict this hypothesis, so therefore the conclusion is that the cAMP mechanism is the mechanism that causes ultrasound pacing in cardiomyocytes.

Chapter 4

Discussion

The previous presented results provide statements regarding ultrasonic pacing of cardiomyocytes and cardiomyocyte response. In this discussion, used methods and results are discussed. First the limitations of the used methods are discussed, after which the results are discussed and limitations are identified.

Overall, the used samples and methods are very complex; over 250 video captures were saved, from which only 50% was useful for analysis due to missing frames, tissue detachment and minor setup vibrations. Apart from the 250 video captures, experiments were started but video software or pulse generators did not work out as set. What should also be remarked is the complexity and time effort of tissue culturing and sample preparation, even before the tissue can be placed at the coverslips. Concluding, the experiments are sophisticated and consist of multiple crucial steps. Therefore it could be that the results based on the captured videos are not a realistic representation of the average cardiomyocyte behaviour.

The samples were obtained as described in subsection 3.1. The samples were made of ventricular cells; it is known that atrial and ventricular cells do not behave equally. Thus it is not possible to convert the results one-on-one to atrial cells, experiments at atrial tissue should take place before the effects can be known.

Additionally, tissue age during experiments plays a role. Kohut states that fibroblasts are the mechano-electrical transducers of the heart [57]. Tissue 'age' at the membrane would therefore be a variable of interest since the ratio fibroblasts to cardiomyocytes increases over time. For example the ultrasound can be more effective at older tissue sample, because transduction in the tissue is elevated.

Another remark is that embryonic bodies consist of a large tissue construct, in which the individual cells communicate with each other. Therefore studying single cells would be useful to determine if the effect on embryonic bodies equals the effect on microtissue and single cells.

Besides, the tissues used for the experiments were constructed by one researcher. Although strict culturing protocols were followed, small variations in lab techniques can affect the outcome. The results should be equal on tissues cultured by other researchers; at the moment it is not known if that is the case. If it's not the case yet, the protocols should be adapted such that interperson variations are avoided as much as possible.

Within the setup the medium temperature is controlled. The experiments were performed at 37 °C, which enable the cells to contract naturally. Performing the experiments at a lower temperature (for example 25 °C) would result in a slower automaticity frequency, which enables the researchers to use a larger interval between automaticity and ultrasound PRF.

Another aspect of interest is matrigel, which is used to crosslink the tissues to the Mylar coverslips by natural polymers. Ultrasound is applied to the samples while they are attached to the Mylar by matrigel. Matrigel and the membrane can absorb the ultrasound or damp the tissue vibrations. To determine if this plays a role, the matrigel volume that is added can be varied. Besides, the thickness of the mylar can be varied. It is not reducible to what extend it played a part in the current results.

The setup is quite complex; inadequate handling and incorrect alignment needs to be avoided at all times. Besides, the settings to get the correct ultrasound pulse are complicated. One should pay attention to all submenus at the various pulse delay generators in order to not overlook a detail that can have a huge effect. Since there are so many settings, the probability of problems accumulates. This can cause damage to the setup, for example to the ultrasound transducer, the hydrophone or the tissue.

Next point of attention is the alignment of the ultrasound focus and the microscope focus. The focus of an ultrasound transducer depends amongst others on the center frequency of the ultrasound. Since alignment takes place at 1 MHz and some measurements are performed at 1.5 MHz, the focus shifts. Therefore microscope focus does not depict the ultrasound focus and the resulting pressure differs from the calculated pressure.

The experimental methods consist of a relatively short waiting time, an ultrasound time and lastly post-US time. In order to extend the datasets available, longer phases before, during and after ultrasound are helpful to study for example the recovery time to the natural contraction frequency of the tissue. This would also increase the sample size for statistical analysis. The only disadvantage is longer experiment duration, but experiment duration is subordinate to the complex protocol that has to be followed before starting a measurement with certain ultrasound parameters.

During these experiments 50 frames per second were captured. But obtaining data at a higher framerate would increase the samplerate. This allows the researcher for perceiving smaller variations, for example in contraction force development and contraction speed this would be beneficial. Besides, the total pulse duration can be determined with higher accuracy.

Most experiments were performed in technical triplo, however at most two out of three experiments resulted in data useful for analysis. Therefore is recommended to perform at least five measurements so ideally three (or more) technical repeats are available for analysis. Also, the subsection 3.3 compares 1.0 MHz pulses of 3.7 MPa with 1.5 MHz pulses of 5.0 MPa. Adapted contraction features can not be solely directed to the center frequency difference nor the pressure interval.

During these experiments bright field videos were obtained, after which PIV analysis resulted in tissue displacement values. Van Meer et al. have shown that various cellular mechanisms result in variations in action potential, calcium flux and contraction speed [24]. In this thesis only contraction parameters were studied. When also the action potential and calcium are studied, the results pointing towards one specific biological mechanism can become even stronger. Calcium imaging could provide information about the proportional intracellular calcium concentration. Calcium imaging requires a fluorescent dye, which can photobleach. The molecule structure of the dye is amended by the light, wherafter the fluorescence capacity decreases. If a researcher wants to quantify the calcium concentration over time, it is necessary to perform 'blanco' measurements without ultrasound pulses to account for photobleaching by light exposure. The degree and speed of photobleaching can be determined and this can be used to distinct slow intracellular calcium decrease or increase from photobleaching.

During data processing the kernel size, range size, overlap percentage and scaling factor determine the sensitivity for small movements and very large movements. The values used for this thesis are a tradeoff between analysis time and analysis sensitivity. However, a smaller kernel size, larger range, higher overlap percentage and smaller scaling factor will increase the sensitivity for contractions. This should result in more accurate contraction shapes and therefore a better comparison between contraction shape variables would be possible.

In order to obtain displacement data, the user of the analysis script should indicate a frame that is not involved in the contraction. It may result in displacement data with a baseline that does not equal zero micrometers. However it is expected that the displacement between contractions is constant and very small. Other than the elevated baseline, the displacement peaks are very high. Comparison of the displacement peak values is therefore not useful between various measurements, since the baseline varies per measurement. This could be solved by using another user input, or later on deleting the elevated baseline or implementing an automatic function that selects a frame without contraction.

The contraction duration was determined as the time interval between maximum speed and minimum speed. However, it is more common to define the contraction duration as the time interval between contraction onset and offset. This was decided since the available framerate in combination with the smoothness of the data was not enough to apply a uniform method to determine the contraction onset and offset time, leading to the full contraction duration time.

The result section is divided in three parts. In the first part isolated measurements are shown, wherein various outcomes are displayed. In this section it is visible that even during ultrasound, no uniform response was achieved within an experiment. Although, in the next sections, all data during ultrasound has been merged. Therefore one cannot distinguish between three measurements of which in one case the contractions are adapted for the full ultrasound duration, or three measurements in which the contractions were altered during one-third of the ultrasound time.

In this thesis, conclusions are drawn based on median values and 25th and 75th percentile values. In order to apply ultrasound pacing in studies that require a constant pacing frequency, an additional analysis should take place. This analysis should account for pacing success rate per measurement. Another measure of interest is 'longest success interval' which is the longest time duration of all synchronized contractions. These measures are necessary to quantify if the tissue response is constant and long-lasting, which are desired quantities in pacing.

Large variations of the ratio contraction frequency to PRF were achieved after ultrasound. This can be explained by the occurrence of measurements in which the contraction frequency after ultrasound decreased gradually on one hand, and measurement were after ultrasound a quick recovery to the original contraction frequency occurred.

When the resulting contraction shapes are compared to the contraction shapes of hiPSCs by Van Meer et al., a different contraction duration can be found [24]. The contraction durations in hiPSCs are around 200 ms, whereas in these experiments full contraction durations around 450 ms are found. However, the time from maximum contraction speed to maximum relaxation speed is around 200 ms. This variations can be due to the different origin of the tissues, or the varying circumstances in which the tissues are studied. For example the attachment of the tissues to coverslips, the controlled temperature, the shape of the tissues, e.g. monolayer versus embryonic bodies. Finding out the cause of these variations is important in order to apply the results in *in vitro* disease modeling, drug screening and study of drug pharmacology.

One of the future applications of cardiomyocyte pacing by ultrasound was defined as disease modelling. But ultrasound pacing uses the internal cellular modes of action to accomplish pacing. Therefore, application of ultrasound to diseased tissues could have another outcome than at healthy tissue. I would suggest to study the behaviour of diseased tissues and compare it to healthy tissue, before using the ultrasound pacing in studies of drug pharmacology in diseased tissue.

Chapter 5

Conclusion

In this thesis the effect of ultrasound on cardiomyocytes was studied in terms of frequency response and contraction features. Also, the ultrasound parameter space was explored. The first subquestion is: *"What is the mechanism driving cell contraction?"*

Based on the increased contraction force, increased contraction & relaxation speeds and decreased contraction duration, the mechanism driving cell contraction is enhancement of the complete contractile cascade by beta-adrenergic stimulation or inhibition of PDE3. It is one of the three known working mechanism of cardioactive drugs [24]. The ultrasound mode of action that enables this enhancement is not identified, just as the optimal ultrasound parameters for pacing. Although, it's known that increased pulse duration lead to increased effect, just as increased center frequency and pressure.

The second subquestion is: *"What is the behaviour of the cells within the ultrasound parameter space?"*

Within the studied parameter space, tissue response to ultrasound was found for pulse durations of 0.5 ms to 1.0 ms. Shorter pulse durations were studied, longer pulse durations were not studied. The responses were periods of several seconds in which the contraction frequency increased towards the pulse repetition frequency. Furthermore, the contraction and relaxation speeds increased; the median speed even tripled for 0.7 ms pulses of 1.5 MHz. Last but not least the contraction duration was decreased. 1.5 MHz, 5.0 MPa pulses do have larger effect than 1.0 MHz, 3.7 MPa pulses on the speed increase and maximum displacement peaks, thus contraction force.

Last subquestion is: *"How to best control the contractile rate?"*

As explained in the result and discussion sections, the tissue response was not uniform for all measurements of one condition. Furthermore, the examined ultrasound parameter space is small and contains more than just one parameter of variation. Also, the tissue response during one measurement did not last for long, so more repeats are necessary to collect even more evidence for the identified mechanisms and increase the success rate.

The subquestions lead to an answer regarding the main research question: *"Can ultrasound control cardiomyocyte pacing?"*

Ultrasound is able to induce cardiomyocyte contractions and accomplishes this via the cAMP mechanism. However, during these experiments the tissue response to non-varying ultrasound pulses was not constant and did not last for long. Furthermore, with the examined parameter space, the main ultrasound mechanism could not be identified and therefore the ideal ultrasound parameters for controlled pacing are not known. However, the biological mechanism that adapts the contraction dynamics is identified and this knowledge is very useful. It gives direction to follow-up studies.

Chapter 6

Recommendations

Based on experiences during experiments and new insights during writing, recommendations are done to improve future research. The recommendations are structured as the method section and discussion section; from sample via setup and experimental methods to data analysis.

First of all the start-up time of an experiment is very long due to complexity of the setup. Also, many measurements do not result in data that can be analysed. Therefore the setup should become less complex, for example by using predefined setting sets in the different devices and reducing the amount of devices. Also, the camera settings should be critically reviewed again, for example the exposure time. Last but not least the setup should be placed at a table that is more stable.

Moreover, testing at ventricular tissue, experiments at atrial tissue should take place. Furthermore, single-cell and microtissue measurements would be a nice addition: testing on single cells eliminates the effect of tissue dynamics, such as paracrine pathways. Another recommendation is to include the tissue fibroblast content and maturity in the measurement labeling and eventually in the parameter set. As described in the discussion (chapter 4), fibroblasts are the mechano-electrical transducers of the heart and fibroblast content increases with tissue age. Furthermore, Van Meer et al. state that in their experiments due to tissue immaturity some effects of drugs are undetectable. Thus the tissue maturity should also be determined, in order to later on link them to results.

During these experiments a 1.0 MHz transducer was used. In addition a 5.0 MHz and 10.0 MHz transducer are available. Before a new transducer can be used, it should be calibrated: the input voltage should be related to the output pressure. Besides, the microscope focus should be aligned with the new ultrasound transducer focus.

As explained before, the experimental methods consists of three relatively short phases regarding to ultrasound status. Increasing the phase durations will result in more data within a measurement and allow analysis on the longevity of tissue response in terms of increased contraction frequency and force. Next the frequency difference between the automaticity and the pulse repetition frequency can be altered. Later on, one could add more phases with increasing PRF in order to account for the statement of Williams that cardiomyocytes synchronize to mechanical perturbations with a limited frequency difference of 25% [18]. It would be helpful to vary the relative frequency difference, to see if outcomes vary with varying frequency difference. Decreasing the temperature of the bath would result in a slower automaticity, which allows for a larger PRF range. The PRF is on one hand limited by the automaticity rhythm, on the other hand by the transducer: it can be ruined by a too large PRF.

The conclusions are based on the contraction features. Additionally action potential and calcium concentration can be used to quantify tissue response to ultrasound pulses. Therefore I recommend to use a voltage sensitive dye and a calcium dye. In appendix B calcium imaging, including theory, methods and a protocol, is planned out. It requires adaptations to the sample preparations. Since Van Meer et al. were capable of doing this to hiPSCs, it should also be possible to ultrasound paced EBs.

Taking the analysis to a higher level can on one hand be done by obtaining more data, on the other hand the analysis can be further elaborated by including a success rate per sample, a success duration and a success rate per experimental parameter set e.g. when performing three technical and three biological repeats. Another way is to divide the cell dynamics during ultrasound into 3 parts; the initial part without variation in contraction frequency but with change in contraction force, the middle part in which changes occur in contraction frequency, contraction speed et cetera and the last part in which the frequency and speed is constant. For application in drug screening it is helpful to know what the 'startup' duration is and for how long a consistent frequency can be kept, just as the

success rate per sample and per ultrasound setting.

Another method to obtain clearer results is by using a higher framerate. This results in a higher time resolution, which increases the frequency resolution. It also provides more detailed information about the speed during contraction and relaxation. Furthermore, it enables to define contraction start and end time more precisely.

In order to further address the initial research questions, follow-up research can focus either on the ultrasound mechanisms that are involved, or extension of the ultrasound parameter set or trying to strengthen the conclusion regarding the biological mechanism.

In order to study the ultrasound mechanisms, it is very helpful to design an experimental set that maximizes the effect of cavitation and minimizes acoustic radiation force and vice versa. Another method to identify the major mechanisms is to design a parameter set that has comparable mechanical indices or equal acoustic radiation force. In appendix B in table B.1 such a set is designed based on approximations from chapter 1. Aside from center frequency, pulse repetition frequency and peak to peak pressure, extension of the ultrasound parameter set can be done towards changes in energy deposition, for example study the effect of two 0.5 ms pulses with 0.1 ms rest inbetween, in comparison with the effect of a single 1.0 ms pulse. This will allow the tissue to 'recover' from the heat generation and allows the researcher to compare the effects.

The beta-adrenergic stimulation pathway can be studied by adding inhibitors of this pathway to the medium such as beta blockers, β_2 agonists and α_2 agonists, to see if the pacing still occurs. If the pacing still occurs whereas the pathway is prohibited, the pathway is not dominant in ultrasound pacing. Another small sidestep is to study the ion ports that are suspected to be involved in ultrasound pacing.

Calcium imaging is a nice method to obtain a measure for intracellular calcium concentration. Furthermore, there are techniques to combine calcium tracking with membrane potential tracking and even tissue movement tracking. These methods do not include ultrasound, but it should be possible to implement this as well.

Another suggestion is to rethink the future application of the ultrasound pacing; if you want to apply it to diseased tissue, but the ultrasound pacing mechanism is also altered in such tissues, electrical pacing is a better option. What also would contribute to the understanding of ultrasound pacing, is studying the contraction dynamics during electrical or optogenetic pacing. Since the ultrasound mechanism causing contractions is not yet known, knowledge about the electrical pacing pathway can speed up this research direction as well. When various pacing methods can be compared in terms of working mechanism, benefits and limitations, it allows for choosing the right pacing method for each specific application.

Bibliography

- [1] Marc Dwenger et al. “Chronic optical pacing conditioning of h-iPSC engineered cardiac tissues”. In: *Journal of Tissue Engineering* 10 (Jan. 2019), p. 204173141984174. DOI: 10.1177/2041731419841748. URL: <https://doi.org/10.1177/2041731419841748>.
- [2] John C. Williams and Emilia Entcheva. “Optogenetic versus Electrical Stimulation of Human Cardiomyocytes: Modeling Insights”. In: *Biophysical Journal* 108.8 (Apr. 2015), pp. 1934–1945. DOI: 10.1016/j.bpj.2015.03.032. URL: <https://doi.org/10.1016/j.bpj.2015.03.032>.
- [3] Andrew William Chen et al. “Preliminary findings on ultrasound modulation of the electromechanical function of human stem-cell-derived cardiomyocytes”. In: *2017 IEEE International Ultrasonics Symposium (IUS)*. IEEE, Sept. 2017. DOI: 10.1109/ultsym.2017.8091621. URL: <https://doi.org/10.1109/ultsym.2017.8091621>.
- [4] Jan Kubanek et al. “Ultrasound modulates ion channel currents.” In: *Scientific reports* 6 (2016), p. 24170.
- [5] Verena Schwach. *Acoustical pacing of advanced human cardiac microtissues as platform to model heart rhythm disorders: sonogenetics in human stem cell-derived cardiomyocytes*. Grant proposal.
- [6] Diane Dalecki et al. “Effects of pulsed ultrasound on the frog heart: I. Thresholds for changes in cardiac rhythm and aortic pressure”. In: *Ultrasound in Medicine & Biology* 19.5 (Jan. 1993), pp. 385–390. DOI: 10.1016/0301-5629(93)90057-u. URL: [https://doi.org/10.1016/0301-5629\(93\)90057-u](https://doi.org/10.1016/0301-5629(93)90057-u).
- [7] Truong An Tran et al. “On the Mechanisms of Ultrasound Contrast Agents-Induced Arrhythmias”. In: *Ultrasound in Medicine & Biology* 35.6 (2009), pp. 1050–1056. ISSN: 0301-5629. DOI: <https://doi.org/10.1016/j.ultrasmedbio.2008.11.015>. URL: <http://www.sciencedirect.com/science/article/pii/S0301562908005802>.
- [8] Amit Livneh et al. “Extracorporeal acute cardiac pacing by High Intensity Focused Ultrasound”. In: *Progress in Biophysics and Molecular Biology* 115.2-3 (Aug. 2014), pp. 140–153. DOI: 10.1016/j.pbiomolbio.2014.08.007. URL: <https://doi.org/10.1016/j.pbiomolbio.2014.08.007>.
- [9] E. B. Buiocchi et al. “Transthoracic cardiac ultrasonic stimulation induces a negative chronotropic effect”. In: *IEEE Transactions on Ultrasonics, Ferroelectrics, and Frequency Control* 59.12 (Dec. 2012), pp. 2655–2661. DOI: 10.1109/TUFFC.2012.2506.
- [10] A. Miwa and N. Kudo. “Study on effects of pressure and duration of ultrasound pulse on pulsation of cultured cardiomyocytes”. In: *2016 IEEE International Ultrasonics Symposium (IUS)*. Sept. 2016, pp. 1–4. DOI: 10.1109/ULTSYM.2016.7728441.
- [11] Nobuki Kudo and Masaya Yamamoto. “An Experimental Model Using Cultured Cardiac Myocytes for a Study of the Generation of Premature Ventricular Contractions Under Ultrasound Exposure”. In: *AIP Conference Proceedings* 1359.1 (2011), pp. 318–321. DOI: 10.1063/1.3607925. eprint: <https://aip.scitation.org/doi/pdf/10.1063/1.3607925>. URL: <https://aip.scitation.org/doi/abs/10.1063/1.3607925>.
- [12] S.C. Calaghan and E. White. “The role of calcium in the response of cardiac muscle to stretch”. In: *Progress in Biophysics and Molecular Biology* 71.1 (1999), pp. 59–90. ISSN: 0079-6107. DOI: [https://doi.org/10.1016/S0079-6107\(98\)00037-6](https://doi.org/10.1016/S0079-6107(98)00037-6). URL: <http://www.sciencedirect.com/science/article/pii/S0079610798000376>.
- [13] T.A. Tran et al. “Effect of ultrasound-activated microbubbles on the cell electrophysiological properties”. In: *Ultrasound in Medicine & Biology* 33.1 (2007), pp. 158–163. ISSN: 0301-5629. DOI: <https://doi.org/10.1016/j.ultrasmedbio.2006.07.029>. URL: <http://www.sciencedirect.com/science/article/pii/S0301562906017704>.

- [14] MAX J LAB. “Mechanosensitive-Mediated Interaction, Integration, and Cardiac Control”. In: *Annals of the New York Academy of Sciences* 1080.1 (2006), pp. 282–300. DOI: 10.1196/annals.1380.022. eprint: <https://nyaspubs.onlinelibrary.wiley.com/doi/pdf/10.1196/annals.1380.022>. URL: <https://nyaspubs.onlinelibrary.wiley.com/doi/abs/10.1196/annals.1380.022>.
- [15] William D. O’Brien. “Ultrasound–biophysics mechanisms”. In: *Progress in Biophysics and Molecular Biology* 93.1 (2007). Effects of ultrasound and infrasound relevant to human health, pp. 212–255. ISSN: 0079-6107. DOI: <https://doi.org/10.1016/j.pbiomolbio.2006.07.010>. URL: <http://www.sciencedirect.com/science/article/pii/S0079610706000915>.
- [16] Zahra Izadifar, Paul Babyn, and Dean Chapman. “Mechanical and Biological Effects of Ultrasound: A Review of Present Knowledge”. In: *Ultrasound in Medicine Biology* 43.6 (2017), pp. 1085–1104. ISSN: 0301-5629. DOI: <https://doi.org/10.1016/j.ultrasmedbio.2017.01.023>. URL: <http://www.sciencedirect.com/science/article/pii/S0301562917300522>.
- [17] Guillaume Gilbert et al. “Calcium Signaling in Cardiomyocyte Function”. In: *Cold Spring Harbor Perspectives in Biology* (2019). DOI: 10.1101/cshperspect.a035428. eprint: <http://cshperspectives.cshlp.org/content/early/2019/07/15/cshperspect.a035428.full.pdf+html>. URL: <http://cshperspectives.cshlp.org/content/early/2019/07/15/cshperspect.a035428.abstract>.
- [18] B.J. Williams and M.T.A. Saif. “Phase Dependent Mechanosensitivity in Cardiomyocytes”. In: *Experimental Mechanics* 59.3 (Mar. 2019), pp. 387–393. ISSN: 1741-2765. DOI: 10.1007/s11340-019-00472-9. URL: <https://doi.org/10.1007/s11340-019-00472-9>.
- [19] Tulio E. Bertorini. “1 - Neuromuscular Anatomy and Function”. In: *Neuromuscular Case Studies*. Ed. by Tulio E. Bertorini. Philadelphia: Butterworth-Heinemann, 2008, pp. 1–25. ISBN: 978-0-7506-7332-7. DOI: <https://doi.org/10.1016/B978-0-7506-7332-7.50005-2>. URL: <http://www.sciencedirect.com/science/article/pii/B9780750673327500052>.
- [20] Walter F. Boron MD PhD. *Medical Physiology*. Saunders, Nov. 2008. Chap. 22. ISBN: 1416031154. URL: <https://www.xarg.org/ref/a/1416031154/>.
- [21] Elaine Nicpon Marieb. *Human anatomy physiology / Elaine N. Marieb, R.N., Ph. D., Holyoke Community College, Katja Hoehn, M.D., Ph. D., Mount Royal University*. eng. Tenth edition. Boston: Pearson. ISBN: 9780321927040.
- [22] Brandon J. Biesiadecki et al. “Tri-modal regulation of cardiac muscle relaxation intracellular calcium decline, thin filament deactivation, and cross-bridge cycling kinetics”. In: *Biophysical Reviews* 6.3-4 (July 2014), pp. 273–289. DOI: 10.1007/s12551-014-0143-5. URL: <https://doi.org/10.1007/s12551-014-0143-5>.
- [23] Donald M. Bers. “16 - Excitation–Contraction Coupling”. In: *Cardiac Electrophysiology: From Cell to Bedside (Seventh Edition)*. Ed. by Douglas P. Zipes, José Jalife, and William G. Stevenson. Seventh Edition. Elsevier, 2018, pp. 151–159. ISBN: 978-0-323-44733-1. DOI: <https://doi.org/10.1016/B978-0-323-44733-1.00016-X>. URL: <http://www.sciencedirect.com/science/article/pii/B978032344733100016X>.
- [24] Berend J. van Meer et al. “Simultaneous measurement of excitation-contraction coupling parameters identifies mechanisms underlying contractile responses of hiPSC-derived cardiomyocytes”. In: *Nature Communications* 10.1 (Sept. 2019). DOI: 10.1038/s41467-019-12354-8. URL: <https://doi.org/10.1038/s41467-019-12354-8>.
- [25] Donald W. Hilgemann. “Control of cardiac contraction by sodium: Promises, reckonings, and new beginnings”. In: *Cell Calcium* 85 (Jan. 2020), p. 102129. DOI: 10.1016/j.ceca.2019.102129. URL: <https://doi.org/10.1016/j.ceca.2019.102129>.
- [26] Emily R. Pfeiffer et al. “Biomechanics of Cardiac Electromechanical Coupling and Mechanoelectric Feedback”. In: *Journal of Biomechanical Engineering* 136.2 (Feb. 2014). DOI: 10.1115/1.4026221. URL: <https://doi.org/10.1115/1.4026221>.
- [27] Donald M Bers. “Regulation of cellular calcium in cardiac myocytes”. In: *Comprehensive Physiology* (2011), pp. 335–387.
- [28] D.M. Bers. “Cardiac excitation-contraction coupling”. In: *Nature* 415.6868 (2002). cited By 2558, pp. 198–205. DOI: 10.1038/415198a.
- [29] N. Balakina-Vikulova et al. “Mechano-Electric Feedbacks in a New Model of the Excitation-Contraction Coupling in Human Cardiomyocytes”. In: *2018 Computing in Cardiology Conference (CinC)*. Vol. 45. Sept. 2018, pp. 1–4. DOI: 10.22489/CinC.2018.065.

- [30] Viviane Timmermann et al. “An integrative appraisal of mechano-electric feedback mechanisms in the heart”. In: *Progress in Biophysics and Molecular Biology* 130 (Nov. 2017), pp. 404–417. DOI: 10.1016/j.pbiomolbio.2017.08.008. URL: <https://doi.org/10.1016/j.pbiomolbio.2017.08.008>.
- [31] Peter Kohl, Frederick Sachs, and Michael R Franz. *Cardiac mechano-electric coupling and arrhythmias*. Oxford University Press, 2011.
- [32] M J Lab. “Contraction-excitation feedback in myocardium. Physiological basis and clinical relevance.” In: *Circulation Research* 50.6 (1982), pp. 757–766. DOI: 10.1161/01.RES.50.6.757. eprint: <https://www.ahajournals.org/doi/pdf/10.1161/01.RES.50.6.757>. URL: <https://www.ahajournals.org/doi/abs/10.1161/01.RES.50.6.757>.
- [33] T. Alexander Quinn and Peter Kohl. “Mechano-sensitivity of cardiac pacemaker function: Pathophysiological relevance, experimental implications, and conceptual integration with other mechanisms of rhythmicity”. In: *Progress in Biophysics and Molecular Biology* 110.2 (2012). SI: Beating Heart, pp. 257–268. ISSN: 0079-6107. DOI: <https://doi.org/10.1016/j.pbiomolbio.2012.08.008>. URL: <http://www.sciencedirect.com/science/article/pii/S0079610712000752>.
- [34] Barbara Calabrese et al. “Mechanosensitivity of N-Type Calcium Channel Currents”. In: *Biophysical Journal* 83.5 (Nov. 2002), pp. 2560–2574. DOI: 10.1016/s0006-3495(02)75267-3. URL: [https://doi.org/10.1016/s0006-3495\(02\)75267-3](https://doi.org/10.1016/s0006-3495(02)75267-3).
- [35] D DIFRANCESCO. “Serious workings of the funny current”. In: *Progress in Biophysics and Molecular Biology* 90.1-3 (Jan. 2006), pp. 13–25. DOI: 10.1016/j.pbiomolbio.2005.05.001. URL: <https://doi.org/10.1016/j.pbiomolbio.2005.05.001>.
- [36] Wei Lin et al. “Dual Stretch Responses of mHCN2 Pacemaker Channels: Accelerated Activation, Accelerated Deactivation”. In: *Biophysical Journal* 92.5 (Mar. 2007), pp. 1559–1572. DOI: 10.1529/biophysj.106.092478. URL: <https://doi.org/10.1529/biophysj.106.092478>.
- [37] Catherine E. Morris and Peter F. Juranka. “Lipid Stress at Play: Mechanosensitivity of Voltage-Gated Channels”. In: *Mechanosensitive Ion Channels, Part B*. Elsevier, 2007, pp. 297–338. DOI: 10.1016/s1063-5823(06)59011-8. URL: [https://doi.org/10.1016/s1063-5823\(06\)59011-8](https://doi.org/10.1016/s1063-5823(06)59011-8).
- [38] Catherine E. Morris and Peter F. Juranka. “Nav Channel Mechanosensitivity: Activation and Inactivation Accelerate Reversibly with Stretch”. In: *Biophysical Journal* 93.3 (Aug. 2007), pp. 822–833. DOI: 10.1529/biophysj.106.101246. URL: <https://doi.org/10.1529/biophysj.106.101246>.
- [39] Diane Dalecki et al. “Thresholds for premature ventricular contractions in frog hearts exposed to lithotripter fields”. In: *Ultrasound in Medicine Biology* 17.4 (1991), pp. 341–346. ISSN: 0301-5629. DOI: [https://doi.org/10.1016/0301-5629\(91\)90133-H](https://doi.org/10.1016/0301-5629(91)90133-H). URL: <http://www.sciencedirect.com/science/article/pii/S030156299190133H>.
- [40] Nils Hersch et al. “The constant beat: cardiomyocytes adapt their forces by equal contraction upon environmental stiffening”. In: *Biology Open* 2.3 (2013), pp. 351–361. DOI: 10.1242/bio.20133830. eprint: <https://bio.biologists.org/content/2/3/351.full.pdf>. URL: <https://bio.biologists.org/content/2/3/351>.
- [41] Mark S. Link et al. “An Experimental Model of Sudden Death Due to Low-Energy Chest-Wall Impact (Comotio Cordis)”. In: *New England Journal of Medicine* 338.25 (1998). PMID: 9632447, pp. 1805–1811. DOI: 10.1056/NEJM199806183382504. eprint: <https://doi.org/10.1056/NEJM199806183382504>. URL: <https://doi.org/10.1056/NEJM199806183382504>.
- [42] Ohad Cohen and Samuel A. Safran. “Theory of frequency response of mechanically driven cardiomyocytes”. In: *Scientific Reports* 8.1 (Feb. 2018). DOI: 10.1038/s41598-018-20307-2. URL: <https://doi.org/10.1038/s41598-018-20307-2>.
- [43] Hai Hu and Frederick Sachs. “Stretch-Activated Ion Channels in the Heart”. In: *Journal of Molecular and Cellular Cardiology* 29.6 (1997), pp. 1511–1523. ISSN: 0022-2828. DOI: <https://doi.org/10.1006/jmcc.1997.0392>. URL: <http://www.sciencedirect.com/science/article/pii/S0022282897903928>.
- [44] Peter Kohl et al. “Sudden cardiac death by Commotio cordis: role of mechano—electric feedback”. In: *Cardiovascular Research* 50.2 (May 2001), pp. 280–289. ISSN: 0008-6363. DOI: 10.1016/S0008-6363(01)00194-8. eprint: <http://oup.prod.sis.lan/cardiavasres/article-pdf/50/2/280/766437/50-2-280.pdf>. URL: [https://doi.org/10.1016/S0008-6363\(01\)00194-8](https://doi.org/10.1016/S0008-6363(01)00194-8).

- [45] Sarbjot Kaur et al. “Stretch modulation of cardiac contractility: importance of myocyte calcium during the slow force response”. In: *Biophysical Reviews* 12.1 (Jan. 2020), pp. 135–142. DOI: 10.1007/s12551-020-00615-6. URL: <https://doi.org/10.1007/s12551-020-00615-6>.
- [46] Heping Cheng and W. J. Lederer. “Calcium Sparks”. In: *Physiological Reviews* 88.4 (2008). PMID: 18923188, pp. 1491–1545. DOI: 10.1152/physrev.00030.2007. eprint: <https://doi.org/10.1152/physrev.00030.2007>. URL: <https://doi.org/10.1152/physrev.00030.2007>.
- [47] P. Greillier et al. “Therapeutic Ultrasound for the Heart: State of the Art”. In: *IRBM* 39.4 (Aug. 2018), pp. 227–235. DOI: 10.1016/j.irbm.2017.11.004. URL: <https://doi.org/10.1016/j.irbm.2017.11.004>.
- [48] F. Marquet et al. “Non-invasive cardiac pacing with image-guided focused ultrasound”. In: *Scientific Reports* 6 (2016). DOI: 10.1038/srep36534.
- [49] Alan G. MacRobbie et al. “Thresholds for premature contractions in murine hearts exposed to pulsed ultrasound”. In: *Ultrasound in Medicine & Biology* 23.5 (Jan. 1997), pp. 761–765. DOI: 10.1016/s0301-5629(97)00049-5. URL: [https://doi.org/10.1016/s0301-5629\(97\)00049-5](https://doi.org/10.1016/s0301-5629(97)00049-5).
- [50] Diane Dalecki et al. “Premature cardiac contractions produced by ultrasound and microbubble contrast agents in mice”. In: *Acoustics Research Letters Online* 6.3 (2005), pp. 221–226. DOI: 10.1121/1.1935467. eprint: <https://doi.org/10.1121/1.1935467>. URL: <https://doi.org/10.1121/1.1935467>.
- [51] Diane Dalecki, Carol H. Raeman, and Edwin L. Carstensen. “Effects of pulsed ultrasound on the frog heart: II. An investigation of heating as a potential mechanism”. In: *Ultrasound in Medicine & Biology* 19.5 (Jan. 1993), pp. 391–398. DOI: 10.1016/0301-5629(93)90058-v. URL: [https://doi.org/10.1016/0301-5629\(93\)90058-v](https://doi.org/10.1016/0301-5629(93)90058-v).
- [52] Diane Dalecki et al. “Effects of pulsed ultrasound on the frog heart: III. The radiation force mechanism”. In: *Ultrasound in Medicine & Biology* 23.2 (1997), pp. 275–285. ISSN: 0301-5629. DOI: [https://doi.org/10.1016/S0301-5629\(96\)00209-8](https://doi.org/10.1016/S0301-5629(96)00209-8). URL: <http://www.sciencedirect.com/science/article/pii/S0301562996002098>.
- [53] Mark A. Hanson. *Health effects of exposure to ultrasound and infrasound: report of the independent advisory group on non-ionising radiation*. Health Protection Agency, Feb. 2010. URL: <https://eprints.soton.ac.uk/348624/>.
- [54] Andrew Fleischman et al. “Ultrasound-induced modulation of cardiac rhythm in neonatal rat ventricular cardiomyocytes”. In: *Journal of Applied Physiology* 118.11 (June 2015), pp. 1423–1428. DOI: 10.1152/jappphysiol.00980.2014. URL: <https://doi.org/10.1152/jappphysiol.00980.2014>.
- [55] Diane Dalecki. “Mechanical Bioeffects of Ultrasound”. In: *Annual Review of Biomedical Engineering* 6.1 (2004). PMID: 15255769, pp. 229–248. DOI: 10.1146/annurev.bioeng.6.040803.140126. eprint: <https://doi.org/10.1146/annurev.bioeng.6.040803.140126>. URL: <https://doi.org/10.1146/annurev.bioeng.6.040803.140126>.
- [56] Douglas L. Miller, Chunyan Dou, and Benedict R. Lucchesi. “Are ECG Premature Complexes Induced by Ultrasonic Cavitation Electrophysiological Responses to Irreversible Cardiomyocyte Injury?” In: *Ultrasound in Medicine & Biology* 37.2 (2011), pp. 312–320. ISSN: 0301-5629. DOI: <https://doi.org/10.1016/j.ultrasmedbio.2010.11.012>. URL: <http://www.sciencedirect.com/science/article/pii/S0301562910006435>.
- [57] Andrew R. Kohut et al. “The potential of ultrasound in cardiac pacing and rhythm modulation”. In: *Expert Review of Medical Devices* 13.9 (Aug. 2016), pp. 815–822. DOI: 10.1080/17434440.2016.1217772. URL: <https://doi.org/10.1080/17434440.2016.1217772>.
- [58] Jacques S. Abramowicz et al. “Fetal Thermal Effects of Diagnostic Ultrasound”. In: *Journal of Ultrasound in Medicine* 27.4 (2008), pp. 541–559. DOI: 10.7863/jum.2008.27.4.541. eprint: <https://onlinelibrary.wiley.com/doi/pdf/10.7863/jum.2008.27.4.541>. URL: <https://onlinelibrary.wiley.com/doi/abs/10.7863/jum.2008.27.4.541>.
- [59] Jan Kubanek et al. “Ultrasound elicits behavioral responses through mechanical effects on neurons and ion channels in a simple nervous system”. In: *Journal of Neuroscience* (2018). ISSN: 0270-6474. DOI: 10.1523/JNEUROSCI.1458-17.2018. eprint: <https://www.jneurosci.org/content/early/2018/02/20/JNEUROSCI.1458-17.2018.full.pdf>. URL: <https://www.jneurosci.org/content/early/2018/02/20/JNEUROSCI.1458-17.2018>.

- [60] Richard D. Rabbitt et al. “Heat pulse excitability of vestibular hair cells and afferent neurons”. In: *Journal of Neurophysiology* 116.2 (2016). PMID: 27226448, pp. 825–843. DOI: 10.1152/jn.00110.2016. eprint: <https://doi.org/10.1152/jn.00110.2016>. URL: <https://doi.org/10.1152/jn.00110.2016>.
- [61] Melvin E. Stratmeyer et al. “Fetal Ultrasound”. In: *Journal of Ultrasound in Medicine* 27.4 (2008), pp. 597–605. DOI: 10.7863/jum.2008.27.4.597. eprint: <https://onlinelibrary.wiley.com/doi/pdf/10.7863/jum.2008.27.4.597>. URL: <https://onlinelibrary.wiley.com/doi/abs/10.7863/jum.2008.27.4.597>.
- [62] T.G. Leighton. “5 - Effects and Mechanisms”. In: *The Acoustic Bubble*. Ed. by T.G. Leighton. Academic Press, 1994, pp. 439–590. ISBN: 978-0-12-441920-9. DOI: <https://doi.org/10.1016/B978-0-12-441920-9.50010-9>. URL: <http://www.sciencedirect.com/science/article/pii/B9780124419209500109>.
- [63] Armen P. Sarvazyan, Oleg V. Rudenko, and Wesley L. Nyborg. “Biomedical Applications of Radiation Force of Ultrasound: Historical Roots and Physical Basis”. In: *Ultrasound in Medicine & Biology* 36.9 (Sept. 2010), pp. 1379–1394. DOI: 10.1016/j.ultrasmedbio.2010.05.015. URL: <https://doi.org/10.1016/j.ultrasmedbio.2010.05.015>.
- [64] D G Allen and J C Kentish. “Calcium concentration in the myoplasm of skinned ferret ventricular muscle following changes in muscle length.” In: *The Journal of Physiology* 407.1 (1988), pp. 489–503. DOI: 10.1113/jphysiol.1988.sp017427. eprint: <https://physoc.onlinelibrary.wiley.com/doi/pdf/10.1113/jphysiol.1988.sp017427>. URL: <https://physoc.onlinelibrary.wiley.com/doi/abs/10.1113/jphysiol.1988.sp017427>.
- [65] S Kurihara and K Komukai. “Tension-dependent changes of the intracellular Ca²⁺ transients in ferret ventricular muscles.” In: *The Journal of Physiology* 489.3 (Dec. 1995), pp. 617–625. DOI: 10.1113/jphysiol.1995.sp021077. URL: <https://doi.org/10.1113/jphysiol.1995.sp021077>.
- [66] D.M. Bers. “Calcium fluxes involved in control of cardiac myocyte contraction”. In: *Circulation Research* 87.4 (2000), pp. 275–281. DOI: 10.1161/01.RES.87.4.275.
- [67] Meaghan A. O’Reilly and Kullervo Hynynen. “Emerging non-cancer applications of therapeutic ultrasound”. In: *International Journal of Hyperthermia* 31.3 (2015), pp. 310–318. DOI: 10.3109/02656736.2015.1004375. eprint: <https://doi.org/10.3109/02656736.2015.1004375>. URL: <https://doi.org/10.3109/02656736.2015.1004375>.
- [68] Jagannathan Sundaram, Berlyn R. Mellein, and Samir Mitragotri. “An Experimental and Theoretical Analysis of Ultrasound-Induced Permeabilization of Cell Membranes”. In: *Biophysical Journal* 84.5 (2003), pp. 3087–3101. ISSN: 0006-3495. DOI: [https://doi.org/10.1016/S0006-3495\(03\)70034-4](https://doi.org/10.1016/S0006-3495(03)70034-4). URL: <http://www.sciencedirect.com/science/article/pii/S0006349503700344>.
- [69] Ryo Suzuki et al. “Effective gene delivery with novel liposomal bubbles and ultrasonic destruction technology”. In: *International Journal of Pharmaceutics* 354.1 (2008). Special Issue in Honor of Prof. Tsuneji Nagai, pp. 49–55. ISSN: 0378-5173. DOI: <https://doi.org/10.1016/j.ijpharm.2007.10.034>. URL: <http://www.sciencedirect.com/science/article/pii/S0378517307008629>.
- [70] Evan C Unger et al. “Local drug and gene delivery through microbubbles”. In: *Progress in Cardiovascular Diseases* 44.1 (2001). Contrast Echocardiography, pp. 45–54. ISSN: 0033-0620. DOI: <https://doi.org/10.1053/pcad.2001.26443>. URL: <http://www.sciencedirect.com/science/article/pii/S0033062001000184>.
- [71] S. Ibsen et al. “Sonogenetics is a non-invasive approach to activating neurons in *Caenorhabditis elegans*”. In: *Nature Communications* 6 (2015). cited By 87. DOI: 10.1038/ncomms9264. URL: <https://www.scopus.com/inward/record.uri?eid=2-s2.0-84941769671&doi=10.1038%2fncomms9264&partnerID=40&md5=1e0c162944f528937a7c1d491229927b>.
- [72] Verena Schwach and Robert Passier. “Generation and purification of human stem cell-derived cardiomyocytes”. In: *Differentiation* 91.4-5 (Apr. 2016), pp. 126–138. DOI: 10.1016/j.diff.2016.01.001. URL: <https://doi.org/10.1016/j.diff.2016.01.001>.
- [73] Jeroen Bugter. *In vitro modeling of cardiac arrhythmia*. Master Thesis. 2020.
- [74] K.R. Gee et al. “Chemical and physiological characterization of fluo-4 Ca²⁺-indicator dyes”. In: *Cell Calcium* 27.2 (Feb. 2000), pp. 97–106. DOI: 10.1054/ceca.1999.0095. URL: <https://doi.org/10.1054/ceca.1999.0095>.
- [75] *Fluo Calcium Indicators*. MP 01240. Via <https://www.thermofisher.com/>. Molecular Probes. Feb. 2011.

Appendix A

Extra figures

A.1 Contractions: histograms and shape

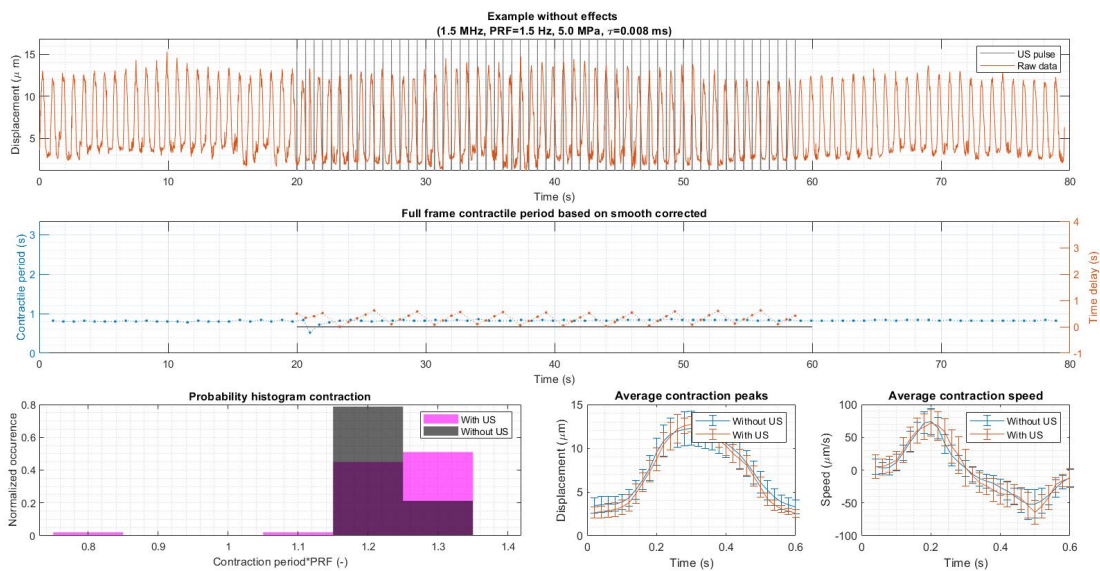


Figure A.1: Overview of tissue displacement, contraction periods, average contraction peak and average contraction speed.

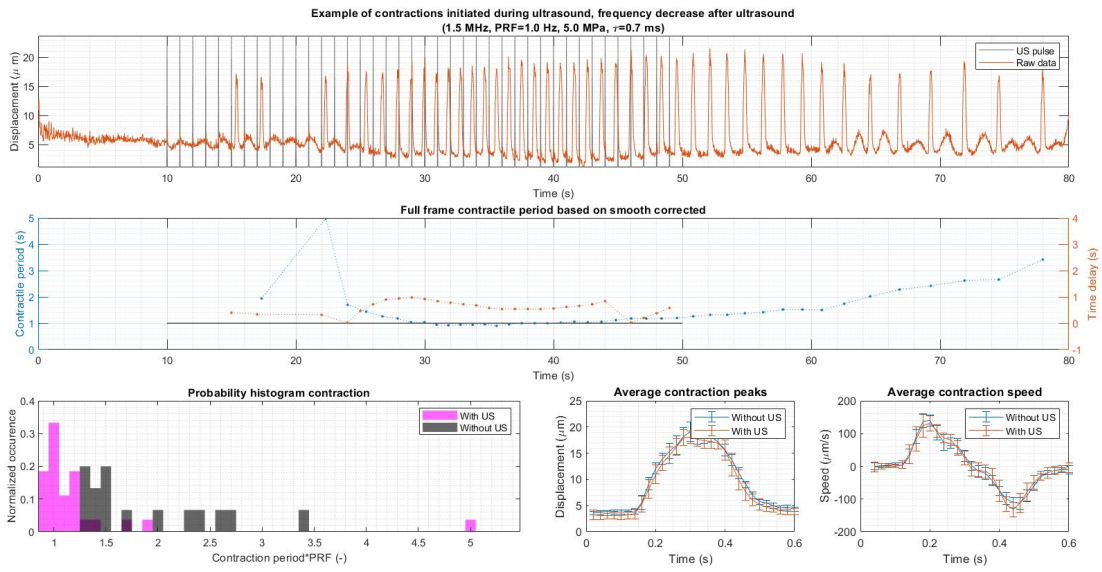


Figure A.2: Overview of tissue displacement, contraction periods, average contraction peak and average contraction speed.

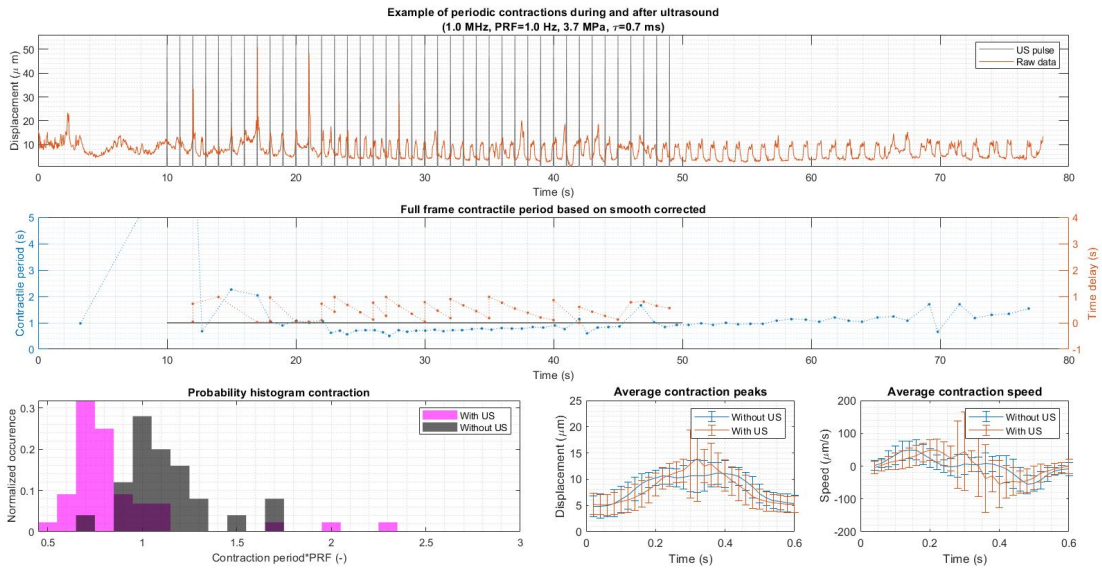


Figure A.3: Overview of tissue displacement, contraction periods, average contraction peak and average contraction speed.

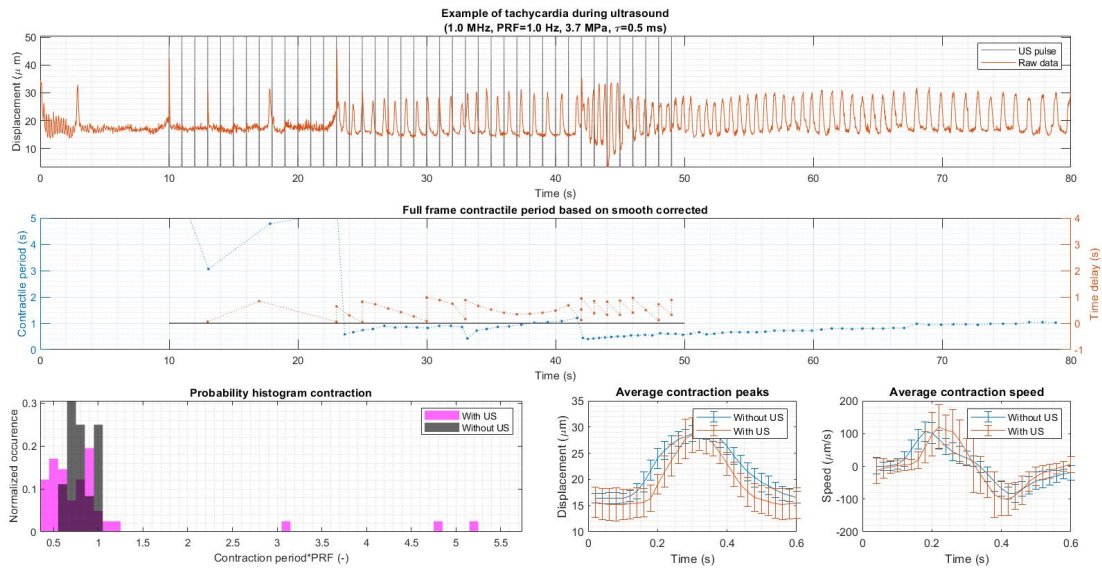


Figure A.4: Overview of tissue displacement, contraction periods, average contraction peak and average contraction speed.

A.2 Histogram view

Another series consisting of 4 videos of 60 seconds pre-US, 60 seconds US and 60 seconds post US at 1.0 MHz, 3.7MPa and 1.5Hz PRF is shown in the following figures. In figure A.5 the contraction period without ultrasound is constant, it decreases with increasing US pulse duration. The peak maxima, peak area and speed maxima are not constant without ultrasound (figures A.6, A.7 and A.8 respectively) so therefore can not be compared with US.

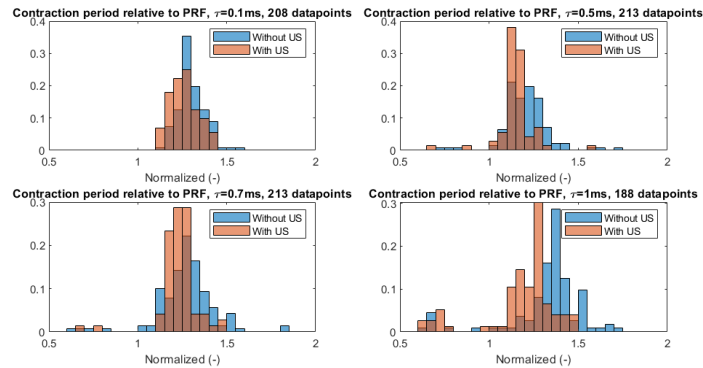


Figure A.5: Contraction period per pulse duration, 1.0 MHz, 3.7MPa, 1.5Hz.

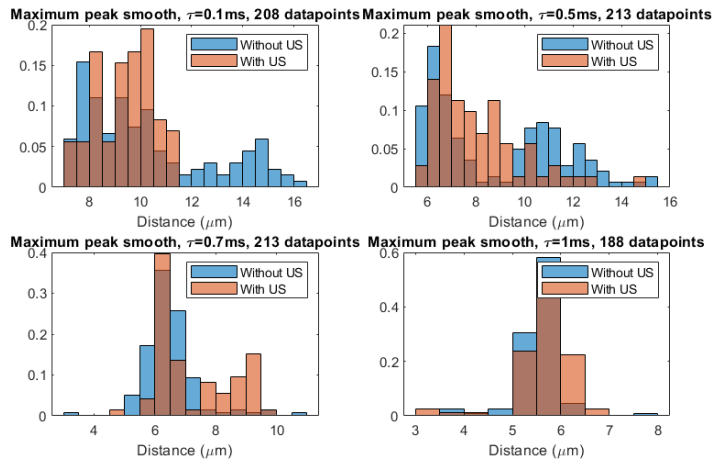


Figure A.6: Peak maxima per pulse duration, 1.0 MHz, 3.7MPa, 1.5Hz.

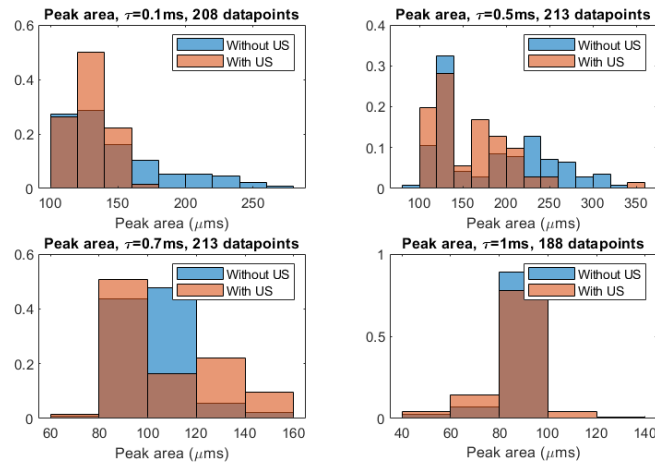


Figure A.7: Peak area per pulse duration, 1.0 MHz, 3.7MPa, 1.5Hz.

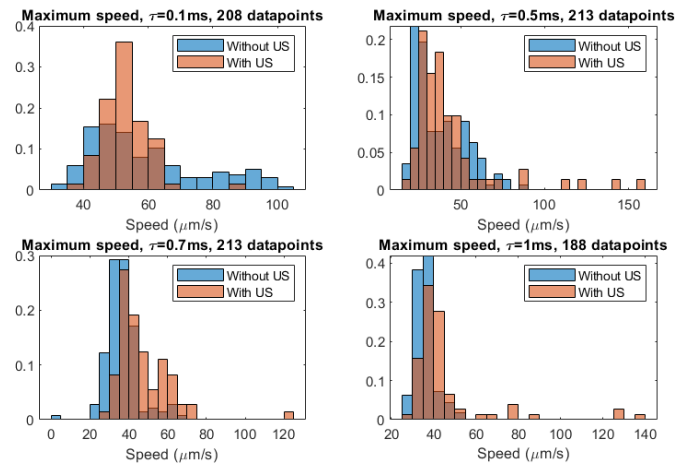


Figure A.8: Speed maxima per pulse duration, 1.0 MHz, 3.7MPa, 1.5Hz.

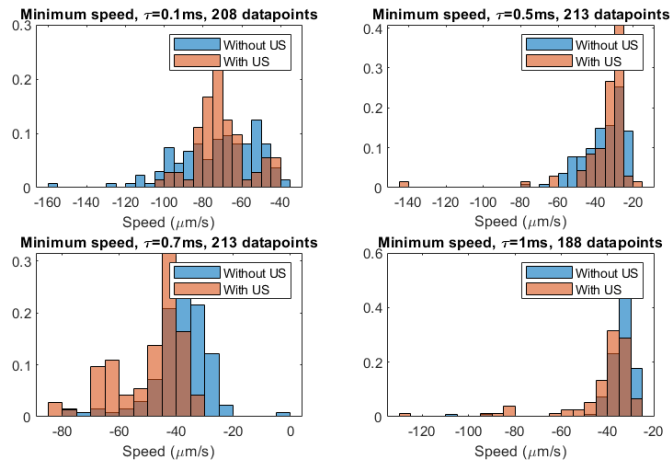


Figure A.9: Speed minima per pulse duration, 1.0 MHz, 3.7MPa, 1.5Hz.

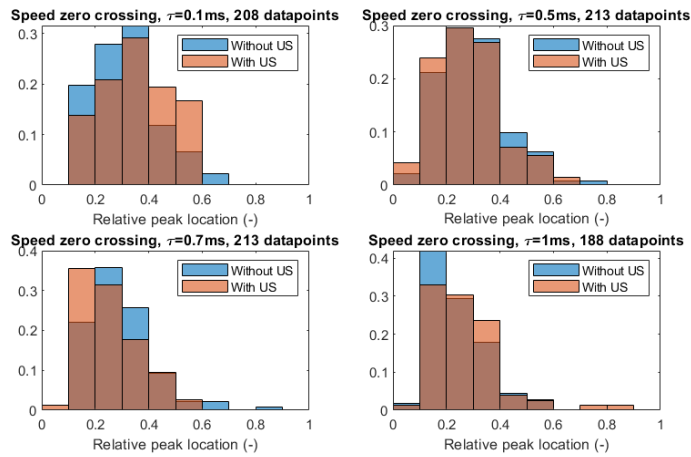


Figure A.10: Speed zero-crossing per pulse duration, 1.0 MHz, 3.7MPa, 1.5Hz.

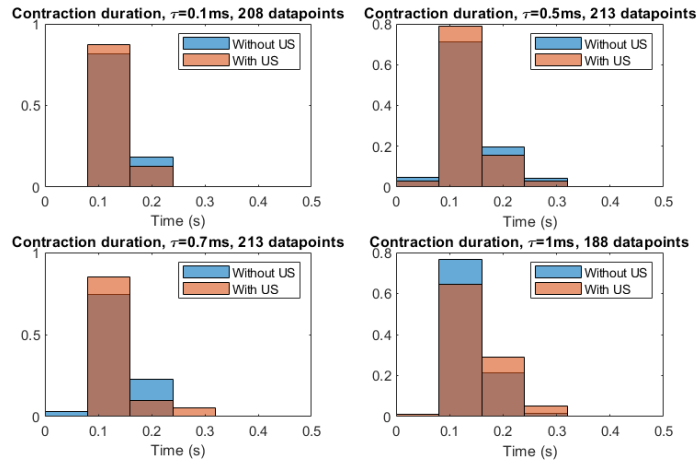


Figure A.11: Peak duration per pulse duration, 1.0 MHz, 3.7MPa, 1.5Hz.

Appendix B

Recommendation calcium imaging

B.1 Theory

To track the intracellular calcium ion concentration ($[Ca^{2+}]$) indicators are used. An example is fluo-4. It is a fluorescent compound that undergoes large fluorescence enhancement upon binding Ca^{2+} [74]. Main fluo-4 characteristics are a maximal excitation wavelength 494 nm for ion-bound and 491 nm for ion-free, maximal emission wavelength of 516 nm with a dissociation constant of 345 nM. Figure B.1 depicts the spectrum of the light source (Ushio America 102D mercury bulb 100W), fluo-4 excitation & emission and excitation & emission filters.

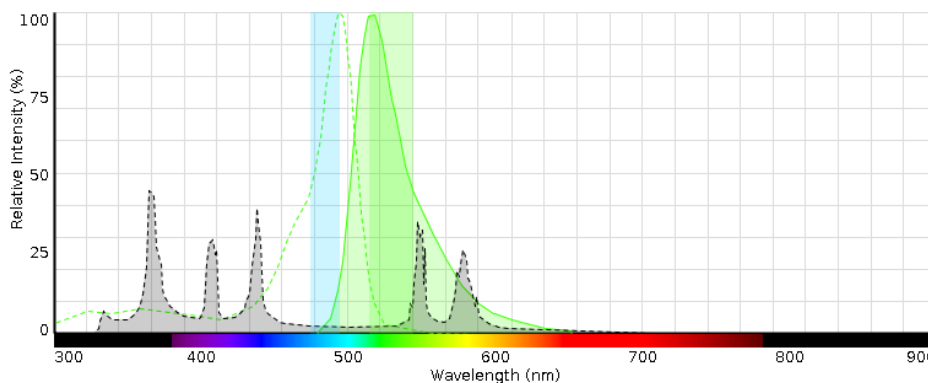


Figure B.1: ThermoFisher spectraviewer of fluo-4 with FITC excitation and emission filters [75]. The dark grey spectrum is the mercury light, the green is the fluo-4 spectrum; dotted is excitation, filled is emission. The light blue band is the excitation filter and the light green band is the emission filter.

B.2 Method

Before measurements can start, the tissue sample has to be dyed. This is done by FLUO-4-AM. FLUO-4-AM is diluted (1 mM) into an aliquot of DMSO stock solution. Thereafter the stock is diluted into the medium (BPEL) in a final concentration of $1 \mu M$, this is defined as the dyeing solution. Next off the medium at the EBs is removed and replaced by 0.4 mL dyeing solution. The sample is stained for 30 minutes at $37^\circ C$. After staining the EBs are washed with dye-free medium and for two hours the samples are ready for experiments.

B.3 Experiments

Several experiment sets are designed. In each set (A, B, C, D, and E) one parameter will be varied. Each experiment set will be performed three times a three different tissues, so nine times in total. An overview of the experiment sets is stated in table B.1.

The standard measurement is used in all sets; PRF 1.5Hz, centre frequency 1.5 MHz, pulse duration 1.0 ms, and

peak to peak pressure 5 MPa. In set A the pulse duration is studied. In set B the centre frequency is studied from 0.7 MHz to 1.5 MHz. In set C the pressure is varied: C1, C3, and C5 can be compared to study the effect of pressure, whereas C2 can be compared with A1 and C4 can be compared with A2 to study the effect of the maximum temperature increase (see equation 1.3), since the Q values are equal. In set D the total pulse time of 1.0 ms is divided into 1, 5, or 10 bursts of 1.0, 0.2, or 0.1 ms respectively. Set E studies cavitation; E1 and E2 can be compared with A3 because the mechanical index is equal. Set F studies acoustic radiation force; F1 and F2 can be compared with A3 because the acoustic radiation force is approximately equal. Each experiment consists of 100 seconds before the ultrasound, 100 seconds during ultrasound and 100 seconds after the ultrasound application.

Table B.1: Overview of proposed experiment plan

Measurement	Pressure (MPa)	PRF (Hz)	# bursts per PRF	Burst duration (ms)	Rest after burst (ms)	Total pulse time (ms)	f_c (MHz)	Duty cycle
A1	5.00	1.5	1	0.500	0.00	0.500	1.5	100%
A2	5.00	1.5	1	0.700	0.00	0.700	1.5	100%
A3, B3, C5, D3	5.00	1.5	1	1.000	0.00	1.000	1.5	100%
B1	5.00	1.5	1	1.000	0.00	1.000	0.7	100%
B2	5.00	1.5	1	1.000	0.00	1.000	1.0	100%
B4	5.00	1.5	1	1.000	0.00	1.000	1.3	100%
C1	2.50	1.5	1	1.000	0.00	1.000	1.5	100%
C2	3.54	1.5	1	1.000	0.00	1.000	1.5	100%
C3	3.75	1.5	1	1.000	0.00	1.000	1.5	100%
C4	4.18	1.5	1	1.000	0.00	1.000	1.5	100%
D1	5.00	1.5	5	0.200	0.10	1.000	1.5	67%
D2	5.00	1.5	10	0.100	0.10	1.000	1.5	50%
E1	3.42	1.5	1	1.000	0.00	1.000	0.7	100%
E2	4.10	1.5	1	1.000	0.00	1.000	1.0	100%
F1	2.33	1.5	1	1.000	0.00	1.000	0.7	100%
F2	3.33	1.5	1	1.000	0.00	1.000	1.0	100%

B.4 Data analysis

In order to analyze the calcium imaging, the videos have to be analyzed.

- Load the videos
- Select ROI at frame 1
- Analysis of pixel intensities
 1. On raw data; average pixel intensity of ROI for each frame.
 2. Data with background subtraction; subtract the last frame as background from each frame. Calculate resulting pixel intensities within ROI.
 3. Data with average frame subtraction (normalization). Make use of $\Delta F/F_0 = (F - \bar{F})/\bar{F}$
- Plot the pixel intensities in time domain and frequency domain

The pixel intensities represent the relative intracellular calcium concentration. By high pass filtering (above 0.3 Hz), the photobleaching drift can be removed. As a result the speed of calcium influx before, during and after ultrasound application can be compared. Furthermore, cross-correlations can be used to compare calcium behaviour.

Appendix C

Matlab scrips

C.1 Script to process .tif files to one .AVI file

Fully written by Dafne Groener.

```
1 %% This file converts .tiff files to 1 .AVI file
2 clc; clear all; close all;
3
4 %% Step 1: select all xiseq files (=same name as folders) that need to be analyzed
5 % ask for the files
6 % Select as many xiseq files if you want, but only in the same folder!!
7 [all_files , path] = uigetfile('*.xiseq', 'multiselect', 'on');
8 tic
9 %% Step 2: Find the folder for each measurement and find the folder
10 % Loop for all files
11 for jj=1:length(all_files)
12     % Add a folder for the results
13     % Find all the slashes
14     pobar = strfind(path, '\');
15     % Construct the correct foldername
16     folder=join([path(1:pobar(end)) all_files(jj)]);
17     folder{1,1}(pobar(end)+1)='';
18     folder{1,1}(end-5:end)='';
19     folder=join([folder '_files']);
20     folder{1,1}(end-6)='';
21     % Open the cell
22     yourfolder=folder{1,1};
23
24     % Find the amount of frames; number of tif files in 'yourfolder'
25     a = dir(fullfile(yourfolder, '*.tif'));
26     framenumbers=length(a);
27
28     % Define the video
29     videoname=all_files(jj);
30     videoname=videoname{1,1}(1:end-6);
31     v = VideoWriter([path videoname, '.avi'], 'Motion JPEG AVI');
32     v.FrameRate=50;
33     open(v);
34
35     % Add all framenumbers to the video
36     for jk=1:framenumbers
37         framename=char(['00000000', num2str(jk)]);
```

```

38     framename=framename(end-5:end);
39     A=imread([yourfolder '\ ' framename '.tif']);
40     writeVideo(v,A);
41     end
42     close(v);
43 end
44 toc

```

C.2 Script to do PIV analysis at .AVI movies

Fully written by Guillaume Lajoinie, including functions used in the script.

```

1  %% this code and the dependant codes are written by G. Lajoinie , April 2020
2
3
4  %%%%%%%%%%%%%%%%%%%%%%%%%%%%%%%%%%%%%%%%%%%%%%%%%%%%%%%%%%%%%%%%%%%%%%%%%
5  %%%%%%%%%%%%%%%%%%%%%%%%%%%%%%%%%%%%%%%%%%%%%%%%%%%%%%%%%%%%%%%%%%%%%%%%%
6  %%%%%%%%%%%%%%%%%%%%%%%%%%%%%%%%%%%%%%%%%%%%%%%%%%%%%%%%%%%%%%%%%%%%%%%%%
7
8
9  % when action is required, you will be prompted in the command window
10 display('when action is required, you will be prompted in the command window');
11
12 % the mat file are automatically saved.
13
14 % You may want to change the variable "resize_factor"
15 % it is now set to 3, which accelerates the analysis by ~10x. if you
16 % decrease it, it will be slower, but more precise. 3 is a good compromise.
17 %(increasing it will decrease your precision)
18
19
20 % I would not play with the other settings
21
22
23 %%% note: one could add a distance penalization on the cross-correlation
24
25
26 %%%%%%%%%%%%%%%%%%%%%%%%%%%%%%%%%%%%%%%%%%%%%%%%%%%%%%%%%%%%%%%%%%%%%%%%%
27 %%%%%%%%%%%%%%%%%%%%%%%%%%%%%%%%%%%%%%%%%%%%%%%%%%%%%%%%%%%%%%%%%%%%%%%%%
28 %%%%%%%%%%%%%%%%%%%%%%%%%%%%%%%%%%%%%%%%%%%%%%%%%%%%%%%%%%%%%%%%%%%%%%%%%
29
30
31
32
33 %%% Clear the workspace etc.
34
35 clear all
36 clc
37 close all
38
39 % select the folders and adapt files so it only contains the files of
40 % interest
41 fold = uigetdir('', 'select the folder containing the movies');
42 files = dir(fold);
43 files(1:2) = [];

```

```

44 %%
45 addpath(genpath('G:/for dafne'))
46 addpath(genpath('G:/05. Experimental data'))
47 % make a cell that contains the moveis of interest
48 movie_list = {};
49
50 for i = 1:length(files)
51
52     if ~isempty(strfind(files(i).name, '.avi'))
53         movie_list{end+1} = files(i).name;
54     end
55 end
56
57 movie_list = movie_list';
58
59 % Make a new folder to save the results in later on
60 step_1_fol = 'Step_1_analysis';
61 if ~.isdir(step_1_fol)
62     mkdir(step_1_fol);
63 end
64 %% Analysis for all movies
65 for jj = 1:length(movie_list)
66
67     % Identify the movie of interest and folder of interest and xiseq file
68     % of interest
69     filoc = movie_list{jj};
70     paloc = [fold '/'];
71     fi_xim = [filoc(1:end-4) '.xiseq'];
72
73     if isfile([step_1_fol '/step_1_' filoc(1:end-4) '.mat'])
74
75     else
76         try
77             time = import_time_sptamps([paloc fi_xim]);
78             time = time./(2^32-1).*2.*pi-pi;
79             time = unwrap(time);
80             time = (time+pi)./2./pi.*(2^32-1);
81
82             time = time.*1e-6;
83             time(1) = []; % first frme is the reference for the analysis
84             time(end) = []; % the last number os a rubbish nan
85         catch
86
87             time = [];
88
89         end
90
91     % Define variables
92     kernell = 64;
93     range = 156;
94     overlap = floor(kernell/2);
95     resize_factor = 3;
96
97 %%
98 % Input: filoc (char: video name), paloc (char: folder name), resize_factor
99 % (variable), kernell(variable), range(variable), overlap(variable)

```

```

100
101 % Output: disp_1 (?), disp_2(?), XCorr_val (?), XCorr_contrast (?), kernell
102 % (adapted by function due to resize factor), range (adapted by function
103 % due to resize factor), overlap (adapted by function due to resize factor).
104     [disp_1 , disp_2 , XCorr_val , XCorr_contrast , kernell , range , overlap] ...
105     = My_PIV_2_func(filoc , paloc , resize_factor , kernell , range , overlap);
106 % Save the result
107     save([step_1_fol '/step_1_' filoc(1:end-4) '.mat'])
108     end
109 end

```

C.2.1 Functions used in the script

```

1 function [disp_1 , disp_2 , XCorr_val , XCorr_contrast , kernell , range , overlap] ...
2     = My_PIV_2_func(filoc , paloc , resize_factor , kernell , range , overlap)
3
4
5
6 %%%%%%%%%%%%%%%%%%%%%%%%%%%%%%%%%%%%%%%%%%%%%%%%%%%%%%%%%%%%%%%%%%%%%%%%%
7 %%%%%%%%%%%%%%%%%%%%%%%%%%%%%%%%%%%%%%%%%%%%%%%%%%%%%%%%%%%%%%%%%%%%%%%%%
8 %%%%%%%%%%%%%%%%%%%%%%%%%%%%%%%%%%%%%%%%%%%%%%%%%%%%%%%%%%%%%%%%%%%%%%%%%
9
10
11 % when action is required, you will be prompted in the commend window
12 display('when action is required, you will be prompted in the commend window');
13
14 % the final variables are in the last section:
15 % mean_displacement
16 % Mean_dis_x
17 % Mean_dis_y
18
19 % the mat file ad the figure are automatically saved.
20
21 % You may want to change the variable "resize_factor"
22 % it is now set to 3, which accelerates the analysis by ~10x. if you
23 % decrease it, it will be slower, but more precise. 3 is a good compromise.
24 % (increasing it will decrease your precision)
25
26 % the section from line 277 onwards is difficult
27 % you will probably need to visualize by temporarily putting the variable
28 % plot_int to 1
29 % and subsequently change the variable "xcorr_lim".
30
31 % I would not play with the other settings
32
33
34 %%% note: one could add a distance penalization on the cross-correlation
35
36
37 %%%%%%%%%%%%%%%%%%%%%%%%%%%%%%%%%%%%%%%%%%%%%%%%%%%%%%%%%%%%%%%%%%%%%%%%%
38 %%%%%%%%%%%%%%%%%%%%%%%%%%%%%%%%%%%%%%%%%%%%%%%%%%%%%%%%%%%%%%%%%%%%%%%%%
39 %%%%%%%%%%%%%%%%%%%%%%%%%%%%%%%%%%%%%%%%%%%%%%%%%%%%%%%%%%%%%%%%%%%%%%%%%
40
41
42 % [fi , pa] = uigetfile('*.avi');
43

```

```

44 %% Step 1: read the video
45 mov = VideoReader([paloc filoc]);
46 % initialize min_fr and max_fr
47 min_fr = zeros(1,mov.NumberOfFrames);
48 max_fr = zeros(1,mov.NumberOfFrames);
49 %%
50 tic
51 % for every frame
52 for i = 1:mov.NumberOfFrames
53     % Display at which percentage the analysis is
54     clc
55     display((i-1)/(mov.NumberOfFrames-1)*100)
56     % Read in the frame of interest
57     I = read(mov,i);
58     I = I(:,:,1);
59
60     % Define the minimum and maximum value of the frame
61     min_fr(i) = min(I(:));
62     max_fr(i) = max(I(:));
63
64 end
65
66 toc
67 % Define the minimum and maximum value of the video
68 min_mov = min(min_fr)
69 max_mov = max(max_fr)
70
71 % define the delta between the maximum and minimum video value
72 Delt = max_mov-min_mov;
73
74 %% settings
75
76 %%%%%%%%%%%%%%%%%%%%%%%%%%%%%%%%%%%%%%%%%%%%%%%%%%%%%%%%%%%%%%%%%%%%%%%%%
77
78 % resize_factor = 3;
79 resize_factor_corr = 3;
80
81 % kernell = 64;
82 kernell = kernell/resize_factor;
83 kernell = 2*round(kernell/2)
84
85 %% range should not be too much bigger than the kernel for images with large
86 %% intensity variation
87 % range = 156;
88 range = range/resize_factor;
89 range = range + 2*kernell;
90 range = 2*round(range/2);
91 range = max(kernell, range)
92
93 %% xcorr_contrast_lim = 3;
94 %% xcorr_lim = 2e-3
95
96 overlap = floor(overlap/resize_factor)
97 % overlap = floor(kernell/2) ; % kernell; %
98
99 %%%%%%%%%%%%%%%%%%%%%%%%%%%%%%%%%%%%%%%%%%%%%%%%%%%%%%%%%%%%%%%%%%%%%%%%%

```

```

100
101 % sub-parameter
102 % Set the reference frame; the middle frame in this case
103 i = floor(mov.NumberOfFrames/2);
104 Iref = read(mov,i);
105 Iref = double(Iref(:,:,1));
106 % Use bicubic interpolation to resize the frame
107 Iref = imresize(Iref, 1/resize_factor, 'bicubic');
108
109 % Normalize the reference frame
110 Iref = Iref-min_mov;
111 Iref = Iref./Delt;
112
113 % Define the image size
114 Im_size = size(Iref);
115 % Define the noverlap
116 Noverlap = ceil((range)/2)
117 N1 = floor((Im_size(1)-2*Noverlap-1)/overlap)
118 N2 = floor((Im_size(2)-2*Noverlap-1)/overlap)
119
120 % display the frame
121 figure(1);
122 % surf(Iref, 'edgecolor', 'none')
123 imagesc(Iref)
124
125 % put 2 rectangles at the frame
126 width = kernell; % whatever
127 height = kernell; % whatever...
128 xCenter = floor(size(Iref,2)/2); % Wherever...
129 yCenter = floor(size(Iref,1)/2); % Wherever...
130 xLeft = xCenter - width/2;
131 yBottom = yCenter - height/2;
132 hold all
133 rectangle('Position', [xLeft, yBottom, width, height], 'EdgeColor', 'k', 'FaceColor',
            'none', 'LineWidth', 1);
134
135 width = range-2*kernell; % whatever
136 height = range-2*kernell; % whatever...
137 xCenter = floor(size(Iref,2)/2); % Wherever...
138 yCenter = floor(size(Iref,1)/2); % Wherever...
139 xLeft = xCenter - width/2;
140 yBottom = yCenter - height/2;
141 hold all
142 rectangle('Position', [xLeft, yBottom, width, height], 'EdgeColor', 'k', 'FaceColor',
            'none', 'LineWidth', 1);
143 hold off
144
145 %% Initialize several variables
146 XCorr_val = zeros(N1,N2,mov.NumberOfFrames);
147 XCorr_contrast = zeros(N1,N2,mov.NumberOfFrames);
148 disp_1 = zeros(N1,N2,mov.NumberOfFrames);
149 disp_2 = zeros(N1,N2,mov.NumberOfFrames);
150
151 display_int_plot = 0;
152
153 tic

```

```

154
155 for i = 2: mov.NumberOfFrames
156
157     %% Show the percentage of analysis
158     clc
159     display(i);
160     display((i-1)/(mov.NumberOfFrames-1)*100)
161     toc
162     % Read, resize and normalize the frame of interest
163     I = read(mov,i);
164     I = double(I(:, :, 1));
165     I = imresize(I, 1/resize_factor, 'bicubic');
166
167     I = I-min_mov;
168     I = I./Delt;
169 %     GPU_I = gpuArray(I);
170 % Parallel computing
171 parfor j = 1:N1
172     for k = 1:N2
173
174         po_sm1 = range/2+(j-1)*overlap+1;
175         po_sm2 = range/2+(k-1)*overlap+1;
176
177         ref_mat = Iref( po_sm1-kernell/2:po_sm1+kernell/2 ,    po_sm2-kernell
178             /2:po_sm2+kernell/2 );
179
180         sub_mat = I( po_sm1-range/2:po_sm1+range/2 , ...
181             po_sm2-range/2:po_sm2+range/2 );
182
183         sub_mat = sub_mat-mean(sub_mat(:));
184         ref_mat = ref_mat-mean(ref_mat(:));
185
186         XC = xcorr2(sub_mat, ref_mat);
187
188         XC(1:kernell,:) = [];
189         XC(:,1:kernell) = [];
190         XC(end-kernell+1:end,:) = [];
191         XC(:,end-kernell+1:end) = [];
192
193         XC = imresize(XC,resize_factor_corr, 'bicubic');
194
195         [~, pos1] = max(max(XC'));
196         [temp, pos2] = max(max(XC));
197
198         if pos1 >= size(XC,1)-1 || pos1 <= 2
199             pos1 = nan;
200             pos2 = nan;
201         end
202         if pos2 >= size(XC,2)-1 || pos2 <= 2
203             pos1 = nan;
204             pos2 = nan;
205         end
206
207         delt = ceil(size(XC,1)/2);
208

```

```

209
210     pos1 = (pos1)-delt;
211     pos2 = (pos2)-delt;
212     stdtep = std(XC(:));
213
214     XCorr_contrast(j,k,i) = temp/stdtep;
215
216     temp = (temp)./kernell^2;
217
218     XCorr_val(j,k,i) = sqrt(temp);
219     disp_1(j,k,i) = pos1;
220     disp_2(j,k,i) = pos2;
221 end
222 end
223
224 if display_int_plot
225     figure(4)
226     subplot(2,2,1);
227     imagesc(XCorr_val(:,:,i));
228     title('correlation value')
229     colorbar
230     subplot(2,2,2);
231     imagesc(XCorr_contrast(:,:,i));
232     title('correlation contrast')
233     colorbar
234
235     subplot(2,2,3);
236     imagesc(disp_1(:,:,i));
237     title('coord 1 disp')
238     colorbar
239     subplot(2,2,4);
240     imagesc(disp_2(:,:,i));
241     title('coord 2 disp')
242     colorbar
243
244     drawnow
245 end
246 end
247 toc
248 %%
249 % save('temp.mat');

```

C.3 Script to define the movement of the tissue based on the PIV analysis results

In this script also the contractions are isolated and the section 1 of the results is developed. **Fully written by Guillaume Lajoinie including subsequent functions.**

```
1 %% this code and the dependant codes are written by G. Lajoinie , April 2020
2
3
4 %%%%%%%%%%%%%%%%%%%%%%%%%%%%%%%%%%%%%%%%%%%%%%%%%%%%%%%%%%%%%%%%%%%%%%%%%
5 %%%%%%%%%%%%%%%%%%%%%%%%%%%%%%%%%%%%%%%%%%%%%%%%%%%%%%%%%%%%%%%%%%%%%%%%%
6 %%%%%%%%%%%%%%%%%%%%%%%%%%%%%%%%%%%%%%%%%%%%%%%%%%%%%%%%%%%%%%%%%%%%%%%%%
7
8
9 % when action is required , you will be prompted in the command window
10 display('when action is required , you will be prompted in the command window');
11
12 % the mat file and the figure are automatically saved.
13
14 % you will be able to visualize the cross-correlation values to set the
15 % variable 'xcorr_lim' if necessary. The higher this variable , the more you
16 % remove data. This variable aims at removing the measured displacements
17 % with a low correlation value , and thus a large uncertainty
18
19
20 % I would not play with the other settings
21
22
23 %%% note: one could add a dstance penalization on the cross-correlation
24
25
26 %%%%%%%%%%%%%%%%%%%%%%%%%%%%%%%%%%%%%%%%%%%%%%%%%%%%%%%%%%%%%%%%%%%%%%%%%
27 %%%%%%%%%%%%%%%%%%%%%%%%%%%%%%%%%%%%%%%%%%%%%%%%%%%%%%%%%%%%%%%%%%%%%%%%%
28 %%%%%%%%%%%%%%%%%%%%%%%%%%%%%%%%%%%%%%%%%%%%%%%%%%%%%%%%%%%%%%%%%%%%%%%%%
29
30
31
32
33 %%% Clearing ans selecting folder
34 clear all
35 clc
36 close all
37
38 fold2 = uigetdir('','select the folder containing the first step analysis');
39 files2 = dir(fold2);
40 files2(1:2) = [];
41
42 % define the files for analysis
43 piv_list = {};
44 for i = 1:length(files2)
45     if ~isempty(strfind(files2(i).name, '.mat'))
46         piv_list{end+1} = files2(i).name;
47     end
48 end
49 end
```

```

50 piv_list = piv_list';
51 % Make folders to save the results
52 step_2_fol = 'Step_2_analysis_Dafne';
53 if ~isdir(step_2_fol)
54     mkdir(step_2_fol);
55 end
56 if ~isdir('figures_PIV')
57     mkdir('figures_PIV');
58 end
59 %% For all files of interest
60 for i = 211:length(piv_list)
61 % load the file
62     filoc2 = piv_list{i};
63     paloc2 = [fold2 '/'];
64
65     load([paloc2 filoc2], 'time', 'disp_1', 'disp_2', 'XCorr_val', 'XCorr_contrast',
        'resize_factor');
66 %     load([paloc2 filoc2]);
67 % this section will help you choosing "xcorr_lim" if need be
68 % Define some variables
69     num = floor(size(XCorr_val,3)/2);
70     XCorr_val_temp = XCorr_val(:, :, num);
71     XCorr_contrast_temp = XCorr_contrast(:, :, num);
72     disp_1_temp = disp_1(:, :, num);
73     disp_2_temp = disp_2(:, :, num);
74
75     % display correlation value, correlation contrast, coord1, coord2
76     figure(5)
77     subplot(2,2,1);
78     imagesc(XCorr_val_temp);
79     title('correlation value')
80     colorbar
81     subplot(2,2,2);
82     imagesc(XCorr_contrast_temp);
83     title('correlation contrast (unused)')
84     colorbar
85     subplot(2,2,3);
86     imagesc(disp_1_temp);
87     title('coord 1 displacement')
88     colorbar
89     subplot(2,2,4);
90     imagesc(disp_2_temp);
91     title('coord 2 displacement')
92     colorbar
93     drawnow
94 %%
95     plot_int = 0;
96     xcorr_lim = max(XCorr_val_temp(:))/2 ; % 0.025;
97
98     [mean_displacement, Mean_dis_x, Mean_dis_y, displacement, disp_1_map_3,
        disp_2_map_3] ...
99     = analysis_step_2(disp_1, disp_2, XCorr_val, XCorr_contrast, xcorr_lim, plot_int,
        resize_factor);
100
101
102 %%

```

```

103     if ~isempty(time)
104
105         h141 = figure(141);
106         set(h141,'position',[50 50 700 700])
107
108
109         subplot(3,1,1)
110         plot(time-time(1),mean_displacement)
111         grid on
112         xlabel('time (s)');
113         ylabel('displacement (pixels)');
114
115         subplot(3,1,2)
116         plot(time-time(1),Mean_dis_x)
117         grid on
118         xlabel('time (s)');
119         ylabel('x displacement (pixels)');
120
121         subplot(3,1,3)
122         plot(time-time(1),Mean_dis_y)
123         grid on
124         xlabel('time (s)');
125         ylabel('y displacement (pixels)');
126
127     else
128
129         h141 = figure(141);
130         set(h141,'position',[50 50 700 700])
131
132
133         subplot(3,1,1)
134         plot(mean_displacement)
135         grid on
136         xlabel('frame number');
137         ylabel('displacement (pixels)');
138
139         subplot(3,1,2)
140         plot(Mean_dis_x)
141         grid on
142         xlabel('frame number');
143         ylabel('x displacement (pixels)');
144
145         subplot(3,1,3)
146         plot(Mean_dis_y)
147         grid on
148         xlabel('frame number');
149         ylabel('y displacement (pixels)');
150
151
152     end
153
154
155     %%
156
157     save(['G:\for dafne\PIV_new\' step_2_fol '/step_2_' filoc2(1:end-4) '.mat']);
158

```

```

159     saveas(h141,[ 'G:\for dafne\PIV_new\figures_PIV' '/step_2_' filoc2(1:end-4) '.
        fig'], 'fig');
160     saveas(h141,[ 'G:\for dafne\PIV_new\figures_PIV' '/step_2_' filoc2(1:end-4) '.
        eps'], 'epsc');
161
162
163
164 end

```

C.3.1 Functions used in the script

```

1 function [mean_displacement, Mean_dis_x, Mean_dis_y, displacement, disp_1_map_3,
        disp_2_map_3] ...
2     = analysis_step_2(disp_1, disp_2, XCorr_val, XCorr_contrast, xcorr_lim, plot_int,
        resize_factor)
3
4
5 %% filter depending on max displacment and on corr contrast
6
7 disp_1_filt = zeros(size(disp_1));
8 disp_2_filt = zeros(size(disp_2));
9
10 % xcorr_lim = 0.025;
11
12 % plot_int = 0;
13 tic
14
15 for i = 2: size(disp_1,3)
16
17     clc
18     display(i);
19     display((i-1)/(size(disp_1,3)-1)*100)
20     toc
21
22     XCorr_val_temp = XCorr_val(:, :, i);
23     XCorr_contrast_temp = XCorr_contrast(:, :, i);
24     disp_1_temp = disp_1(:, :, i);
25     disp_2_temp = disp_2(:, :, i);
26
27
28
29     XCorr_val_temp_2 = XCorr_val_temp;
30
31     disp_1_temp( XCorr_val_temp < xcorr_lim) = nan;
32     disp_2_temp( XCorr_val_temp < xcorr_lim) = nan;
33
34
35     disp_2_filt(:, :, i) = disp_2_temp;
36     disp_1_filt(:, :, i) = disp_1_temp;
37
38     XCorr_val_temp = XCorr_val_temp_2;
39
40 if plot_int
41
42     figure(5)
43     subplot(2,2,1);

```

```

44     imagesc(XCorr_val_temp);
45     title('reliable correlation value')
46     colorbar
47     subplot(2,2,2);
48     imagesc(XCorr_contrast_temp);
49     title('reliable correlation contrast')
50     colorbar
51
52     subplot(2,2,3);
53     imagesc(disp_1_temp);
54     title('reliable coord 1 disp')
55     colorbar
56     subplot(2,2,4);
57     imagesc(disp_2_temp);
58     title('reliable coord 2 disp')
59     colorbar
60
61     drawnow
62 end
63
64 end
65
66
67 %%
68
69
70
71 disp_1_map = zeros(size(disp_1,1)*size(disp_1,2),size(disp_1,3));
72 disp_2_map = zeros(size(disp_1,1)*size(disp_1,2),size(disp_1,3));
73
74 plot_int = 0;
75 tic
76
77 for i = 2: size(disp_1,3)
78
79     disp_1_temp = disp_1_filt(:, :, i);
80     disp_2_temp = disp_2_filt(:, :, i);
81
82
83     disp_1_map(:, i) = disp_1_temp(:);
84     disp_2_map(:, i) = disp_2_temp(:);
85
86 end
87
88
89 % figure(10);
90 % subplot(2,1,1)
91 % imagesc(disp_1_map)
92 % colorbar
93 % subplot(2,1,2)
94 % imagesc(disp_2_map)
95 % colorbar
96
97 %%
98 co_rem = 0.1;
99

```

```

100 for i = size(displ_map,1):-1:1
101
102
103     clc
104     display((i-1)/(size(displ_map,1)-1)*100)
105
106     line1 = displ_map(i,:);
107     line2 = disp2_map(i,:);
108
109     if sum(isnan(line1))>length(line1)*co_rem
110         displ_map(i,:) = [];
111         disp2_map(i,:) = [];
112     elseif sum(isnan(line2))>length(line2)*co_rem
113         displ_map(i,:) = [];
114         disp2_map(i,:) = [];
115     end
116
117
118 end
119
120
121 % figure(11);
122 % subplot(2,1,1)
123 % imagesc(displ_map)
124 % colorbar
125 % subplot(2,1,2)
126 % imagesc(disp2_map)
127 % colorbar
128 % %
129
130 %%
131
132 displ_map_2 = displ_map;
133 disp2_map_2 = disp2_map;
134
135
136 displ_map_2(:,1) = [];
137 disp2_map_2(:,1) = [];
138
139
140 for i = 1:1:size(displ_map,1)
141
142     %%
143     line1 = displ_map_2(i,:);
144     x = 1:length(line1);
145     y = 1:length(line1);
146
147     x(isnan(line1)) = [];
148     line1(isnan(line1)) = [];
149
150
151     line1 = interp1(x,line1,y,'linear','extrap');
152
153
154     TF = fft(line1);
155     TF(floor(length(TF)/2):end) = 0;

```

```

156     TF(1:50) = 0;
157
158     line1filt = 2.*real(ifft(TF));
159
160     disp_1_map_2(i,:) = line1filt;
161
162     %%
163     line2 = disp_2_map_2(i,:);
164     x = 1:length(line2);
165     y = 1:length(line2);
166
167     x(isnan(line2)) = [];
168     line2(isnan(line2)) = [];
169
170
171     line2 = interp1(x,line2,y,'linear','extrap');
172
173
174     TF = fft(line2);
175     TF(floor(length(TF)/2):end) = 0;
176     TF(1:50) = 0;
177
178     line2filt = 2.*real(ifft(TF));
179
180     disp_2_map_2(i,:) = line2filt;
181
182     %%
183
184 end
185
186 % figure(12);
187 % subplot(2,1,1)
188 % imagesc(disp_1_map_2)
189 % colorbar
190 % subplot(2,1,2)
191 % imagesc(disp_2_map_2)
192 % colorbar
193
194 %%
195
196
197 disp_1_map_3 = disp_1_map_2;
198 disp_2_map_3 = disp_2_map_2;
199
200
201 % line1filt = mean(disp_1_map_3,1);
202 line1filt = disp_1_map_3(1,:);
203
204 A = floor(length(line1filt)/2)-floor(length(line1filt)/15);
205 B = floor(length(line1filt)/2)+floor(length(line1filt)/15);
206 Temp_mat = disp_1_map_3(:,A:B);
207
208
209 figure(30);
210 imagesc(Temp_mat);
211 title('click on non-contractile area in tr figure');

```

```

212 caxis ([median(Temp_mat(:))-1*std(Temp_mat(:)) median(Temp_mat(:))+1*std(Temp_mat(:)
    ) ] );
213 % idea: use median instead of mean, use 1*std instead of 1.
214 display('click on non-contractile area in tr figure');
215 a = round(ginput(1));
216 a = a(1)
217 a = a+A-1;
218
219 Mlin1 = mean(disp_1_map_3(: , a-2:a+2)');
220 Mlin2 = mean(disp_2_map_3(: , a-2:a+2)');
221
222
223 disp_1_map_3 = disp_1_map_3'-Mlin1;
224 disp_1_map_3 = disp_1_map_3';
225
226 disp_2_map_3 = disp_2_map_3'-Mlin2;
227 disp_2_map_3 = disp_2_map_3';
228
229
230 figure(13);
231 subplot(2,1,1)
232 imagesc(disp_1_map_3)
233 caxis ([mean(disp_1_map_3(:))-3*std(disp_1_map_3(:)) mean(disp_1_map_3(:))+3*std(
    disp_1_map_3(:)) ] );
234 colorbar
235
236 subplot(2,1,2)
237 imagesc(disp_2_map_3)
238 colorbar
239 caxis ([mean(disp_2_map_3(:))-3*std(disp_2_map_3(:)) mean(disp_2_map_3(:))+3*std(
    disp_2_map_3(:)) ] );
240
241
242 %%
243
244 displacement = resize_factor.*sqrt(disp_1_map_3.^2+disp_2_map_3.^2);
245
246 % figure(14);
247 % imagesc(displacement)
248
249 mean_displacement = mean(displacement);
250 Mean_dis_x = resize_factor.*mean(disp_1_map_3);
251 Mean_dis_y = resize_factor.*mean(disp_2_map_3);
252
253 % h141 = figure(141);
254 % subplot(3,1,1)
255 % plot(mean_displacement)
256 % grid on
257 % xlabel('time (frame number)');
258 % ylabel('displacement (pixels)');
259 %
260 % subplot(3,1,2)
261 % plot(Mean_dis_x)
262 % grid on
263 % xlabel('time (frame number)');
264 % ylabel('x displacement (pixels)');

```

```

265 %
266 % subplot(3,1,3)
267 % plot(Mean-dis-y)
268 % grid on
269 % xlabel('time (frame number)');
270 % ylabel('y displacement (pixels)');
271 %
272 %
273 % %%
274 %
275 % save([fi(1:end-4) '.mat']);
276 % saveas(h141,[fi(1:end-4) '.fig'], 'fig');

```

C.4 Script to extract contractions and determine contraction parameters

Written by Dafne Groener.

C.4.1 Results subsection 2

```

1 clc
2 clear all
3 close all
4
5 % Step 1: Select all the data of interest
6 [PEAKSFORANALYSIS, pa] = uigetfile('*.mat', 'multiselect', 'on');
7
8 %% Pre-allocate
9 peak_matrix_all=[];
10 video_ID_all='';
11 PRF_all=[];
12 tau_all=[];
13 freq_all=[];
14 USstatus_all=[];
15 delaytime_all=[];
16 contrperiod_all=[];
17 %% Analysis video by video
18 for k1=1:length(PEAKSFORANALYSIS)
19     peak_matrix=[];
20     video_ID='';
21     PRF=[];
22     TAU=[];
23     FREQ=[];
24     delaytime_matrix=[];
25     contrperiod_matrix=[];
26
27     peak_matrix=load(PEAKSFORANALYSIS{1,k1}, 'peak_matrix');
28     peak_matrix=peak_matrix.peak_matrix;
29     if size(peak_matrix,2)>30
30         peak_matrix(:,1:10)=[];
31         peak_matrix(:,end-9:end)=[];
32     end
33     delaytimes=load(PEAKSFORANALYSIS{1,k1}, 'time_delay');
34     delaytimes=delaytimes.time_delay;
35

```

```

36   contrperiod_matrix=load(PEAKSFORANALYSIS{1,k1}, 'delta_t_full_filt');
37   contrperiod_matrix=contrperiod_matrix.delta_t_full_filt;
38   contrperiod_matrix=[NaN, contrperiod_matrix];
39   contrperiod_matrix(:,size(peak_matrix)+1:end)=[];
40
41   peak_matrix_USstatus=load(PEAKSFORANALYSIS{1,k1}, 'peak_matrix_USstatus');
42   peak_matrix_USstatus=peak_matrix_USstatus.peak_matrix_USstatus;
43   duringUS=find(peak_matrix_USstatus==1);
44   peak_matrix_USstatus(duringUS(end)+1:end)=2;
45
46   video_ID=PEAKSFORANALYSIS{1,k1};
47   PRF=load(PEAKSFORANALYSIS{1,k1}, 'PRF');
48   PRF=PRF.PRF;
49   FREQ_index=strfind(video_ID, 'MHz');
50   FREQ=str2num(video_ID((FREQ_index)-3:(FREQ_index)-1));
51   TAU_index=strfind(video_ID, 'ms');
52   TAU=str2num(video_ID((TAU_index)-5:(TAU_index)-1));
53   TAU=TAU(:,end);
54
55   video_ID_="";
56   centerfrequency=[];
57   pulserепetitionfreq=[];
58   pulseduration=[];
59   for ii=1:size(peak_matrix,1)
60       video_ID_{ii,:}=video_ID;
61       pulserепetitionfreq(ii,:)=PRF;
62       centerfrequency(ii,:)=FREQ;
63       pulseduration(ii,:)=TAU;
64   end
65   centerfrequency=centerfrequency(:,end);
66
67   delaytime_matrix=nan(size(centerfrequency));
68
69   [M,~]=find(peak_matrix_USstatus==1);
70   zz=0;
71   for kk=1:length(delaytimes)
72       zz=zz+1;
73       delaytime_matrix(M)=delaytimes(zz);
74   end
75
76   video_ID_all={video_ID_all;video_ID_};
77   peak_matrix_all=[peak_matrix_all;peak_matrix];
78   PRF_all=[PRF_all;pulserепetitionfreq];
79   tau_all=[tau_all;pulseduration];
80   freq_all=[freq_all;centerfrequency];
81   USstatus_all=[USstatus_all; peak_matrix_USstatus];
82   contrperiod_all=[contrperiod_all, contrperiod_matrix];
83   delaytime_all=[delaytime_all; delaytime_matrix];
84 end
85   contrfreq_all=1./contrperiod_all;
86   %% Define the speed matrix
87   speed_matrix_all=[];
88   speed_matrix_all_smooth=[];
89   peak_matrix_all_smooth=[];
90   for ii=1:length(tau_all);
91       peak_matrix_all_smooth(ii,:)=smooth(peak_matrix_all(ii,:),3);

```

```

92 end
93 speed_matrix_all_smooth=diff(peak_matrix_all_smooth ,1 ,2);
94 stepsize=0.02;
95 speed_matrix_all_smooth=speed_matrix_all_smooth/stepsize;
96
97 %% Analysis of the peaks
98 max_peak_smooth=nanmax(peak_matrix_all_smooth ');
99 min_peak_smooth=nanmin(peak_matrix_all_smooth ');
100 area_peak_smooth=trapz(peak_matrix_all_smooth ');
101
102 [max_speed_smooth , index_max_speed_smooth]=nanmax(speed_matrix_all_smooth ');
103 [min_speed_smooth , index_min_speed_smooth]=nanmin(speed_matrix_all_smooth (:,
    index_max_speed_smooth:end) ');
104 index_min_speed_smooth=index_min_speed_smooth+index_max_speed_smooth;
105
106 peak_time=[0.02:0.02:0.750];
107 %% Plot the figures
108 close all
109 A=categories(categorical(tau_all));
110 % Get rid of the smallest category (0.03 s, only 1 measurement)
111 A(8)=A(9);
112 A(9)=[];
113
114 max_speed_noUS_median=[];
115 max_speed_noUS_fquant=[];
116 max_speed_noUS_lquant=[];
117 max_speed_US_median=[];
118 max_speed_US_fquant=[];
119 max_speed_US_lquant=[];
120 max_speed_aUS_median=[];
121 max_speed_aUS_fquant=[];
122 max_speed_aUS_lquant=[];
123 pulseduration_xarray=[];
124
125 min_speed_noUS_median=[];
126 min_speed_noUS_fquant=[];
127 min_speed_noUS_lquant=[];
128 min_speed_US_median=[];
129 min_speed_US_fquant=[];
130 min_speed_US_lquant=[];
131 min_speed_aUS_median=[];
132 min_speed_aUS_fquant=[];
133 min_speed_aUS_lquant=[];
134
135 for zz=1:length(A)
136     set=str2num(A{zz ,:});
137     max_speed_noUS_median(zz)=nanmedian(max_speed_smooth(USstatus_all==0&tau_all==
        set));
138     max_speed_noUS_fquant(zz)=max_speed_noUS_median(zz)-quantile((max_speed_smooth(
        USstatus_all==0&tau_all==set)),0.25);
139     max_speed_noUS_lquant(zz)=quantile((max_speed_smooth(USstatus_all==0&tau_all==
        set)),0.75)-max_speed_noUS_median(zz);
140     max_speed_US_median(zz)=nanmedian(max_speed_smooth(USstatus_all==1&tau_all==set
        ));
141     max_speed_US_fquant(zz)=max_speed_US_median(zz)-quantile((max_speed_smooth(
        USstatus_all==1&tau_all==set)),0.25);

```

```

142     max_speed_US_lquant (zz)=quantile ((max_speed_smooth (USstatus_all==1&tau_all==set
    ) ),0.75)-max_speed_US_median (zz);
143     max_speed_aUS_median (zz)=nanmedian (max_speed_smooth (USstatus_all==2&tau_all==
    set));
144     max_speed_aUS_fquant (zz)=max_speed_US_median (zz)-quantile ((max_speed_smooth (
    USstatus_all==2&tau_all==set)),0.25);
145     max_speed_aUS_lquant (zz)=quantile ((max_speed_smooth (USstatus_all==2&tau_all==
    set)),0.75)-max_speed_US_median (zz);
146
147     min_speed_noUS_median (zz)= -1.*median (min_speed_smooth (USstatus_all==0&tau_all
    ==set));
148     min_speed_noUS_fquant (zz)= min_speed_noUS_median (zz)-(-1.*quantile ((
    min_speed_smooth (USstatus_all==0&tau_all==set)),0.25));
149     min_speed_noUS_lquant (zz)= -1.*quantile ((min_speed_smooth (USstatus_all==0&
    tau_all==set)),0.75)-(min_speed_noUS_median (zz));
150     min_speed_US_median (zz)= -1.*median (min_speed_smooth (USstatus_all==1&tau_all==
    set));
151     min_speed_US_fquant (zz)= min_speed_US_median (zz)-(-1.*quantile ((
    min_speed_smooth (USstatus_all==1&tau_all==set)),0.25));
152     min_speed_US_lquant (zz)=-1.*quantile ((min_speed_smooth (USstatus_all==1&tau_all
    ==set)),0.75)-min_speed_US_median (zz);
153     min_speed_aUS_median (zz)= -1.*median (min_speed_smooth (USstatus_all==2&tau_all==
    set));
154     min_speed_aUS_fquant (zz)= min_speed_aUS_median (zz)-(-1.*quantile ((
    min_speed_smooth (USstatus_all==2&tau_all==set)),0.25));
155     min_speed_aUS_lquant (zz)=-1.*quantile ((min_speed_smooth (USstatus_all==2&tau_all
    ==set)),0.75)-min_speed_aUS_median (zz);
156     pulseduration_xarray (zz)=set;
157 end
158 xarray_pd=[1:length (pulseduration_xarray)];
159
160 figure
161 subplot (2,1,1)
162 errorbar (xarray_pd ,max_speed_noUS_median ,max_speed_noUS_fquant ,
    max_speed_noUS_lquant , 'd', 'LineWidth', 1)
163 hold on
164 errorbar (xarray_pd ,max_speed_US_median ,max_speed_US_fquant ,max_speed_US_lquant , 'h',
    'LineWidth', 1)
165 errorbar (xarray_pd ,max_speed_aUS_median ,max_speed_aUS_fquant ,max_speed_aUS_lquant , '
    s', 'LineWidth', 1)
166 xlabel ('\tau (ms)')
167 ylabel ('V_{max} (\mu m/s)')
168 title ('Maximum speed during contraction')
169 legend ('Before ultrasound', 'During ultrasound', 'After ultrasound', 'Location', '
    northwest')
170 grid minor
171 xlim ([0 length (pulseduration_xarray)+1])
172 ylim ([30 350])
173 xticklabels ([""; A])
174
175 subplot (2,1,2)
176 errorbar (xarray_pd ,min_speed_noUS_median ,min_speed_noUS_fquant ,
    min_speed_noUS_lquant , 'd', 'LineWidth', 1)
177 hold on
178 errorbar (xarray_pd ,min_speed_US_median ,min_speed_US_fquant ,min_speed_US_lquant , 'h',
    'LineWidth', 1)

```

```

179 errorbar(xarray_pd , min_speed_aUS_median , min_speed_aUS_fquant , min_speed_aUS_lquant , '
      s' , 'LineWidth' , 1)
180 xlabel( '\tau (ms) ' )
181 ylabel( 'V_{max} (\mu m/s) ' )
182 title( 'Maximum speed during relaxation ' )
183 legend( 'Before ultrasound' , 'During ultrasound' , 'After ultrasound' , 'Location' , '
      northwest ' )
184 grid minor
185 xlim([0 length(pulseduration_xarray)+1])
186 xticklabels(['" ; A])
187 ylim([30 350])
188
189 max_peak_noUS_median = [];
190 max_peak_noUS_fquant = [];
191 max_peak_noUS_lquant = [];
192 max_peak_US_median = [];
193 max_peak_US_fquant = [];
194 max_peak_US_lquant = [];
195 max_peak_aUS_median = [];
196 max_peak_aUS_fquant = [];
197 max_peak_aUS_lquant = [];
198
199 for zz=1:length(A)
200     set=str2num(A{zz , :} ) ;
201     max_peak_noUS_median(zz)=nanmedian( max_peak_smooth( USstatus_all==0&tau_all==set
      ) ) ;
202     max_peak_noUS_fquant(zz)=max_peak_noUS_median(zz)-quantile( (max_peak_smooth(
      USstatus_all==0&tau_all==set) ) , 0.25) ;
203     max_peak_noUS_lquant(zz)=quantile( (max_peak_smooth( USstatus_all==0&tau_all==set
      ) ) , 0.75)-max_peak_noUS_median(zz) ;
204     max_peak_US_median(zz)=nanmedian( max_peak_smooth( USstatus_all==1&tau_all==set) )
      ;
205     max_peak_US_fquant(zz)=max_peak_US_median(zz)-quantile( (max_peak_smooth(
      USstatus_all==1&tau_all==set) ) , 0.25) ;
206     max_peak_US_lquant(zz)=quantile( (max_peak_smooth( USstatus_all==1&tau_all==set) )
      , 0.75)-max_peak_US_median(zz) ;
207     max_peak_aUS_median(zz)=nanmedian( max_peak_smooth( USstatus_all==2&tau_all==set)
      ) ;
208     max_peak_aUS_fquant(zz)=max_peak_aUS_median(zz)-quantile( (max_peak_smooth(
      USstatus_all==2&tau_all==set) ) , 0.25) ;
209     max_peak_aUS_lquant(zz)=quantile( (max_peak_smooth( USstatus_all==2&tau_all==set)
      ) , 0.75)-max_peak_aUS_median(zz) ;
210 end
211
212 figure
213 errorbar(xarray_pd , max_peak_noUS_median , max_peak_noUS_fquant , max_peak_noUS_lquant , '
      d' , 'LineWidth' , 1)
214 hold on
215 errorbar(xarray_pd , max_peak_US_median , max_peak_US_fquant , max_peak_US_lquant , 'h' , '
      LineWidth' , 1)
216 errorbar(xarray_pd , max_peak_aUS_median , max_peak_aUS_fquant , max_peak_aUS_lquant , 's' ,
      'LineWidth' , 1)
217 xlabel( '\tau (ms) ' )
218 ylabel( 'Maximum peak (\mu m) ' )
219 title( 'Maximum peak ' )

```

```

220 legend('Before ultrasound', 'During ultrasound', 'After ultrasound', 'Location', '
        northwest')
221 grid minor
222 xlim([0 length(pulseduration_xarray)+1])
223 xticklabels(['"; A])
224 ylim([5 15])
225
226 area_peak_noUS_median = [];
227 area_peak_noUS_fquant = [];
228 area_peak_noUS_lquant = [];
229 area_peak_US_median = [];
230 area_peak_US_fquant = [];
231 area_peak_US_lquant = [];
232 area_peak_aUS_median = [];
233 area_peak_aUS_fquant = [];
234 area_peak_aUS_lquant = [];
235
236 for zz=1:length(A)
237     set=str2num(A{zz, :});
238     area_peak_noUS_median(zz)=nanmedian(area_peak_smooth(USstatus_all==0&tau_all==
        set));
239     area_peak_noUS_fquant(zz)=area_peak_noUS_median(zz)-quantile((area_peak_smooth(
        USstatus_all==0&tau_all==set)), 0.25);
240     area_peak_noUS_lquant(zz)=quantile((area_peak_smooth(USstatus_all==0&tau_all==
        set)), 0.75)-area_peak_noUS_median(zz);
241     area_peak_US_median(zz)=nanmedian(area_peak_smooth(USstatus_all==1&tau_all==set
        ));
242     area_peak_US_fquant(zz)=area_peak_US_median(zz)-quantile((area_peak_smooth(
        USstatus_all==1&tau_all==set)), 0.25);
243     area_peak_US_lquant(zz)=quantile((area_peak_smooth(USstatus_all==1&tau_all==set
        )), 0.75)-area_peak_US_median(zz);
244     area_peak_aUS_median(zz)=nanmedian(area_peak_smooth(USstatus_all==2&tau_all==
        set));
245     area_peak_aUS_fquant(zz)=area_peak_aUS_median(zz)-quantile((area_peak_smooth(
        USstatus_all==2&tau_all==set)), 0.25);
246     area_peak_aUS_lquant(zz)=quantile((area_peak_smooth(USstatus_all==2&tau_all==
        set)), 0.75)-area_peak_aUS_median(zz);
247 end
248
249 figure
250 errorbar(xarray_pd, area_peak_noUS_median, area_peak_noUS_fquant,
        area_peak_noUS_lquant, 'd', 'LineWidth', 1)
251 hold on
252 errorbar(xarray_pd, area_peak_US_median, area_peak_US_fquant, area_peak_US_lquant, 'h',
        'LineWidth', 1)
253 errorbar(xarray_pd, area_peak_aUS_median, area_peak_aUS_fquant, area_peak_aUS_lquant, '
        s', 'LineWidth', 1)
254 xlabel('\tau (ms)')
255 ylabel('Peak area (\mums)')
256 title('Peak area')
257 legend('Before ultrasound', 'During ultrasound', 'After ultrasound', 'Location', '
        northwest')
258 grid minor
259 xlim([0 length(pulseduration_xarray)+1])
260 xticklabels(['"; A])
261 ylim([100 250])

```

```

262
263 contraction_dur_noUS_median = [];
264 contraction_dur_noUS_fquant = [];
265 contraction_dur_noUS_lquant = [];
266 contraction_dur_US_median = [];
267 contraction_dur_US_fquant = [];
268 contraction_dur_US_lquant = [];
269 contraction_dur_aUS_median = [];
270 contraction_dur_aUS_fquant = [];
271 contraction_dur_aUS_lquant = [];
272 for zz=1:length(A)
273     set=str2num(A{zz,:});
274     contraction_dur_noUS_median(zz)=nanmedian(0.02*(index_min_speed_smooth(
        USstatus_all==0&tau_all==set)-index_max_speed_smooth(USstatus_all==0&tau_all
        ==set)));
275     contraction_dur_noUS_fquant(zz)=contraction_dur_noUS_median(zz)-quantile(0.02*(
        index_min_speed_smooth(USstatus_all==0&tau_all==set)-index_max_speed_smooth(
        USstatus_all==0&tau_all==set)),0.25);
276     contraction_dur_noUS_lquant(zz)=quantile(0.02*(index_min_speed_smooth(
        USstatus_all==0&tau_all==set)-index_max_speed_smooth(USstatus_all==0&tau_all
        ==set)),0.75)-contraction_dur_noUS_median(zz);
277     contraction_dur_US_median(zz)=nanmedian(0.02*(index_min_speed_smooth(
        USstatus_all==1&tau_all==set)-index_max_speed_smooth(USstatus_all==1&tau_all
        ==set)));
278     contraction_dur_US_fquant(zz)=contraction_dur_US_median(zz)-quantile(0.02*(
        index_min_speed_smooth(USstatus_all==1&tau_all==set)-index_max_speed_smooth(
        USstatus_all==1&tau_all==set)),0.25);
279     contraction_dur_US_lquant(zz)=quantile(0.02*(index_min_speed_smooth(
        USstatus_all==1&tau_all==set)-index_max_speed_smooth(USstatus_all==1&tau_all
        ==set)),0.75)-contraction_dur_US_median(zz);
280     contraction_dur_aUS_median(zz)=nanmedian(0.02*(index_min_speed_smooth(
        USstatus_all==2&tau_all==set)-index_max_speed_smooth(USstatus_all==2&tau_all
        ==set)));
281     contraction_dur_aUS_fquant(zz)=contraction_dur_aUS_median(zz)-quantile(0.02*(
        index_min_speed_smooth(USstatus_all==2&tau_all==set)-index_max_speed_smooth(
        USstatus_all==2&tau_all==set)),0.25);
282     contraction_dur_aUS_lquant(zz)=quantile(0.02*(index_min_speed_smooth(
        USstatus_all==2&tau_all==set)-index_max_speed_smooth(USstatus_all==2&tau_all
        ==set)),0.75)-contraction_dur_aUS_median(zz);
283 end
284
285 figure
286 errorbar(xarray_pd,contraction_dur_noUS_median,contraction_dur_noUS_fquant,
        contraction_dur_noUS_lquant,'d','LineWidth',1)
287 hold on
288 errorbar(xarray_pd,contraction_dur_US_median,contraction_dur_US_fquant,
        contraction_dur_US_lquant,'h','LineWidth',1)
289 errorbar(xarray_pd,contraction_dur_aUS_median,contraction_dur_aUS_fquant,
        contraction_dur_aUS_lquant,'s','LineWidth',1)
290 xlabel('\tau (ms)')
291 ylabel('Peak duration (s)')
292 title('Peak duration')
293 legend('Before ultrasound','During ultrasound','After ultrasound','Location',
        'northwest')
294 grid minor
295 xlim([0 length(pulseduration_xarray)+1])

```

```

296 xticklabels(['"; A])
297 ylim([0.10 0.40])
298
299 contrfreq_all_noUS_median = [];
300 contrfreq_all_noUS_fquant = [];
301 contrfreq_all_noUS_lquant = [];
302 contrfreq_all_US_median = [];
303 contrfreq_all_US_fquant = [];
304 contrfreq_all_US_lquant = [];
305 contrfreq_all_aUS_median = [];
306 contrfreq_all_aUS_fquant = [];
307 contrfreq_all_aUS_lquant = [];
308
309 for zz=1:length(A)
310     set=str2num(A{zz,:});
311     contrfreq_all_noUS_median(zz)=nanmedian(contrfreq_all(USstatus_all==0&tau_all==
        set)./PRF_all(USstatus_all==0&tau_all==set)');
312     contrfreq_all_noUS_fquant(zz)=contrfreq_all_noUS_median(zz)-quantile((
        contrfreq_all(USstatus_all==0&tau_all==set)./PRF_all(USstatus_all==0&tau_all
        ==set)'),0.25);
313     contrfreq_all_noUS_lquant(zz)=quantile((contrfreq_all(USstatus_all==0&tau_all==
        set)./PRF_all(USstatus_all==0&tau_all==set)'),0.75)-
        contrfreq_all_noUS_median(zz);
314     contrfreq_all_US_median(zz)=nanmedian(contrfreq_all(USstatus_all==1&tau_all==
        set)./PRF_all(USstatus_all==1&tau_all==set)');
315     contrfreq_all_US_fquant(zz)=contrfreq_all_US_median(zz)-quantile((contrfreq_all
        (USstatus_all==1&tau_all==set)./PRF_all(USstatus_all==1&tau_all==set)'),
        0.25);
316     contrfreq_all_US_lquant(zz)=quantile((contrfreq_all(USstatus_all==1&tau_all==
        set)./PRF_all(USstatus_all==1&tau_all==set)'),0.75)-contrfreq_all_US_median(
        zz);
317     contrfreq_all_aUS_median(zz)=nanmedian(contrfreq_all(USstatus_all==2&tau_all==
        set)./PRF_all(USstatus_all==2&tau_all==set)');
318     contrfreq_all_aUS_fquant(zz)=contrfreq_all_aUS_median(zz)-quantile((
        contrfreq_all(USstatus_all==2&tau_all==set)./PRF_all(USstatus_all==2&tau_all
        ==set)'),0.25);
319     contrfreq_all_aUS_lquant(zz)=quantile((contrfreq_all(USstatus_all==2&tau_all==
        set)./PRF_all(USstatus_all==2&tau_all==set)'),0.75)-contrfreq_all_aUS_median
        (zz);
320 end
321
322 figure
323 errorbar(xarray_pd,contrfreq_all_noUS_median,contrfreq_all_noUS_fquant,
        contrfreq_all_noUS_lquant,'d','LineWidth',1)
324 hold on
325 errorbar(xarray_pd,contrfreq_all_US_median,contrfreq_all_US_fquant,
        contrfreq_all_US_lquant,'h','LineWidth',1)
326 errorbar(xarray_pd,contrfreq_all_aUS_median,contrfreq_all_aUS_fquant,
        contrfreq_all_aUS_lquant,'s','LineWidth',1)
327 plot([0 length(pulseduration_xarray)+1],[1 1],'LineWidth',1)
328 xlabel('\tau (ms)')
329 ylabel('f_c / PRF (-)')
330 title('Ratio contraction frequency to PRF')
331 legend('Before ultrasound','During ultrasound','After ultrasound','PRF','
        Location','northwest')
332 grid minor

```

```

333 xlim([0 length(pulseduration_xarray)+1])
334 xticklabels(['"; A])
335 ylim([0.3 1.1])
336
337 %%
338 close all
339 figure
340 for zz=1:length(A)
341     set=str2num(A{zz,:});
342     contr_ratio=(contrfreq_all(USstatus_all==1&tau_all==set)./PRF_all(USstatus_all==1&
        tau_all==set));
343     contr_ratio_delaytime=delaytime_all(USstatus_all==1&tau_all==set);
344     contr_ratio_1=contr_ratio_delaytime(contr_ratio<=1.1&contr_ratio>=0.9);
345     ratio_1_median(zz)=nanmedian(contr_ratio_1);
346     ratio_1_fquant(zz)=ratio_1_median(zz)-quantile(contr_ratio_1,0.25);
347     ratio_1_lquant(zz)=quantile(contr_ratio_1,0.75)-ratio_1_median(zz);
348     ratio_1_length(zz)=size(contr_ratio_1,1);
349 end
350
351 figure
352 errorbar(xarray_pd,ratio_1_median,ratio_1_fquant,ratio_1_lquant,'d','LineWidth',
    1)
353 for zy=1:zz
354     text(xarray_pd(zy),0.3,num2str(ratio_1_length(zy)))
355 end
356 xlabel('\tau (ms)')
357 ylabel('Delay after US pulse (s)')
358 title('Delay of contraction after US pulse')
359 legend('During ultrasound','Location','northwest')
360 grid minor
361 xlim([0 length(pulseduration_xarray)+1])
362 xticklabels(['"; A])

```

C.4.2 Results subsection 3

```

1 clc
2 clear all
3 close all
4
5 % Step 1: Select all the data of interest
6 [PEAKSFORANALYSIS, pa] = uigetfile('*.mat','multiselect','on');
7
8 %% Pre-allocate
9 peak_matrix_all=[];
10 video_ID_all='';
11 PRF_all=[];
12 tau_all=[];
13 freq_all=[];
14 USstatus_all=[];
15 delaytime_all=[];
16 contrperiod_all=[];
17 %% Analysis video by video
18 for k1=215:length(PEAKSFORANALYSIS)
19     peak_matrix=[];
20     video_ID='';
21     PRF=[];
22     TAU=[];

```

```

23  FREQ=[];
24  delaytime_matrix=[];
25  contrperiod_matrix=[];
26
27  peak_matrix=load(PEAKSFORANALYSIS{1,k1}, 'peak_matrix');
28  peak_matrix=peak_matrix.peak_matrix;
29  if size(peak_matrix,2)>30
30      peak_matrix(:,1:10)=[];
31      peak_matrix(:,end-9:end)=[];
32  end
33  delaytimes=load(PEAKSFORANALYSIS{1,k1}, 'time_delay');
34  delaytimes=delaytimes.time_delay;
35
36  contrperiod_matrix=load(PEAKSFORANALYSIS{1,k1}, 'delta_t_full_filt');
37  contrperiod_matrix=contrperiod_matrix.delta_t_full_filt;
38  contrperiod_matrix=[NaN, contrperiod_matrix];
39  contrperiod_matrix(:,size(peak_matrix)+1:end)=[];
40
41  peak_matrix_USstatus=load(PEAKSFORANALYSIS{1,k1}, 'peak_matrix_USstatus');
42  peak_matrix_USstatus=peak_matrix_USstatus.peak_matrix_USstatus;
43  duringUS=find(peak_matrix_USstatus==1);
44  peak_matrix_USstatus(duringUS(end)+1:end)=2;
45
46  video_ID=PEAKSFORANALYSIS{1,k1};
47  PRF=load(PEAKSFORANALYSIS{1,k1}, 'PRF');
48  PRF=PRF.PRF;
49  FREQ_index=strfind(video_ID, 'MHz');
50  FREQ=str2num(video_ID((FREQ_index)-3:(FREQ_index)-1));
51  TAU_index=strfind(video_ID, 'ms');
52  TAU=str2num(video_ID((TAU_index)-5:(TAU_index)-1));
53  TAU=TAU(:,end);
54
55  video_ID_='";
56  centerfrequency=[];
57  pulserепetitionfreq=[];
58  pulseduration=[];
59  for ii=1:size(peak_matrix,1)
60      video_ID_{ii,:}=video_ID;
61      pulserепetitionfreq(ii,:)=PRF;
62      centerfrequency(ii,:)=FREQ;
63      pulseduration(ii,:)=TAU;
64  end
65  centerfrequency=centerfrequency(:,end);
66
67  delaytime_matrix=nan(size(centerfrequency));
68
69  [M,~]=find(peak_matrix_USstatus==1);
70  zz=0;
71  for kk=1:length(delaytimes)
72      zz=zz+1;
73      delaytime_matrix(M)=delaytimes(zz);
74  end
75
76  video_ID_all={video_ID_all; video_ID_};
77  peak_matrix_all=[peak_matrix_all; peak_matrix];
78  PRF_all=[PRF_all; pulserепetitionfreq];

```

```

79     tau_all=[tau_all;pulseduration];
80     freq_all=[freq_all;centerfrequency];
81     USstatus_all=[USstatus_all; peak_matrix_USstatus];
82     contrperiod_all=[contrperiod_all, contrperiod_matrix];
83     delaytime_all=[delaytime_all; delaytime_matrix];
84 end
85 %% %% Define the speed matrix
86 contrfreq_all=1./contrperiod_all;
87
88 speed_matrix_all=[];
89 speed_matrix_all_smooth=[];
90 peak_matrix_all_smooth=[];
91 for ii=1:length(tau_all);
92     peak_matrix_all_smooth(ii,:)=smooth(peak_matrix_all(ii,:),3);
93 end
94 speed_matrix_all_smooth=diff(peak_matrix_all_smooth,1,2);
95 stepsize=0.02;
96 speed_matrix_all_smooth=speed_matrix_all_smooth/stepsize;
97
98 %% Analysis of the peaks
99 max_peak_smooth=nanmax(peak_matrix_all_smooth');
100 min_peak_smooth=nanmin(peak_matrix_all_smooth');
101 area_peak_smooth=trapz(peak_matrix_all_smooth');
102
103 [max_speed_smooth, index_max_speed_smooth]=nanmax(speed_matrix_all_smooth');
104 [min_speed_smooth, index_min_speed_smooth]=nanmin(speed_matrix_all_smooth(:,
    index_max_speed_smooth:end)');
105 index_min_speed_smooth=index_min_speed_smooth+index_max_speed_smooth;
106
107 peak_time=[0.02:0.02:0.60];
108 %% Plot the figures
109 close all
110 A=categories(categorical(tau_all));
111 C=A([20:22]);
112 A=C;
113
114 D=categories(categorical(freq_all));
115 E=D([3:4]);
116 D=E;
117
118 max_speed_noUS_median=[];
119 max_speed_noUS_fquant=[];
120 max_speed_noUS_lquant=[];
121 max_speed_US_median=[];
122 max_speed_US_fquant=[];
123 max_speed_US_lquant=[];
124 max_speed_aUS_median=[];
125 max_speed_aUS_fquant=[];
126 max_speed_aUS_lquant=[];
127 pulseduration_xarray=[];
128
129 min_speed_noUS_median=[];
130 min_speed_noUS_fquant=[];
131 min_speed_noUS_lquant=[];
132 min_speed_US_median=[];
133 min_speed_US_fquant=[];

```

```

134 min_speed_US_lquant = [];
135 min_speed_aUS_median = [];
136 min_speed_aUS_fquant = [];
137 min_speed_aUS_lquant = [];
138
139 for zz=1:length(A)
140     set=str2num(A{zz,:});
141     pulseduration_xarray(zz)=set;
142     for yy=1:length(D)
143
144         setD=str2num(D{yy,:});
145         max_speed_noUS_median(zz,yy)=nanmedian(max_speed_smooth(USstatus_all==0&tau_all
146             ==set&freq_all==setD));
147         max_speed_noUS_fquant(zz,yy)=max_speed_noUS_median(zz,yy)-quantile((
148             max_speed_smooth(USstatus_all==0&tau_all==set&freq_all==setD)),0.25);
149         max_speed_noUS_lquant(zz,yy)=quantile((max_speed_smooth(USstatus_all==0&tau_all
150             ==set&freq_all==setD)),0.75)-max_speed_noUS_median(zz,yy);
151         max_speed_US_median(zz,yy)=nanmedian(max_speed_smooth(USstatus_all==1&tau_all==
152             set&freq_all==setD));
153         max_speed_US_fquant(zz,yy)=max_speed_US_median(zz,yy)-quantile((
154             max_speed_smooth(USstatus_all==1&tau_all==set&freq_all==setD)),0.25);
155         max_speed_US_lquant(zz,yy)=quantile((max_speed_smooth(USstatus_all==1&tau_all==
156             set&freq_all==setD)),0.75)-max_speed_US_median(zz,yy);
157         max_speed_aUS_median(zz,yy)=nanmedian(max_speed_smooth(USstatus_all==2&tau_all
158             ==set&freq_all==setD));
159         max_speed_aUS_fquant(zz,yy)=max_speed_aUS_median(zz,yy)-quantile((
160             max_speed_smooth(USstatus_all==2&tau_all==set&freq_all==setD)),0.25);
161         max_speed_aUS_lquant(zz,yy)=quantile((max_speed_smooth(USstatus_all==2&tau_all
162             ==set&freq_all==setD)),0.75)-max_speed_aUS_median(zz,yy);
163
164         min_speed_noUS_median(zz,yy)= -1.*median(min_speed_smooth(USstatus_all==0&
165             tau_all==set&freq_all==setD));
166         min_speed_noUS_fquant(zz,yy)= min_speed_noUS_median(zz,yy)-(-1.*quantile((
167             min_speed_smooth(USstatus_all==0&tau_all==set&freq_all==setD)),0.25));
168         min_speed_noUS_lquant(zz,yy)= -1.*quantile((min_speed_smooth(USstatus_all==0&
169             tau_all==set&freq_all==setD)),0.75)-(min_speed_noUS_median(zz,yy));
170         min_speed_US_median(zz,yy)= -1.*median(min_speed_smooth(USstatus_all==1&tau_all
171             ==set&freq_all==setD));
172         min_speed_US_fquant(zz,yy)= min_speed_US_median(zz,yy)-(-1.*quantile((
173             min_speed_smooth(USstatus_all==1&tau_all==set&freq_all==setD)),0.25));
174         min_speed_US_lquant(zz,yy)=-1.*quantile((min_speed_smooth(USstatus_all==1&
175             tau_all==set&freq_all==setD)),0.75)-min_speed_US_median(zz,yy);
176         min_speed_aUS_median(zz,yy)= -1.*median(min_speed_smooth(USstatus_all==2&
177             tau_all==set&freq_all==setD));
178         min_speed_aUS_fquant(zz,yy)= min_speed_aUS_median(zz,yy)-(-1.*quantile((
179             min_speed_smooth(USstatus_all==2&tau_all==set&freq_all==setD)),0.25));
180         min_speed_aUS_lquant(zz,yy)=-1.*quantile((min_speed_smooth(USstatus_all==2&
181             tau_all==set&freq_all==setD)),0.75)-min_speed_aUS_median(zz,yy);
182
183     end
184 end
185 xarray_pd=[1:length(pulseduration_xarray)];
186 figure
187 subplot(2,2,1)
188 errorbar(xarray_pd,max_speed_noUS_median(:,1),max_speed_noUS_fquant(:,1),

```

```

    max_speed_noUS_lquant(:,1), 'd', 'LineWidth', 1)
172 hold on
173 errorbar(xarray_pd, max_speed_US_median(:,1), max_speed_US_fquant(:,1),
    max_speed_US_lquant(:,1), 'h', 'LineWidth', 1)
174 errorbar(xarray_pd, max_speed_aUS_median(:,1), max_speed_aUS_fquant(:,1),
    max_speed_aUS_lquant(:,1), 's', 'LineWidth', 1)
175 xlabel('\tau (ms)')
176 ylabel('V_{max} (\mum/s)')
177 title('Maximum speed during contraction 1.0MHz')
178 legend('Before ultrasound', 'During ultrasound', 'After ultrasound', 'Location', '
    northwest')
179 grid minor
180 xticks([0 1 2 3 4])
181 xlim([0 length(pulseduration_xarray)+1])
182 ylim([0 350])
183 xticklabels(['"; A])
184
185
186 subplot(2,2,3)
187 errorbar(xarray_pd, min_speed_noUS_median(:,1), min_speed_noUS_fquant(:,1),
    min_speed_noUS_lquant(:,1), 'd', 'LineWidth', 1)
188 hold on
189 errorbar(xarray_pd, min_speed_US_median(:,1), min_speed_US_fquant(:,1),
    min_speed_US_lquant(:,1), 'h', 'LineWidth', 1)
190 errorbar(xarray_pd, min_speed_aUS_median(:,1), min_speed_aUS_fquant(:,1),
    min_speed_aUS_lquant(:,1), 's', 'LineWidth', 1)
191 xlabel('\tau (ms)')
192 ylabel('V_{max} (\mum/s)')
193 title('Maximum speed during relaxation 1.0MHz')
194 legend('Before ultrasound', 'During ultrasound', 'After ultrasound', 'Location', '
    northwest')
195 grid minor
196 xticks([0 1 2 3 4])
197 xlim([0 length(pulseduration_xarray)+1])
198 ylim([0 350])
199 xticklabels(['"; A])
200
201 subplot(2,2,2)
202 errorbar(xarray_pd, max_speed_noUS_median(:,2), max_speed_noUS_fquant(:,2),
    max_speed_noUS_lquant(:,2), 'd', 'LineWidth', 1)
203 hold on
204 errorbar(xarray_pd, max_speed_US_median(:,2), max_speed_US_fquant(:,2),
    max_speed_US_lquant(:,2), 'h', 'LineWidth', 1)
205 errorbar(xarray_pd, max_speed_aUS_median(:,2), max_speed_aUS_fquant(:,2),
    max_speed_aUS_lquant(:,2), 's', 'LineWidth', 1)
206 xlabel('\tau (ms)')
207 ylabel('V_{max} (\mum/s)')
208 title('Maximum speed during contraction 1.5MHz')
209 legend('Before ultrasound', 'During ultrasound', 'After ultrasound', 'Location', '
    northwest')
210 grid minor
211 xticks([0 1 2 3 4])
212 xlim([0 length(pulseduration_xarray)+1])
213 ylim([0 350])
214 xticklabels(['"; A])
215

```

```

216 subplot(2,2,4)
217 errorbar(xarray_pd , min_speed_noUS_median(:,2) , min_speed_noUS_fquant(:,2) ,
           min_speed_noUS_lquant(:,2) , 'd' , 'LineWidth' , 1)
218 hold on
219 errorbar(xarray_pd , min_speed_US_median(:,2) , min_speed_US_fquant(:,2) ,
           min_speed_US_lquant(:,2) , 'h' , 'LineWidth' , 1)
220 errorbar(xarray_pd , min_speed_aUS_median(:,2) , min_speed_aUS_fquant(:,2) ,
           min_speed_aUS_lquant(:,2) , 'p' , 'LineWidth' , 1)
221 xlabel('\tau (ms)')
222 ylabel('V_{max} (\mum/s)')
223 title('Maximum speed during relaxation 1.5MHz')
224 legend('Before ultrasound' , 'During ultrasound' , 'After ultrasound' , 'Location' , '
           northwest')
225 grid minor
226 xticks([0 1 2 3 4])
227 xlim([0 length(pulseduration_xarray)+1])
228 ylim([0 350])
229 xticklabels(['"; A])
230
231 max_peak_noUS_median = [];
232 max_peak_noUS_fquant = [];
233 max_peak_noUS_lquant = [];
234 max_peak_US_median = [];
235 max_peak_US_fquant = [];
236 max_peak_US_lquant = [];
237 max_peak_aUS_median = [];
238 max_peak_aUS_fquant = [];
239 max_peak_aUS_lquant = [];
240
241 for zz=1:length(A)
242     set=str2num(A{zz , :});
243     for yy=1:length(D)
244
245         setD=str2num(D{yy , :});
246         max_peak_noUS_median(zz , yy)=nanmedian(max_peak_smooth(USstatus_all==0&tau_all==
           set&freq_all==setD));
247         max_peak_noUS_fquant(zz , yy)=max_peak_noUS_median(zz , yy)-quantile((
           max_peak_smooth(USstatus_all==0&tau_all==set&freq_all==setD)) , 0.25);
248         max_peak_noUS_lquant(zz , yy)=quantile((max_peak_smooth(USstatus_all==0&tau_all==
           set&freq_all==setD)) , 0.75)-max_peak_noUS_median(zz , yy);
249         max_peak_US_median(zz , yy)=nanmedian(max_peak_smooth(USstatus_all==1&tau_all==
           set&freq_all==setD));
250         max_peak_US_fquant(zz , yy)=max_peak_US_median(zz , yy)-quantile((max_peak_smooth(
           USstatus_all==1&tau_all==set&freq_all==setD)) , 0.25);
251         max_peak_US_lquant(zz , yy)=quantile((max_peak_smooth(USstatus_all==1&tau_all==
           set&freq_all==setD)) , 0.75)-max_peak_US_median(zz , yy);
252         max_peak_aUS_median(zz , yy)=nanmedian(max_peak_smooth(USstatus_all==2&tau_all==
           set&freq_all==setD));
253         max_peak_aUS_fquant(zz , yy)=max_peak_aUS_median(zz , yy)-quantile((max_peak_smooth(
           USstatus_all==2&tau_all==set&freq_all==setD)) , 0.25);
254         max_peak_aUS_lquant(zz , yy)=quantile((max_peak_smooth(USstatus_all==2&tau_all==
           set&freq_all==setD)) , 0.75)-max_peak_aUS_median(zz , yy);
255 end
256 end
257
258 figure

```

```

259 subplot(1,2,1)
260 errorbar(xarray_pd,max_peak_noUS_median(:,1),max_peak_noUS_fquant(:,1),
           max_peak_noUS_lquant(:,1),'d','LineWidth',1)
261 hold on
262 errorbar(xarray_pd,max_peak_US_median(:,1),max_peak_US_fquant(:,1),
           max_peak_US_lquant(:,1),'h','LineWidth',1)
263 errorbar(xarray_pd,max_peak_aUS_median(:,1),max_peak_aUS_fquant(:,1),
           max_peak_aUS_lquant(:,1),'s','LineWidth',1)
264 xlabel('\tau (ms)')
265 ylabel('Maximum peak (\mum)')
266 title('Maximum peak (1.0MHz)')
267 legend('Before ultrasound','During ultrasound','After ultrasound','Location',
         'northwest')
268 grid minor
269 xticks([0 1 2 3 4])
270 xlim([0 4])
271 xticklabels(['"; A])
272 ylim([5 32])
273
274 subplot(1,2,2)
275 errorbar(xarray_pd,max_peak_noUS_median(:,2),max_peak_noUS_fquant(:,2),
           max_peak_noUS_lquant(:,2),'d','LineWidth',1)
276 hold on
277 errorbar(xarray_pd,max_peak_US_median(:,2),max_peak_US_fquant(:,2),
           max_peak_US_lquant(:,2),'h','LineWidth',1)
278 errorbar(xarray_pd,max_peak_aUS_median(:,2),max_peak_aUS_fquant(:,2),
           max_peak_aUS_lquant(:,2),'s','LineWidth',1)
279 xlabel('\tau (ms)')
280 ylabel('Maximum peak (\mum)')
281 title('Maximum peak (1.5MHz)')
282 legend('Before ultrasound','During ultrasound','After ultrasound','Location',
         'northwest')
283 grid minor
284 xticks([0 1 2 3 4])
285 xlim([0 4])
286 xticklabels(['"; A])
287 ylim([5 32])
288
289 area_peak_noUS_median=[];
290 area_peak_noUS_fquant=[];
291 area_peak_noUS_lquant=[];
292 area_peak_US_median=[];
293 area_peak_US_fquant=[];
294 area_peak_US_lquant=[];
295 area_peak_aUS_median=[];
296 area_peak_aUS_fquant=[];
297 area_peak_aUS_lquant=[];
298
299 for zz=1:length(A)
300     set=str2num(A{zz,:});
301
302     for yy=1:length(D)
303
304         setD=str2num(D{yy,:});
305         area_peak_noUS_median(zz,yy)=nanmedian(area_peak_smooth(USstatus_all==0&tau_all
           ==set&freq_all==setD));

```

```

306     area_peak_noUS_fquant (zz ,yy)=area_peak_noUS_median (zz ,yy)-quantile ((
        area_peak_smooth ( USstatus_all==0&tau_all==set&freq_all==setD) ) ,0.25) ;
307     area_peak_noUS_lquant (zz ,yy)=quantile (( area_peak_smooth ( USstatus_all==0&tau_all
        ==set&freq_all==setD) ) ,0.75)-area_peak_noUS_median (zz ,yy) ;
308     area_peak_US_median (zz ,yy)=nanmedian ( area_peak_smooth ( USstatus_all==1&tau_all==
        set&freq_all==setD) ) ;
309     area_peak_US_fquant (zz ,yy)=area_peak_US_median (zz ,yy)-quantile ((
        area_peak_smooth ( USstatus_all==1&tau_all==set&freq_all==setD) ) ,0.25) ;
310     area_peak_US_lquant (zz ,yy)=quantile (( area_peak_smooth ( USstatus_all==1&tau_all==
        set&freq_all==setD) ) ,0.75)-area_peak_US_median (zz ,yy) ;
311 area_peak_aUS_median (zz ,yy)=nanmedian ( area_peak_smooth ( USstatus_all==2&tau_all==set
    &freq_all==setD) ) ;
312     area_peak_aUS_fquant (zz ,yy)=area_peak_aUS_median (zz ,yy)-quantile ((
        area_peak_smooth ( USstatus_all==2&tau_all==set&freq_all==setD) ) ,0.25) ;
313     area_peak_aUS_lquant (zz ,yy)=quantile (( area_peak_smooth ( USstatus_all==2&tau_all
        ==set&freq_all==setD) ) ,0.75)-area_peak_aUS_median (zz ,yy) ;
314 end
315 end
316
317 figure (3)
318 subplot (1 ,2 ,1)
319 errorbar (xarray_pd ,area_peak_noUS_median (: ,1) ,area_peak_noUS_fquant (: ,1) ,
    area_peak_noUS_lquant (: ,1) , 'd' , 'LineWidth' , 1)
320 hold on
321 errorbar (xarray_pd ,area_peak_US_median (: ,1) ,area_peak_US_fquant (: ,1) ,
    area_peak_US_lquant (: ,1) , 'h' , 'LineWidth' , 1)
322 errorbar (xarray_pd ,area_peak_aUS_median (: ,1) ,area_peak_aUS_fquant (: ,1) ,
    area_peak_aUS_lquant (: ,1) , 's' , 'LineWidth' , 1)
323 xlabel ( '\tau (ms)' )
324 ylabel ( 'Peak area (\mums)' )
325 title ( 'Peak area (1.0MHz)' )
326 legend ( 'Before ultrasound' , 'During ultrasound' , 'After ultrasound' , 'Location' , '
    northwest' )
327 grid minor
328 xticks ([0 1 2 3 4])
329 xlim ([0 4])
330 xticklabels ([""; A])
331 ylim ([80 680])
332
333
334 subplot (1 ,2 ,2)
335 errorbar (xarray_pd ,area_peak_noUS_median (: ,2) ,area_peak_noUS_fquant (: ,2) ,
    area_peak_noUS_lquant (: ,2) , 'd' , 'LineWidth' , 1)
336 hold on
337 errorbar (xarray_pd ,area_peak_US_median (: ,2) ,area_peak_US_fquant (: ,2) ,
    area_peak_US_lquant (: ,2) , 'h' , 'LineWidth' , 1)
338 errorbar (xarray_pd ,area_peak_aUS_median (: ,2) ,area_peak_aUS_fquant (: ,2) ,
    area_peak_aUS_lquant (: ,2) , 's' , 'LineWidth' , 1)
339 xlabel ( '\tau (ms)' )
340 ylabel ( 'Peak area (\mums)' )
341 title ( 'Peak area (1.5MHz)' )
342 legend ( 'Before ultrasound' , 'During ultrasound' , 'After ultrasound' , 'Location' , '
    northwest' )
343 grid minor
344 xticks ([0 1 2 3 4])
345 xlim ([0 4])

```

```

346 xticklabels(['"; A])
347 ylim([80 680])
348
349 contraction_dur_noUS_median = [];
350 contraction_dur_noUS_fquant = [];
351 contraction_dur_noUS_lquant = [];
352 contraction_dur_US_median = [];
353 contraction_dur_US_fquant = [];
354 contraction_dur_US_lquant = [];
355 contraction_dur_aUS_median = [];
356 contraction_dur_aUS_fquant = [];
357 contraction_dur_aUS_lquant = [];
358 for zz=1:length(A)
359     set=str2num(A{zz, :});
360
361     for yy=1:length(D)
362
363         setD=str2num(D{yy, :});
364         contraction_dur_noUS_median(zz, yy)=nanmedian(0.02*(index_min_speed_smooth(
            USstatus_all==0&tau_all==set&freq_all==setD)-index_max_speed_smooth(
            USstatus_all==0&tau_all==set&freq_all==setD)));
365         contraction_dur_noUS_fquant(zz, yy)=contraction_dur_noUS_median(zz, yy)-quantile
            (0.02*(index_min_speed_smooth(USstatus_all==0&tau_all==set&freq_all==setD)-
            index_max_speed_smooth(USstatus_all==0&tau_all==set&freq_all==setD)), 0.25);
366         contraction_dur_noUS_lquant(zz, yy)=quantile(0.02*(index_min_speed_smooth(
            USstatus_all==0&tau_all==set&freq_all==setD)-index_max_speed_smooth(
            USstatus_all==0&tau_all==set&freq_all==setD)), 0.75)-
            contraction_dur_noUS_median(zz, yy);
367         contraction_dur_US_median(zz, yy)=nanmedian(0.02*(index_min_speed_smooth(
            USstatus_all==1&tau_all==set&freq_all==setD)-index_max_speed_smooth(
            USstatus_all==1&tau_all==set&freq_all==setD)));
368         contraction_dur_US_fquant(zz, yy)=contraction_dur_US_median(zz, yy)-quantile
            (0.02*(index_min_speed_smooth(USstatus_all==1&tau_all==set&freq_all==setD)-
            index_max_speed_smooth(USstatus_all==1&tau_all==set&freq_all==setD)), 0.25);
369         contraction_dur_US_lquant(zz, yy)=quantile(0.02*(index_min_speed_smooth(
            USstatus_all==1&tau_all==set&freq_all==setD)-index_max_speed_smooth(
            USstatus_all==1&tau_all==set&freq_all==setD)), 0.75)-
            contraction_dur_US_median(zz, yy);
370         contraction_dur_aUS_median(zz, yy)=nanmedian(0.02*(index_min_speed_smooth(
            USstatus_all==2&tau_all==set&freq_all==setD)-index_max_speed_smooth(
            USstatus_all==2&tau_all==set&freq_all==setD)));
371         contraction_dur_aUS_fquant(zz, yy)=contraction_dur_aUS_median(zz, yy)-quantile
            (0.02*(index_min_speed_smooth(USstatus_all==2&tau_all==set&freq_all==setD)-
            index_max_speed_smooth(USstatus_all==2&tau_all==set&freq_all==setD)), 0.25);
372         contraction_dur_aUS_lquant(zz, yy)=quantile(0.02*(index_min_speed_smooth(
            USstatus_all==2&tau_all==set&freq_all==setD)-index_max_speed_smooth(
            USstatus_all==2&tau_all==set&freq_all==setD)), 0.75)-
            contraction_dur_aUS_median(zz, yy);
373 end
374 end
375
376 figure
377 subplot(1, 2, 1)
378 errorbar(xarray_pd, contraction_dur_noUS_median(:, 1), contraction_dur_noUS_fquant
            (:, 1), contraction_dur_noUS_lquant(:, 1), 'd', 'LineWidth', 1)
379 hold on

```

```

380 errorbar(xarray_pd , contraction_dur_US_median (:,1) , contraction_dur_US_fquant (:,1) ,
    contraction_dur_US_lquant (:,1) , 'h' , 'LineWidth' , 1)
381 errorbar(xarray_pd , contraction_dur_aUS_median (:,1) , contraction_dur_aUS_fquant (:,1) ,
    contraction_dur_aUS_lquant (:,1) , 's' , 'LineWidth' , 1)
382 xlabel( '\tau (ms)' )
383 ylabel( 'Peak duration (s)' )
384 title( 'Peak duration (1.0MHz)' )
385 legend( 'Before ultrasound' , 'During ultrasound' , 'After ultrasound' , 'Location' , '
    northwest' )
386 grid minor
387 xticks( [0 1 2 3 4] )
388 xlim( [0 4] )
389 xticklabels( [""; A] )
390 ylim( [0.08 0.24] )
391
392
393 subplot( 1,2,2)
394 errorbar(xarray_pd , contraction_dur_noUS_median (:,2) , contraction_dur_noUS_fquant
    (:,2) , contraction_dur_noUS_lquant (:,2) , 'd' , 'LineWidth' , 1)
395 hold on
396 errorbar(xarray_pd , contraction_dur_US_median (:,2) , contraction_dur_US_fquant (:,2) ,
    contraction_dur_US_lquant (:,2) , 'h' , 'LineWidth' , 1)
397 errorbar(xarray_pd , contraction_dur_aUS_median (:,2) , contraction_dur_aUS_fquant (:,2) ,
    contraction_dur_aUS_lquant (:,2) , 's' , 'LineWidth' , 1)
398 xlabel( '\tau (ms)' )
399 ylabel( 'Peak duration (s)' )
400 title( 'Peak duration (1.5MHz)' )
401 legend( 'Before ultrasound' , 'During ultrasound' , 'After ultrasound' , 'Location' , '
    northwest' )
402 grid minor
403 xticks( [0 1 2 3 4] )
404 xlim( [0 4] )
405 xticklabels( [""; A] )
406 ylim( [0.08 0.24] )
407
408
409 contrfreq_all_noUS_median = [];
410 contrfreq_all_noUS_fquant = [];
411 contrfreq_all_noUS_lquant = [];
412 contrfreq_all_US_median = [];
413 contrfreq_all_US_fquant = [];
414 contrfreq_all_US_lquant = [];
415 contrfreq_all_aUS_median = [];
416 contrfreq_all_aUS_fquant = [];
417 contrfreq_all_aUS_lquant = [];
418
419
420 for zz=1:length(A)
421     set=str2num(A{zz,:});
422
423     for yy=1:length(D)
424
425         setD=str2num(D{yy,:});
426         contrfreq_all_noUS_median(zz,yy)=nanmedian( contrfreq_all( USstatus_all==0&
            tau_all==set&freq_all==setD) ./ PRF_all( USstatus_all==0&tau_all==set&freq_all
            ==setD) ');

```

```

427   contrfreq_all_noUS_fquant (zz ,yy)=contrfreq_all_noUS_median (zz ,yy)-quantile ((
      contrfreq_all ( USstatus_all==0&tau_all==set&freq_all==setD) ./ PRF_all (
      USstatus_all==0&tau_all==set&freq_all==setD) ') ,0.25);
428   contrfreq_all_noUS_lquant (zz ,yy)=quantile (( contrfreq_all ( USstatus_all==0&
      tau_all==set&freq_all==setD) ./ PRF_all ( USstatus_all==0&tau_all==set&freq_all
      ==setD) ') ,0.75)-contrfreq_all_noUS_median (zz ,yy);
429   contrfreq_all_US_median (zz ,yy)=nanmedian ( contrfreq_all ( USstatus_all==1&tau_all
      ==set&freq_all==setD) ./ PRF_all ( USstatus_all==1&tau_all==set&freq_all==setD)
      ');
430   contrfreq_all_US_fquant (zz ,yy)=contrfreq_all_US_median (zz ,yy)-quantile ((
      contrfreq_all ( USstatus_all==1&tau_all==set&freq_all==setD) ./ PRF_all (
      USstatus_all==1&tau_all==set&freq_all==setD) ') ,0.25);
431   contrfreq_all_US_lquant (zz ,yy)=quantile (( contrfreq_all ( USstatus_all==1&tau_all
      ==set&freq_all==setD) ./ PRF_all ( USstatus_all==1&tau_all==set&freq_all==setD)
      ') ,0.75)-contrfreq_all_US_median (zz ,yy);
432   contrfreq_all_aUS_median (zz ,yy)=nanmedian ( contrfreq_all ( USstatus_all==2&tau_all
      ==set&freq_all==setD) ./ PRF_all ( USstatus_all==2&tau_all==set&freq_all==setD)
      ');
433   contrfreq_all_aUS_fquant (zz ,yy)=contrfreq_all_aUS_median (zz ,yy)-quantile ((
      contrfreq_all ( USstatus_all==2&tau_all==set&freq_all==setD) ./ PRF_all (
      USstatus_all==2&tau_all==set&freq_all==setD) ') ,0.25);
434   contrfreq_all_aUS_lquant (zz ,yy)=quantile (( contrfreq_all ( USstatus_all==2&tau_all
      ==set&freq_all==setD) ./ PRF_all ( USstatus_all==2&tau_all==set&freq_all==setD)
      ') ,0.75)-contrfreq_all_aUS_median (zz ,yy);
435   end
436 end
437
438 figure
439 subplot (1,2,1)
440 errorbar (xarray_pd , contrfreq_all_noUS_median (:,1) , contrfreq_all_noUS_fquant (:,1) ,
      contrfreq_all_noUS_lquant (:,1) , 'd' , 'LineWidth' , 1)
441 hold on
442 errorbar (xarray_pd , contrfreq_all_US_median (:,1) , contrfreq_all_US_fquant (:,1) ,
      contrfreq_all_US_lquant (:,1) , 'h' , 'LineWidth' , 1)
443 errorbar (xarray_pd , contrfreq_all_aUS_median (:,1) , contrfreq_all_aUS_fquant (:,1) ,
      contrfreq_all_aUS_lquant (:,1) , 's' , 'LineWidth' , 1)
444 xlabel ( '\tau (ms) ')
445 ylabel ( 'f_c / PRF (-) ')
446 title ( 'Ratio contraction frequency to PRF (1.0MHz) ')
447 legend ( 'Before ultrasound' , 'During ultrasound' , 'After ultrasound' , 'Location' , '
      northwest' )
448 grid minor
449
450 xticks ([0 1 2 3 4])
451 xlim ([0 4])
452 xticklabels (['' ; A])
453 ylim ([0.3 1.3])
454
455 subplot (1,2,2)
456 errorbar (xarray_pd , contrfreq_all_noUS_median (:,2) , contrfreq_all_noUS_fquant (:,2) ,
      contrfreq_all_noUS_lquant (:,2) , 'd' , 'LineWidth' , 1)
457 hold on
458 errorbar (xarray_pd , contrfreq_all_US_median (:,2) , contrfreq_all_US_fquant (:,2) ,
      contrfreq_all_US_lquant (:,2) , 'h' , 'LineWidth' , 1)
459 errorbar (xarray_pd , contrfreq_all_aUS_median (:,2) , contrfreq_all_aUS_fquant (:,2) ,
      contrfreq_all_aUS_lquant (:,2) , 's' , 'LineWidth' , 1)

```

```

460 xlabel( '\tau (ms)')
461 ylabel( 'f_c / PRF (-)')
462 title( 'Ratio contraction frequency to PRF (1.5MHz)')
463 legend( 'Before ultrasound', 'During ultrasound', 'After ultrasound', 'Location', '
         northwest')
464 grid minor
465 xticks([0 1 2 3 4])
466 xlim([0 4])
467 xticklabels(['"; A])
468 ylim([0.3 1.3])
469 %%
470 close all
471 A=categories(categorical(tau_all));
472 C=A([20:22]);
473 A=C;
474 D=categories(categorical(freq_all));
475 E=D([3:4]);
476 D=E;
477
478 pulseduration_xarray=[];
479 ratio_1_median=[];
480 ratio_1_fquant=[];
481 ratio_1_lquant=[];
482 ratio_1_length=[];
483 ratio_non1_median=[];
484 ratio_non1_fquant=[];
485 ratio_non1_lquant=[];
486 ratio_non1_length=[];
487 for zz=1:length(A)
488     set=str2num(A{zz,:});
489
490 %     for yy=1:length(D)
491 %
492 %     setD=str2num(D{yy,:});
493
494 contr_ratio=(contrfreq_all(USstatus_all==1&tau_all==set&freq_all>0.8)./PRF_all(
         USstatus_all==1&tau_all==set&freq_all>0.8)');
495 contr_ratio_delaytime=delaytime_all(USstatus_all==1&tau_all==set&freq_all>0.8);
496 contr_ratio_1=contr_ratio_delaytime(contr_ratio<1.05&contr_ratio>0.949);
497
498 contr_ratio_maxspeed=max_speed_smooth(USstatus_all==1&tau_all==set);
499 contr_ratio_1_maxspeed=contr_ratio_maxspeed(contr_ratio<1.05&contr_ratio>0.949);
500
501 contr_ratio_non1=contr_ratio_delaytime(contr_ratio>=1.05|contr_ratio<=0.949);
502
503 ratio_1_median(zz)=nanmedian(contr_ratio_1);
504 ratio_1_fquant(zz)=ratio_1_median(zz)-quantile(contr_ratio_1,0.25);
505 ratio_1_lquant(zz)=quantile(contr_ratio_1,0.75)-ratio_1_median(zz);
506 ratio_1_length(zz)=size(contr_ratio_1,1);
507 ratio_non1_median(zz)=nanmedian(contr_ratio_non1);
508 ratio_non1_fquant(zz)=ratio_non1_median(zz)-quantile(contr_ratio_non1,0.25);
509 ratio_non1_lquant(zz)=quantile(contr_ratio_non1,0.75)-ratio_non1_median(zz);
510 ratio_non1_length(zz)=size(contr_ratio_non1,1);
511 pulseduration_xarray(zz)=set;
512 end
513 all_delaytime=[];

```

```

514 all_delaytime=delaytime_all(USstatus_all==1&freq_all >0.8&tau_all >0.4&tau_all <1.1)
    ./(PRF_all(USstatus_all==1&freq_all >0.8&tau_all >0.4&tau_all <1.1));
515 all_median=nanmedian(all_delaytime);
516 all_fquant=all_median-quantile(all_delaytime,0.25);
517 all_lquant=quantile(all_delaytime,0.75)-all_median;
518 all_length=size(all_delaytime,1);
519
520 xarray_pd=[1:1:length(pulseduration_xarray)];
521
522 figure
523 errorbar(xarray_pd, ratio_1_median, ratio_1_fquant, ratio_1_lquant, 'd', 'LineWidth',
    1)
524 hold on
525 errorbar(xarray_pd, ratio_non1_median, ratio_non1_fquant, ratio_non1_lquant, 's', '
    LineWidth', 1)
526 errorbar(length(pulseduration_xarray)+1, all_median, all_fquant, all_lquant, 'p', '
    LineWidth', 1)
527
528 for zy=1:zz
529 text(xarray_pd(zy)+0.1,0.1,num2str(ratio_1_length(zy)), 'color', 'b')
530 text(xarray_pd(zy)+0.1,0.2,num2str(ratio_non1_length(zy)), 'color', 'r')
531 end
532 xlabel(' \tau (ms)')
533 ylabel('Delay after US pulse (s)')
534 title('Delay of contraction after US pulse')
535 legend('Contraction frequency 0.95 to 1.05 PRF', 'Contraction frequency above 1.05
    or below 0.95', 'All datapoints', 'Location', 'northwest')
536 grid minor
537 xticks([0 [1:1:length(A)+2]])
538 xlim([0 length(A)+2])
539 xticklabels([""; A;" All"])
540
541 %%
542 close all
543 figure
544
545 for zz=1:length(A)
546     set=str2num(A{zz,:});
547 contr_ratio=(contrfreq_all(USstatus_all==1&tau_all==set)./PRF_all(USstatus_all==1&
    tau_all==set));
548 contr_ratio_delaytime=delaytime_all(USstatus_all==1&tau_all==set);
549 contr_ratio_1=contr_ratio_delaytime(contr_ratio <1.05&contr_ratio >0.949);
550 contr_ratio_non1=contr_ratio_delaytime(contr_ratio >=1.05|contr_ratio <=0.949);
551
552 contr_ratio_maxspeed=max_speed_smooth(USstatus_all==1&tau_all==set);
553 contr_ratio_1_maxspeed=contr_ratio_maxspeed(contr_ratio <1.05&contr_ratio >0.949);
554 contr_ratio_non1_maxspeed=contr_ratio_maxspeed(contr_ratio >=1.05|contr_ratio
    <=0.949);
555
556 plot(contr_ratio_1, contr_ratio_1_maxspeed, '*')
557 hold on
558 plot(contr_ratio_non1, contr_ratio_non1_maxspeed, 'o')
559 end
560 xlabel('Delaytime (s)')
561 ylabel('V_{max} (\text{mm/s})')
562

```

```

563 %%
564
565 % [X,Y]=meshgrid(min(contrperiod_all):0.02:max(contrperiod_all),min(delaytime_all)
      :0.02:max(delaytime_all));
566 % Z=nan(size(X,1),size(X,2));
567 % for pp=1:size(X,2)
568 % for ss=1:size(X,1)
569 %     Z(ss,pp)=nnz(contrperiod_all==X(1,pp)&delaytime_all==Y(ss,1));
570 % end
571 % end
572 %
573 % figure
574 % surf(X,Y,Z)

```